

Dissertation presented to the Instituto Tecnológico de Aeronáutica, in partial fulfillment of the requirements for the degree of Master in Engineering in the Professional Master's Program of Aeronautics and Mechanics Engineering.

Heric Martinez Santos Ballesteros

**DYNAMIC STIFFNESS ENHANCEMENT OF A
FLIGHT CONTROL ACTUATOR USING
CONTROL TECHNIQUES**

Dissertation approved in its final version by signatories below:

Ph.D. Alberto Adade Filho
Advisor

MSc. Raphael das Neves Calvo
Co-advisor

Ph.D. Luiz Carlos Sandoval Góes
Prorector of Graduate Studies and Research

Campo Montenegro
São José dos Campos, SP - Brazil
2015

**Cataloging-in Publication Data
Documentation and Information Division**

Martinez Santos Ballesteros, Heric

Dynamic Stiffness Enhancement of a Flight Control Actuator using control techniques / Heric Martinez Santos Ballesteros.

São José dos Campos, 2015.

175f.

Dissertation of Master in Engineering – Course of Aeronautics and Mechanics Engineering. Area of Aerospace Systems and Mechatronics – Instituto Tecnológico de Aeronáutica, 2015. Advisor: Ph.D. Alberto Adade Filho. Co-advisor: MSc. Raphael das Neves Calvo.

1. Dynamic stiffness. 2. Actuator. 3. Flutter. I. Instituto Tecnológico de Aeronáutica. II. Title.

BIBLIOGRAPHIC REFERENCE

MARTINEZ SANTOS BALLESTEROS, Heric. **Dynamic Stiffness Enhancement of a Flight Control Actuator using control techniques**. 2015. 175f. Dissertation of Master in Engineering – Instituto Tecnológico de Aeronáutica, São José dos Campos.

CESSION OF RIGHTS

AUTHOR'S NAME: Heric Martinez Santos Ballesteros

PUBLICATION TITLE: Dynamic Stiffness Enhancement of a Flight Control Actuator using control techniques.

PUBLICATION KIND/YEAR: Dissertation / 2015

It is granted to Instituto Tecnológico de Aeronáutica permission to reproduce copies of this dissertation and to only loan or to sell copies for academic and scientific purposes. The author reserves other publication rights and no part of this dissertation can be reproduced without the authorization of the author.

Heric Martinez Santos Ballesteros
R. Maria Kfuri, 448
12.242-500 – São José dos Campos–SP

DYNAMIC STIFFNESS ENHANCEMENT OF A FLIGHT CONTROL ACTUATOR USING CONTROL TECHNIQUES

Heric Martinez Santos Ballesteros

Thesis Committee Composition:

Ph.D.	Luiz Carlos Sandoval Góes	President	-	ITA
Ph.D.	Alberto Adade Filho	Advisor	-	ITA
MSc.	Raphael das Neves Calvo	Co-advisor	-	EMBRAER
Eng.	Marcio Matuo	Engineer	-	EMBRAER

ITA

Para Julia, Janet, Edijane e Edilberto
Júnior.

Acknowledgments

I would like to express my deepest gratitude to my advisor, Dr. Alberto Adade Filho and my co-advisor, M.Sc. Raphael das Neves Calvo, for their support, guidance, encouragement and patience throughout this research work.

My sincere appreciation to Carlos Constantino and Eulo Antonio Balvedi Junior for their invaluable support, encouragement and advice on specific points of this work.

I would also like to thank EMBRAER, especially Marcos Gritti, for allowing me to dedicate time to put effort in this work.

I am very grateful to FCMF for the financial support during this research work.

My deepest gratitude and love belong to Julia, whose support and patience kept me going throughout this journey and were with me for all those years.

Last but not least, I would like to thank my family - my mom, grandmother, and aunt - for their love, support, advice, and encouragement.

*“And in the end,
the love you take is equal to the love you make.”*
— SIR PAUL McCARTNEY

Resumo

Em sistemas de comandos de voo, atuadores eletrohidráulicos são responsáveis por mover as superfícies de controle primário das aeronaves atendendo requisitos de desempenho, como resposta temporal e em frequência. Outra responsabilidade dos mesmos é a supressão de flutter da superfície de controle, atendendo requisitos de rigidez dinâmica e de amortecimento. Em um projeto clássico de atuador, o cumprimento de tais requisitos gera atuadores não-ótimos, penalizando o desempenho da aeronave. O objetivo deste trabalho é investigar diferentes estratégias de controle de posição do atuador que atendam os requisitos de desempenho e aumentem a rigidez dinâmica do atuador.

Uma metodologia clássica de dimensionamento de atuadores primários é desenvolvida e validada utilizando um modelo baseado em (CONSTANTINO, 2010) com modificações para a análise de rigidez dinâmica. O desempenho do atuador para diferentes controladores clássicos (P, PI, PD, PID) é analisado, e uma abordagem de controle moderno usando a estratégia de controle LQR com um observador linear de ordem reduzida, além de uma realimentação de estado parcial, usando apenas variáveis medidas, são desenvolvidas. Ambas estratégias apresentaram bom desempenho, superando o do controle PD, e aumentando a rigidez dinâmica do atuador especialmente para frequências acima de 10 Hz.

O desempenho dos controladores modernos permitiu a redução da área do pistão em um selo. O atuador com área reduzida operando com realimentação de estados ou de saída apresentou um excelente desempenho e uma melhoria notável da rigidez dinâmica. Assim, é possível projetar um atuador de comandos de voo otimizado, utilizando uma abordagem de controle moderno, que reduziria o consumo hidráulico, o peso e tamanho do atuador, trazendo benefícios para o desempenho da aeronave.

Abstract

In flight control systems, electro-hydraulic actuators are responsible for moving the aircraft primary control surfaces while complying with performance requirements, such as time and frequency response. Another responsibility is the control surface flutter suppression, translated into dynamic stiffness and damping requirements. In a classical actuator design, compliance with those requirements leads to non-optimal actuators and penalizes the aircraft overall performance. This work aims to investigate different actuator's position control strategies seeking compliance with performance requirements and enhancing the actuator's dynamic stiffness.

A primary actuator classic sizing methodology is developed and validated using an actuator model, based on (CONSTANTINO, 2010), with modifications to improve the dynamic stiffness analysis. Actuator performance is evaluated for different classical controllers (P, PI, PD, and PID). In addition, a modern control approach using an LQR control strategy and a linear reduced-order observer, and a partial-state (output) feedback control using only the measured variables were developed. Both strategies presented good performance, overcoming the PD strategy, and enhanced the actuator's dynamic stiffness especially for frequencies above 10 Hz.

These modern controllers' performance allowed a piston area reduction of one seal size. The reduced area actuator with full-state and partial-state feedback control presented great performance and an outstanding enhancement of the dynamic stiffness. Thus, it is feasible to design an optimized flight control actuator, taking credit of a modern control approach that would reduce hydraulic consumption, and the actuator's weight and size, bringing benefits to the aircraft performance.

List of Figures

FIGURE 2.1 – Control Surface Dynamics	28
FIGURE 2.2 – Definition of Secant Bulk Modulus Source: (HODGES, 1996)	31
FIGURE 2.3 – Definition of Tangent Bulk Modulus Source: (HODGES, 1996)	31
FIGURE 2.4 – Example of the effect of the pressure on the bulk modulus of a typical mineral based hydraulic fluid at constant temperature. Source: (RABIE, 2009)	32
FIGURE 2.5 – Example of the effect of the temperature on the bulk modulus of a typical mineral based hydraulic fluid at constant pressure. Source: (RABIE, 2009)	33
FIGURE 2.6 – Example of variation of the fluid effective bulk modulus with volume of entrapped air. Source: (CORTELLINE; GOES, 2010)	33
FIGURE 2.7 – Aircraft classical coordinate sign convention. Source: (SCHMIDT, 1998)	34
FIGURE 2.8 – Conventional mechanical flight control system. Source: (PRATT, 2000)	35
FIGURE 2.9 – Irreversible Flight Control System with hydraulic actuator Source: (DAEROSPACE, 2015)	36
FIGURE 2.10 – F/A-18E/F Super Hornet rudder actuator. Source: (WOODWARD, 2015)	37
FIGURE 2.11 – Typical actuator using electrohydraulic servovalves - Dowty Aerospace. Source: (PRATT, 2000)	37
FIGURE 2.12 – Typical flight control actuator dynamic stiffness and damping boundaries. Source: (PRATT, 2000)	39
FIGURE 2.13 – Block diagram of hydromechanical position control servo. Source: (MERRITT, 1967)	40

FIGURE 3.1 – Actuator installation and RLC triangle. Adapted from (CONSTANTINO, 2010)	43
FIGURE 3.2 – Balanced hydraulic actuator, rod and piston seals. Source: (DAEROSPACE, 2015)	44
FIGURE 3.3 – Complete Primary Flight Control Actuator Design Process	45
FIGURE 3.4 – Flutter requirements - airspeed margin. Source: (MIL-A-8870C, 1993)	46
FIGURE 3.5 – Flutter requirements - damping coefficient. Source: (MIL-A-8870C, 1993)	46
FIGURE 3.6 – Primary Flight Control Actuator and surface.	51
FIGURE 3.7 – Flight Control Actuator, Surface - stiffness components - adapted from (CONSTANTINO, 2010)	54
FIGURE 3.8 – Unbalanced piston - oil column stiffness. Adapted from: (DAEROSPACE, 2015)	55
FIGURE 3.9 – Actuator in neutral position - RLC triangle	58
FIGURE 3.10 –Actuator in extended position - RLC triangle	58
FIGURE 3.11 –Actuator in retracted position - RLC triangle	59
FIGURE 4.1 – Actuator Hydraulic Schematic	63
FIGURE 4.2 – Schematic of a two-stage electrohydraulic servovalve with force feedback and a flapper nozzle system as first stage (THAYER, 1965)	64
FIGURE 4.3 – Hydraulic Actuation System Model overview	69
FIGURE 4.4 – Hydraulic System Model	70
FIGURE 4.5 – Actuation System Model	72
FIGURE 4.6 – Actuator Electronics System Model	73
FIGURE 4.7 – Actuator Model	73
FIGURE 4.8 – Actuator Model - Valves Dynamics	75
FIGURE 4.9 – Actuator Model - Cylinder Dynamics	76
FIGURE 4.10 –Actuator Model - Sensor Dynamics	77
FIGURE 4.11 –Surface Kinematics Model	77
FIGURE 4.12 –Bulk Modulus modifications	79
FIGURE 4.13 –Actuator chamber with fluid and air. Source: (RABIE, 2009)	80

FIGURE 4.14 –EHSV 1st Stage Moog model valve in Simulink	85
FIGURE 4.15 –Simulated EHSV 1st Stage Frequency Response	86
FIGURE 4.16 –Schematic of a two-stage electrohydraulic servo valve with force feed-back and a flapper nozzle system as first stage [adapted from Moog]	87
FIGURE 4.17 –Friction due to O-ring seal compression and hardness. Source:(PARKER, 2007)	88
FIGURE 4.18 –Friction due to fluid pressure. Source:(PARKER, 2007)	88
FIGURE 4.19 –Friction force implementation for piston and rod groove applications	90
FIGURE 4.20 –Friction force implementation for piston and rod groove applications .	92
FIGURE 4.21 –Actuator Position Control Loop with piston position feedback . . .	93
FIGURE 4.22 –Inlet check valve. Source:(CONSTANTINO, 2010)	93
FIGURE 4.23 –Cutaway view of a typical LVDT sensor. Source: (MACROSENSORS, 2015)	94
FIGURE 4.24 –LVDT error - for a LVDT range of +/ – 4in	95
FIGURE 4.25 –LVDT model implemented	96
FIGURE 4.26 –Step Response - proportional controller gain $K_p = 40 \text{ mA/in}$. . .	97
FIGURE 4.27 –Step Response - Overview	98
FIGURE 4.28 –Step Response - Stiffness Analysis	99
FIGURE 4.29 –Step Response - EHSV Analysis	100
FIGURE 4.30 –Linear Load x Surface Rate	101
FIGURE 4.31 –Rudder actuator's frequency response for different fluid temperatures	102
FIGURE 4.32 –Dynamic Stiffness test in hot temperature - compliant with requirement	103
FIGURE 5.1 – EHSV flow output x EHSV current	105
FIGURE 5.2 – Time response for different EHSV flow output	106
FIGURE 5.3 – Frequency Response for different EHSV flow output	107
FIGURE 5.4 – Dynamic Stiffness for different EHSV flow output	108
FIGURE 5.5 – Time Response for different proportional gains	110
FIGURE 5.6 – Step Response for different proportional gains	111
FIGURE 5.7 – Frequency Response for different proportional gains	112

FIGURE 5.8 – Dynamic Stiffness test for different proportional gains	113
FIGURE 5.9 – Dynamic Stiffness Response for different control loop's update rates	114
FIGURE 5.10 –Dynamic Stiffness Response for different internal leakage values . . .	115
FIGURE 5.11 –Discrete parallel PID implementation	118
FIGURE 5.12 –Time Response for different integral gains	119
FIGURE 5.13 –Step Response for different integral gains	120
FIGURE 5.14 –Frequency Response for different integral gains	121
FIGURE 5.15 –Dynamic Stiffness test for different integral gains	122
FIGURE 5.16 –Time Response for different derivative gains	123
FIGURE 5.17 –Step Response for different derivative gains	124
FIGURE 5.18 –Frequency Response for different derivative gains	125
FIGURE 5.19 –Dynamic Stiffness test for different derivative gains	126
FIGURE 5.20 –Time Response for PID controllers	127
FIGURE 5.21 –Frequency Response for PID controllers	128
FIGURE 5.22 –Dynamic Stiffness test for PID controllers	129
FIGURE 5.23 –Time response for different classic controllers	130
FIGURE 5.24 –Frequency response for different classic controllers	131
FIGURE 5.25 –Dynamic Stiffness for different classic controllers	132
FIGURE 5.26 –Phase delay x Dynamic Stiffness	133
FIGURE 5.27 –Nonlinear and linear model comparison - EHSV 1st stage states - EHSV 1 mA step at 0.5 s	136
FIGURE 5.28 –Nonlinear and linear model comparison - ΔP state - EHSV 1 mA step at 0.5 s	137
FIGURE 5.29 –Nonlinear and linear model comparison - Piston states - EHSV 1 mA step at 0.5 s	138
FIGURE 5.30 –Time Response for modern controllers	144
FIGURE 5.31 –Time Response for modern controllers	145
FIGURE 5.32 –Frequency Response for modern controllers	146
FIGURE 5.33 –Dynamic Stiffness for modern controllers	147
FIGURE 6.1 – Time Response - Different controllers - new design	150

FIGURE 6.2 – Frequency Response - Different controllers - new design	152
FIGURE 6.3 – Dynamic Stiffness - Different controllers - new design	153
FIGURE 6.4 – Dynamic Stiffness - Preliminary vs. Optimal design comparison . .	155
FIGURE A.1 – Time Response - ON-OFF controller	162
FIGURE A.2 – Frequency Response - ON-OFF controller	163
FIGURE A.3 – Dynamic Stiffness - ON-OFF controller	164
FIGURE A.4 – EHSV first stage dynamics model	167
FIGURE A.5 – EHSV 2nd stage and ΔP dynamics	168
FIGURE A.6 – Simplified P_1 dynamics	168
FIGURE A.7 – Simplified Piston dynamics model	169
FIGURE A.8 – Δ pressure sensor output with noise	170
FIGURE A.9 – Actuator's time response for modern controller and with ΔP sensor noise	171
FIGURE A.10 – Actuator's frequency response for modern controller and with ΔP sensor noise	172
FIGURE A.11 – Dynamic Stiffness performance comparison for modern controller with and without ΔP sensor noise	173

List of Tables

TABLE 2.1 – SAE AIR1362 - Bulk Modulus type selection	31
TABLE 3.1 – Rudder Actuator Kinematics	59
TABLE 3.2 – Rudder Actuator Design Results	60
TABLE 3.3 – Rudder Actuation System Design Characteristics	60
TABLE 3.4 – Actuator Design	61
TABLE 3.5 – Preliminary Actuator compliance with design requirements	62
TABLE 4.1 – Rudder Actuator Design - Time Response Requirements Compliance	97
TABLE 4.2 – Rudder Actuator Design - Frequency Response Requirements Compliance	101
TABLE 5.1 – Rudder Actuator Design - Time Response Requirements Compliance EHSV study	106
TABLE 5.2 – Rudder Actuator Design - Frequency Response Requirements Compliance EHSV study	107
TABLE 5.3 – Rudder Actuator Design - Time Response Requirements Compliance P controller	110
TABLE 5.4 – Rudder Actuator Design - Frequency Response Requirements Compliance P controller	112
TABLE 5.5 – Rudder Actuator Design - Time Response Requirements Compliance PI controller	119
TABLE 5.6 – Rudder Actuator Design - Frequency Response Requirements Compliance PI controller	121
TABLE 5.7 – Rudder Actuator Design - Time Response Requirements Compliance PD controller	123

TABLE 5.8 – Rudder Actuator Design - Frequency Response Requirements Compliance PD controller	125
TABLE 5.9 – Different PID designs proposed	127
TABLE 5.10 – Rudder Actuator Design - Time Response Requirements Compliance PID controller	128
TABLE 5.11 – Rudder Actuator Design - Frequency Response Requirements Compliance PID controller	129
TABLE 5.12 – Different classical controller design proposed	130
TABLE 5.13 – Rudder Actuator Design - Time Response Requirements Compliance Classic controllers	131
TABLE 5.14 – Rudder Actuator Design - Frequency Response Requirements Compliance Classic controllers	132
TABLE 5.15 – Rudder Actuator Design - Time Response Requirements Compliance Modern controllers	144
TABLE 5.16 – Rudder Actuator Design - Frequency Response Requirements Compliance Modern controllers	146
TABLE 6.1 – Rudder Actuator New design	149
TABLE 6.2 – New Rudder Actuator against Requirements	149
TABLE 6.3 – Classical controller gains	150
TABLE 6.4 – Rudder Actuator New Design Time Response Requirements Compliance	151
TABLE 6.5 – Rudder Actuator New Design - Frequency Response Requirements Compliance	152
TABLE 6.6 – Rudder Actuator New Design Frequency Response Requirements Compliance	154
TABLE A.1 – Rudder Actuator Design - Time Response Requirements Compliance ON-OFF controller	162
TABLE A.2 – Rudder Actuator Design - Frequency Response Requirements Compliance ON-OFF controller	163
TABLE A.3 – Actuator's time response for modern controller and with ΔP sensor noise	171

TABLE A.4 – Actuator’s frequency response for modern controller and with ΔP sensor noise	172
---------------------------------------------------------------------------------------------------------------	-----

List of Symbols

β	Isothermal Secant Bulk Modulus
ΔP	Liquid Pressure variation
ΔV	Liquid Volume variation
Z	Mechanical Impedance
K	Mechanical Dynamic Stiffness
C	Imaginary part of Mechanical Impedance
w_f	Flutter frequency
V_D	Aircraft dive speed
J	Control surface inertial
c	Control surface rotational damping
K_θ	Control surface rotational stiffness
w_n	Control surface undamped natural frequency
V_L	Aircraft limit speed
t_{ss}	settling time
y_s	control surface position steady state value
R	Horn radius
L	Actuator length in neutral position
L_r	Actuator length in retracted position
L_e	Actuator length in extended position
C	Distance from non-moveable surface and control surface's anchorage point
b_{eff}	Effective arm
HM_{aero}	Control surface aerodynamic hinge moment
HM_{act}	Control surface hinge moment due to actuator force
F_{lin}	Forces in the actuator axis
F_{act}	Actuator output force
A_{act}	Actuator area
δP	Differential pressure between actuator chambers
ΔL	Actuator piston linear displacement
θ	Control surface angular position
θ	Control surface angular position

K_L	Control surface stiffness
$f_{flutter}$	infinite stiffness frequency
ξ	Control surface rotational damping ration
K_{act}	Actuator stiffness
K_R	Anchorage surface stiffness
$K_{\theta_{flutter_{lin}}}$	Control surface equivaelent linear stiffness for flutter suppression
K_{metal}	Actuator's metallic part stiffness
K_{oil}	Actuator's oil column stiffness
β_{mod}	Fluid Bulk Modulus
A_1	Actuator piston area in chamber 1
A_2	Actuator piston area in chamber 2
$K_{oil@neutral}$	Actuator's oil column stiffness at neutral position
S	Actuator' stroke
λ	ratio between K_{metal} and K_{oil}
$A_{act_{flutter}}$	actuator area to meet flutter requirements
α	angle between C and L
β	angle between C and R
γ	angle between L and R
deg	degrees
$A_{act_{load}}$	actuator area to meet load requirements
$K_{act_{flutter}}$	Actuator stiffness to meet flutter requirements
$PistonD$	Actuator piston diameter
$RodD$	Actuator rod diameter
β_M	Fluid-air mixture bulk modulus
β_{oil}	Fluid bulk modulus
F_C	Total friction due to seal compression
K_{iso}	Isothermal process constant
f_C	Friction coefficient due to O-ring compression
F_H	Friction due to fluid pressure
f_H	Friction coefficient due to fluid pressure
A_p	Projected area of seal for piston groove applications
L_p	Length of seal rubbing surface in inches for piston groove applications
A_R	Projected area of seal for rod groove applications
L_R	Length of seal rubbing surface in inches for rod groove applications
F_f	Total seal friction force
x_p	actuator piston position
F_{fs}	Seal friction force
sc	Stribeck coefficient
P_s	Supply pressure or inlet pressure

P_{cv}	Pressure inside the inlet check valve
x_v	EHSV spool position
K_p	proportional discrete PID controller gain
K_i	integral discrete PID controller gain
K_d	derivative discrete PID controller gain

Contents

1	INTRODUCTION	23
1.1	Motivation	23
1.2	Objective	23
1.3	Bibliographic review	24
1.4	Organization	25
2	THEORY BACKGROUND	27
2.1	Flutter	27
2.1.1	Control Surface Flutter	28
2.2	Hydraulic Oil Compressibility - Bulk Modulus	30
2.3	Rudder Actuation Control Systems	34
2.3.1	Flight Control Systems Overview	34
3	FLIGHT CONTROL ACTUATOR DESIGN	43
3.1	Actuator Design Process	43
3.2	Actuator Design Requirements	44
3.2.1	Flutter suppression requirements	44
3.2.2	Safety requirements	48
3.2.3	Actuator control loop requirements	49
3.3	Flight Control Actuator design	50
3.3.1	Actuator Stall Load Requirement	51
3.3.2	Actuation System Rotational Stiffness Requirement	52
3.3.3	Actuator Stiffness required for flutter suppression	54
3.3.4	Actuator Stroke Estimation	57

3.4 Rudder flight control actuator design	59
3.4.1 Stall load compliance design	60
3.4.2 Flutter suppression compliance design	61
3.4.3 Final actuator design	61
4 MODEL CONSTRUCTION	63
4.1 Flight Control Actuator Nonlinear Model	63
4.2 Flight Control Actuation System Simulation Model	67
4.2.1 Hydraulic System	70
4.2.2 Actuation System Model	71
4.3 Flight Control Actuation System Model Modifications	77
4.3.1 Surface simplification	78
4.3.2 Fluid Bulk Modulus Variation	78
4.3.3 Electro-hydraulic servovalve - EHSV	84
4.3.4 Seal Friction	87
4.3.5 Position Control Loop	92
4.3.6 Inlet Check Valve	93
4.3.7 Sensors	94
4.4 Model results and design requirements compliance	96
4.4.1 Time response	96
4.4.2 Frequency Response	101
4.4.3 Dynamic Stiffness	102
5 CONTROL STRATEGIES	104
5.1 Parametric Study	104
5.1.1 EHSV second stage size	104
5.1.2 Proportional Controller	108
5.1.3 Control loop update rate study	113
5.1.4 Internal Leakage	115
5.2 Control Strategies	116
5.2.1 Classic Controllers	116

5.2.2	Modern Controller	133
6	FLIGHT CONTROL ACTUATOR NEW DESIGN	148
6.1	Rudder actuator new design	148
6.2	Actuator Redesign Performance	149
6.2.1	Time Response	150
6.2.2	Frequency Response	151
6.2.3	Dynamic Stiffness	152
6.3	Actuator Design Comparison	153
7	CONCLUSION	156
7.1	Future Works	157
BIBLIOGRAPHY		159
APPENDIX A – GENERAL TOPICS		161
A.1	ON-OFF Controller	161
A.2	Electro-hydraulic Actuator State-space model	164
A.3	Modern controller with Pressure sensor noise	169
ANNEX A – AEROELASTIC AND SAFETY REQUIREMENTS		174
A.1	Control surface flutter suppression requirements	174
A.2	Safety requirements - Flight Control System	175

1 Introduction

This work presents an investigation over the effect of different position control strategies and its impact on a hydraulic actuator dynamic stiffness. The motivation, objective, bibliographic review and organization are presented in the following sections.

1.1 Motivation

Recent aircraft projects have adopted modern flight control systems, bringing performance gains like weight saving, envelope protection and reduced crew workload. Position control of those surfaces is usually performed by electro-hydraulic actuators, which must mitigate conditions leading to catastrophic failures, such as the flutter phenomenon.

The flutter phenomenon may cause severe catastrophic damages to the aircraft. In the aeronautical industry, the control surface flutter can be prevented by the mass balancing of the control surface or by the flight control actuator. When the actuator performs flutter suppression, its design obeys not only typical performance requirements, such as actuation rate, but also aeroelastic stability requirements, such as dynamic stiffness and dynamic damping. Usually, the dynamic stiffness compliance is guaranteed by increasing the actuator piston area. This approach leads to an increase in the actuator's volume and weight. Moreover, the increase of hydraulic flow demand penalizes the aircraft hydraulic system, leading to subsequent weight penalties.

An actuator sizing method that seek compliance with both performance and flutter requirements, and optimize the actuator's size, would bring weight and volume reduction benefits. In addition, it would allow thinner control surfaces design, thus an increase in aircraft global performance.

1.2 Objective

The main objective of this work is to propose an enhancement of the dynamic stiffness of a rudder flight control electro-hydraulic actuator using control techniques in order to

comply with flutter suppression and performance requirements.

The dynamic stiffness enhancement may allow an optimized design of electro-hydraulic actuators without performance withdraws or design requirements noncompliance, and that could bring benefits such as:

- i weight reduction;
- ii volume reduction;
- iii reduced hydraulic consumption.

A classical actuator design will be made using standard tools to comply with performance and flutter suppression requirements. An actuation system model will be developed in order to simulate and validate the electro-hydraulic actuator design.

In order to guarantee compliance with performance requirements and to enhance the actuator's dynamic stiffness, the actuator's position control loop will be designed and evaluated for different control techniques. As a result, the actuator sizing will be revised in order to reduce hydraulic consumption and to maintain its compliance with other requirements.

1.3 Bibliographic review

In (MERRITT, 1967), a complete overview is given on hydraulics fundamentals. Important topics on hydraulic system design, components and control are also available.

A model of a flight control system hydraulic actuation on active-active configuration is constructed in (CONSTANTINO, 2010). The model consists of a servo valve, a hydraulic actuator, a position control loop and control surface with a representative performance up to around 80 Hz. A study of the model behavior on an oscillatory mal-function scenario was also performed, identifying fatigue life consumption of the control surface structure and the need for monitors to detect this failure mode.

A complete overview of aircraft aeroelasticity is presented in (WRIGHT; COOPER, 2007). The dynamic aeroelasticity section describes and analyzes flutter phenomenon including control surface flutter problem faced by the aeronautical industry.

In (THAYER, 1965), an electro-hydraulic servovalve dynamic behavior is represented by equivalent transfer functions. A highlight is the servo valve's block diagram model and parameters presented in its Appendix.

In (BLAIGNAN; SKORMIN, 1993), a flight control actuator dynamic stiffness enhancement using actuator's position control laws is proposed. The author presents a mathe-

matical model of a flight control actuator driven by an electro-hydrostatic servo pump. A dynamic stiffness investigation is carried out by simulation; an estimator of external force is designed to allow the use of a feedforward control strategy. It is presented a significant increase in the actuator dynamic stiffness especially at frequencies below 30 Hz.

A flight control actuator dynamic stiffness increase using actuator robust control laws is proposed in (THOMPSON *et al.*, 1999). This work presents an electro-hydraulic actuator model and a position control feedback based on the Quantitative Feedback Theory (QFT) technique. Both robust piston position tracking and actuator dynamic stiffness enhancement are achieved using QFT. Some hydraulic fluid parameters variation (bulk modulus, temperature, pressure) are considered and the controller design results in a high-order filter, which is a drawback for industry applications.

The modelling of an electro-hydraulic servo valve and hydraulic actuator is performed in (KASHI; SOFFKER, 2004). In this work, a robust position control via sliding mode technique is proposed to take into account some parameters variation such as fluid bulk modulus, fluid temperature and other servo valve parameters. In addition, it is presented a performance comparison between sliding mode technique and a robust PID control with parametric variation, with the latter being more robust presenting less control efforts.

A state-space model of an electro-hydraulic actuator is developed in (KURODE S.; SHIRALKAR, 2013) in order to estimate the force and displacement of the hydraulic actuator. The estimation is performed by a Proportional-Integral Observer (PIO) constructed based on the state-space model. Experimental tests in a test-rig were conducted and the observer showed a good overall estimation of force and piston displacement.

(PARKER, 2007) contains extensive information about basic sealing elastomers, focusing on typical O-ring applications for hydraulic components. Fundamentals of static and dynamic seal design are presented including a detailed formula to estimate dynamic O-ring seal friction based on standard seal sizes used in the industry.

1.4 Organization

Chapter 1 performs an introduction about this work.

Chapter 2 provides a theoretical background for flight control systems, focusing on flutter, hydraulic fluid bulk modulus and dynamic stiffness definitions.

Chapter 3 overviews the actuator classic design process in order to comply with performance and flutter requirements.

Chapter 4 approaches the actuator nonlinear model and its implementation focusing on the modifications from (CONSTANTINO, 2010) and on actuator design validation.

Chapter 5 synthesizes several control strategies adopted to enhance the actuator's dynamic stiffness and to comply with time and frequency performance requirements.

Chapter 6 presents a new actuator design, and performs a comparison between the preliminary and optimal actuator design performance.

Chapter 7 is responsible for conclusions and future work.

2 Theory Background

This chapter provides a theory review about important subjects that will appear all over this work. It is made to be simple. For specific details, please see the indicated references.

2.1 Flutter

Flutter is an aeroelastic phenomenon, an unstable self-excited vibration in which the structure extracts energy from the air stream and it may result in catastrophic structural failure. When the aerodynamic forces associated with motion in two or more modes of vibration of the aircraft structure cause the modes to couple in an unfavorable manner, the flutter occurs.

Flutter speed is the airspeed at which flutter occurs. At this critical speed, the structure sustains oscillation following some initial disturbance. Below flutter speed, the oscillations are damped. Above this speed, in a linear aeroelastic system analysis, one of the aircraft modes of vibration is marginally damped, implicating in sustained oscillations that would lead to structural failures of the aircraft. For nonlinear systems, those oscillations may converge to limit cycle oscillations (LCO's).

Besides flutter speed, another important aeroelastic aspect is the flutter frequency, defined as the frequency at which flutter phenomenon occurs. Generally, the solution adopted to prevent flutter phenomena is to avoid coupling between aeroelastic modes in the flutter frequency.

In the aerospace industry, flutter can appear involving different pairs of interacting modes such as wing bending/torsion, wing torsion/control surface, wing/engine, etc. This work will focus on preventing flutter, which occurs due to control surfaces oscillations only.

2.1.1 Control Surface Flutter

Flutter involving control surfaces occurs more frequently than classical wing bending/torsion flutter and usually results in the loss of control surfaces and/or part of the wing/tail structure (WRIGHT; COOPER, 2007). When control surfaces oscillate around its hinge line, forces are induced in the main surface (e.g. wing) where the control surface is attached. When coupling a main surface bending/torsion movement with a control surface oscillation, it may be possible to observe the flutter phenomenon.

Observing figure 2.1, control surface dynamics can be represented by the sum of the moments around the control surface hinge line:

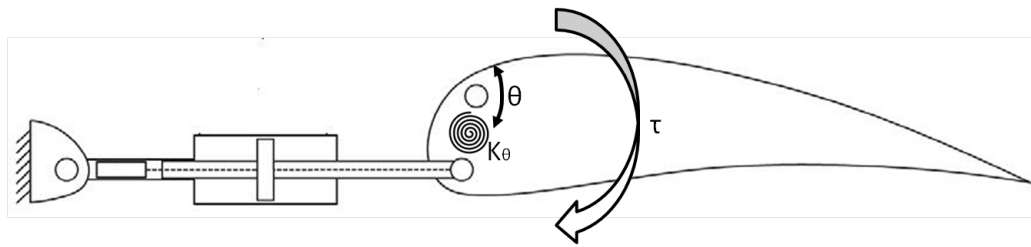


FIGURE 2.1 – Control Surface Dynamics

$$\sum \tau(t) = J\dot{\omega}(t) \quad (2.1)$$

$$\tau(t) - \tau_{reaction}(t) = J\dot{\omega}(t) \quad (2.2)$$

$$\tau(t) - \tau_{damping}(t) - \tau_{spring}(t) = J\dot{\omega}(t) \quad (2.3)$$

$$J\dot{\omega}(t) + c\omega(t) + K_\theta\theta(t) = \tau(t) \quad (2.4)$$

$$J\ddot{\theta}(t) + c\dot{\theta}(t) + K_\theta\theta(t) = \tau(t) \quad (2.5)$$

where θ is the control surface deflection, K_θ , the rotational stiffness and c , the rotational damping. The control surface inertia is represented by J and the rotational damping (c) is composed mainly by the damping originated by the hydraulic fluid in the actuator.

The control surface rotational stiffness term K_θ is composed by the control surface stiffness, the backup structure stiffness (wing or tail) and the actuator stiffness. The actuator stiffness can be divided in two components: one is due to the metallic parts

of the actuator K_{metal} , while the other is based on the hydraulic fluid properties, its operational temperature and pressure, K_{oil} .

The transfer function between applied moment (τ) and the control surface deflection (θ) can be obtained by applying the Laplace transform to the equation 2.5 :

$$\frac{\Theta(s)}{\tau(s)} = \frac{1}{Js^2 + cs + K_\theta} \quad (2.6)$$

The control surface dynamics, presented in equation 2.6, has a characteristic equation of a mass-spring-damper second order system with its undamped natural frequency given by:

$$\omega_n = \sqrt{\frac{K_\theta}{J}} \quad (2.7)$$

One common approach to prevent control surface flutter is to avoid coupling between the control surface rotational mode and the aircraft structure bending/torsion modes. Therefore, one possible solution is to set the control surface natural mode frequency ω_n greater than aircraft bending/torsion modes frequency (ω_f):

$$\omega_f < \omega_n \quad (2.8)$$

From equations 2.7 and 2.8, it is possible to conclude that during an actuation system design, if the control surface inertia J increases, the rotational stiffness shall increase to maintain the control surface natural mode decoupled from the aircraft structure aeroelastic modes.

In the aircraft design, when identified that flutter phenomenon may occur within the aircraft operational envelope, control surface mass balancing, rotational stiffness or rotational damping requirements are necessary to prevent flutter phenomenon.

For a pure mechanical flight control system, generally, mass balancing is the common solution, because control cables do not guarantee the required stiffness to avoid aeroelastic instabilities. In hydraulically powered actuation systems, the compliance with flutter suppression aeroelastic requirements is often guaranteed by the dynamic stiffness, or damping when it is not possible to guarantee the required dynamic stiffness by flight control actuators during full operational time, or even a combination of these two combined with partial mass balancing.

Each flutter suppression method intends to introduce in the control surface actuation system an element to avoid coupling between the control surface mode and the aircraft modes of vibration. In the following chapter, flutter suppression solutions will be discussed in more details.

2.2 Hydraulic Oil Compressibility - Bulk Modulus

The use of hydraulic power has several applications in different aircraft systems such as landing gear, flight control, thrust reverse and brake systems. The hydraulic system supplies other systems with hydraulic fluid, and depending on the choice of the hydraulic fluid, their performance may be influenced. The flight control system suffers major influence, since its flight control actuators are generally hydraulic powered.

While gases are highly compressible, liquids are of very low compressibility, but their compressibility must not be neglected as it affects the dynamic behavior of hydraulic actuation systems and its performance.

The compressibility of a fluid can be defined as its ability to change its volume when subjected to pressure variation. The relation between the fluid volume and pressure variations is known as bulk modulus and is presented in equation 2.9.

$$\beta = -\frac{\Delta P}{\Delta V/V} = -\frac{dP}{dV/V} \quad (2.9)$$

where: β is the Bulk Modulus of the fluid, ΔV is the change in fluid volume due to pressure variation, V is the initial fluid volume and ΔP is the pressure variation.

A high Bulk Modulus indicates low compressibility, fluid volume changes are relatively small and the fluid has high stiffness.

Being a thermodynamic quantity, the temperature variation during operation defines different Bulk Moduli: for constant temperature processes - Isothermal Bulk Modulus, for constant entropy processes - Adiabatic Bulk modulus.

Graphically, the Bulk Modulus can be defined as tangent Bulk Modulus or secant Bulk Modulus. Secant Bulk Modulus is graphically defined as the slope of the line connecting two pressures of pressure x volume curve (figure 2.2), while tangent Bulk Modulus is graphically defined as the tangent line at a point in the pressure x volume graph (figure 2.3).

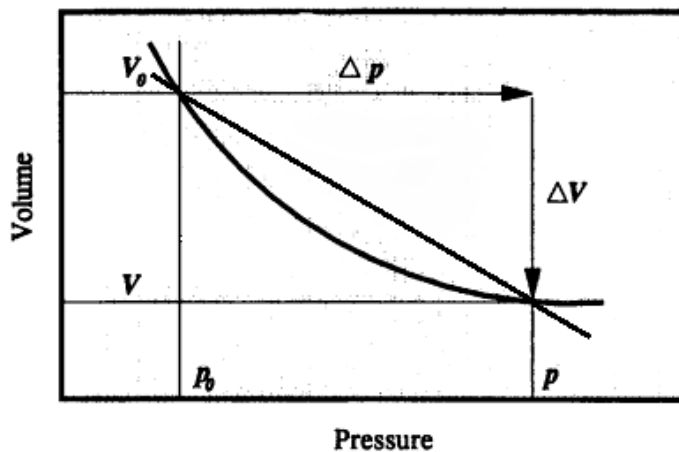


FIGURE 2.2 – Definition of Secant Bulk Modulus Source: (HODGES, 1996)

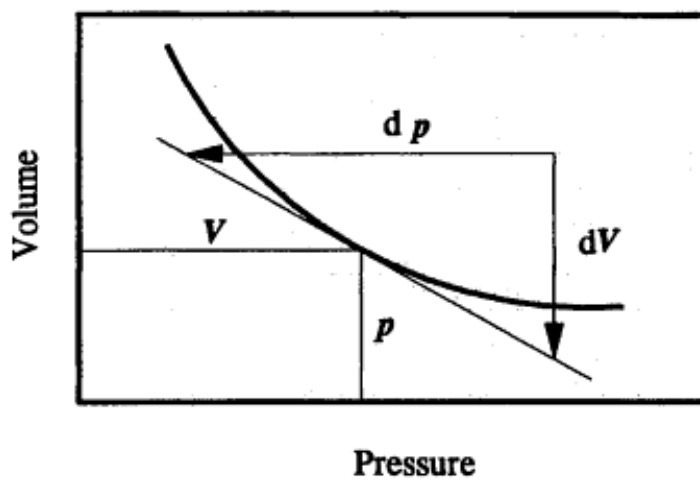


FIGURE 2.3 – Definition of Tangent Bulk Modulus Source: (HODGES, 1996)

According to (AIR1362B, 2008), the selection of the proper bulk modulus type for the hydraulic component design is based on the type of application and the pressure excursion magnitude being performed during its normal operation, as summarized on table 2.1.

TABLE 2.1 – SAE AIR1362 - Bulk Modulus type selection

Function	Pressure Excursion	Bulk Modulus	Application
Dynamic	Small	Adiabatic Tangent	Design of servo systems and actuators
Dynamic	Large	Adiabatic Tangent	Design of hydraulic pumps
Static	Small	Isothermal Tangent	Limited use in air vehicle system design
Dynamic	Large	Isothermal Secant	Limited use in air vehicle system design

For flight control hydraulic actuators design, as per table 2.1, the Bulk Modulus type to be used is the Adiabatic Tangent.

The Bulk Modulus can be interpreted as a measure of fluid compressibility and it is an important fluid property for system design, because it affects stability of hydraulic servo-controlled actuation systems, time response and the available force for limited stroke actuators.

The fluid pressure, temperature and the quantity of entrained air affect the bulk modulus of a hydraulic fluid.

The effects of pressure and temperature on the bulk modulus of typical mineral-based industrial hydraulic fluid are illustrated in figures 2.4 and 2.5. The bulk modulus decreases with a fluid temperature increase, and it increases with a fluid pressure increase.

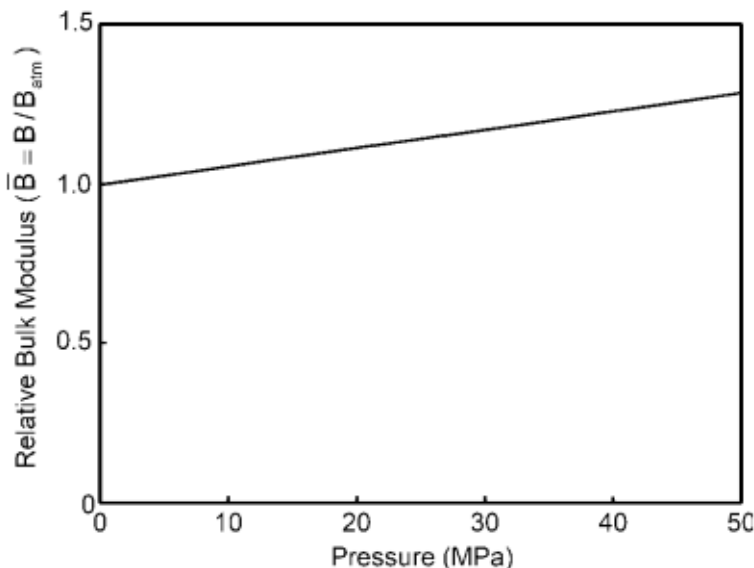


FIGURE 2.4 – Example of the effect of the pressure on the bulk modulus of a typical mineral based hydraulic fluid at constant temperature. Source: (RABIE, 2009)

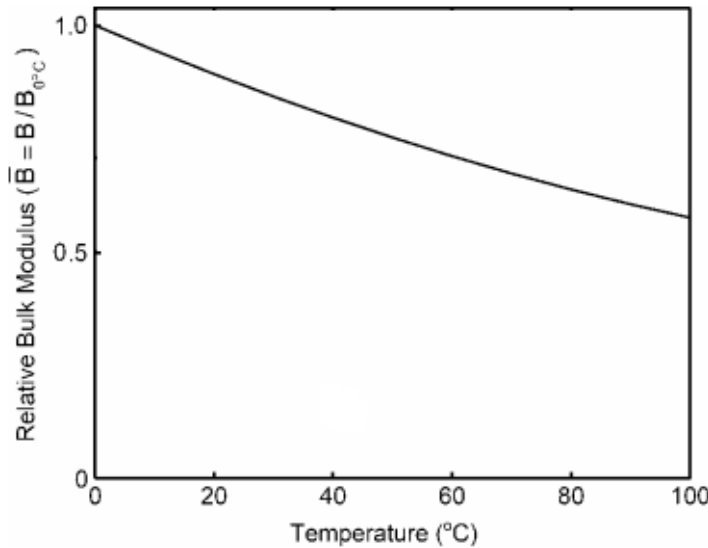


FIGURE 2.5 – Example of the effect of the temperature on the bulk modulus of a typical mineral based hydraulic fluid at constant pressure. Source: (RABIE, 2009)

Figure 2.6 shows the fluid bulk modulus variation with volume of entrained air. For low fluid pressures, small amounts of entrained air have a high influence on the fluid bulk modulus. As the fluid pressure increases, the entrained air effect is reduced.

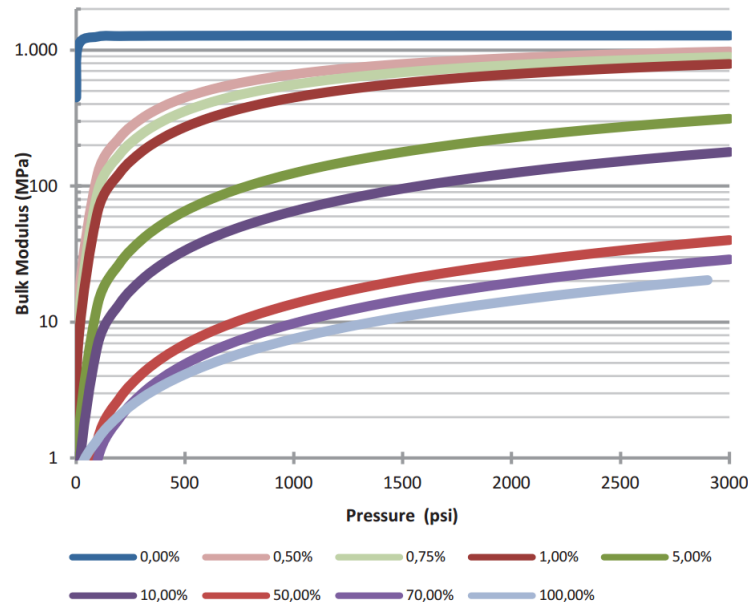


FIGURE 2.6 – Example of variation of the fluid effective bulk modulus with volume of entrapped air. Source: (CORTELLINE; GOES, 2010)

2.3 Rudder Actuation Control Systems

2.3.1 Flight Control Systems Overview

In the study of Flight Mechanics, it is common practice to assume the aircraft as a rigid body, defined by a coordinate system, as shown in figure 2.7. The rigid body dynamics have six degrees-of-freedom: three translations along X, Y and Z and three rotations (pitch, roll and yaw) about these axes. All forces and moments acting on the aircraft can be represented within this framework.

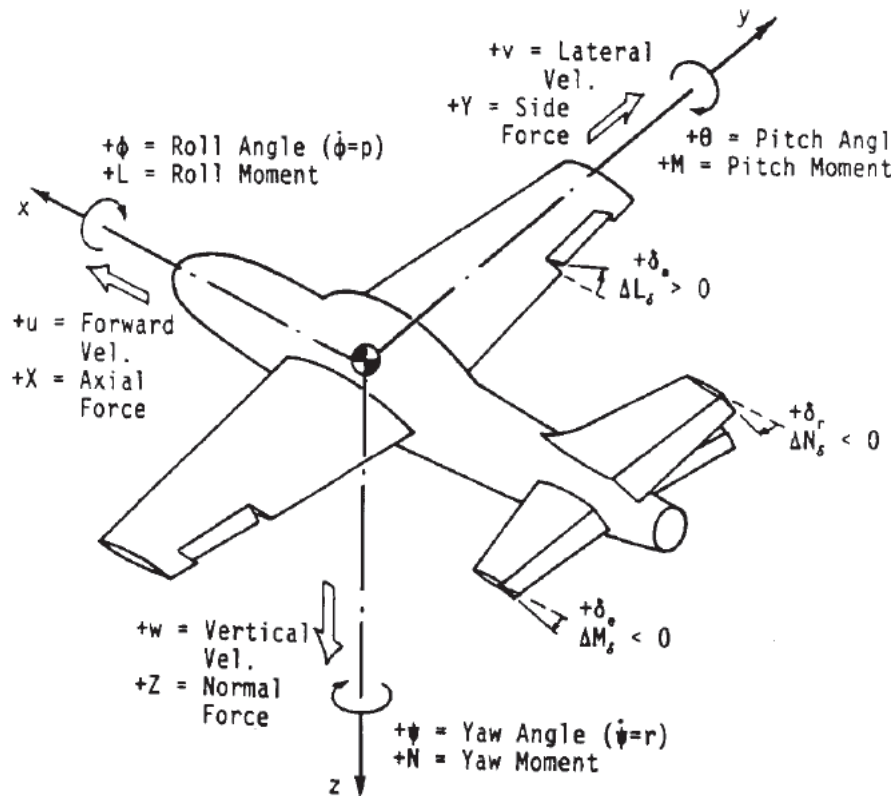


FIGURE 2.7 – Aircraft classical coordinate sign convention. Source: (SCHMIDT, 1998)

The main goal of a flight control system is to enable the pilot to exercise control over the aircraft during all portions of flight.

To achieve flight control, it is necessary to control the forces and moments acting on the vehicle, commanding aircraft's translational and rotational accelerations, and hence its velocities, attitude and position. The Flight Control System (FCS) provides this capability via control surfaces and/or thrusters. The FCS can perform primary functions, such as pitch, roll and yaw control and secondary functions, such as airbrake and high-lift. In the same way, according to their function, the control surfaces can be divided into two groups:

- i Primary surfaces: responsible for roll, pitch and yaw control. Generally, the surfaces encompassed are elevators, rudder, ailerons and spoilers (with rolling function aid).
- ii Secondary surfaces: responsible for flight control secondary functions (airbrake, high-lift). The surfaces encompassed are flaps, slats, horizontal stabilizer and trim tabs.

In this work, the focus will be on the primary functions since the aim is to study the rudder's actuation control system.

2.3.1.1 Conventional Flight Control Systems

In conventional Flight Control Systems, there is a mechanic connection between the pilot cockpit controls and the control surfaces, which are responsible for maneuvering the aircraft. A pilot input is transmitted by cables, pulleys, rods and chains to the control surface, guaranteeing a highly reliable system, easy to maintain and low cost. An example of a conventional FCS can be observed in figure 2.8.

Because, the feedback of aerodynamic forces on the control surfaces are transmitted directly to the pilot, this conventional FCS can be classified as a reversible flight control system.

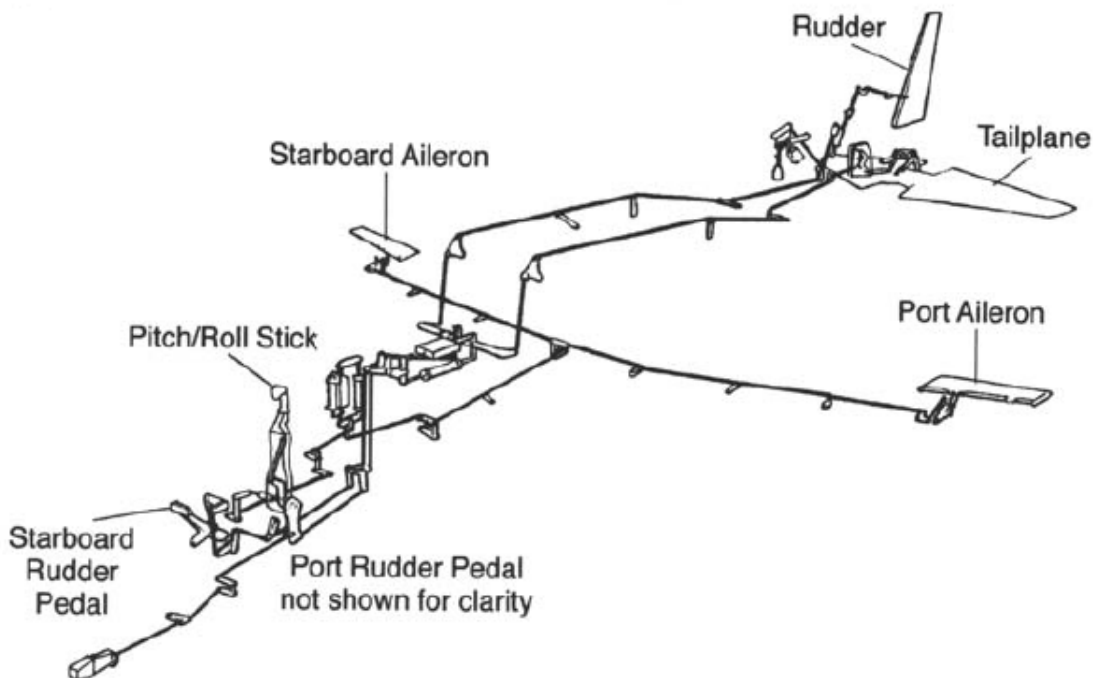


FIGURE 2.8 – Conventional mechanical flight control system. Source: (PRATT, 2000)

With aircraft evolution in size and speed, high loads on flight control surfaces were observed, and the force to move control surfaces against the aerodynamic forces grew, exceeding pilot physical capabilities. To overcome this limitation, hydraulic boosters

and/or hydraulic powered actuators were used to boost the pilot's effort to move the control surfaces. Nevertheless, conventional FCS became more complex, heavier, with more components, and expensive. A conventional hydraulic powered FCS example is shown in figure 2.9.

With the insertion of a hydraulic actuator in the system, the feedback of aerodynamic forces on the control surface are not transmitted directly to the pilot, this system is known as irreversible flight control system.

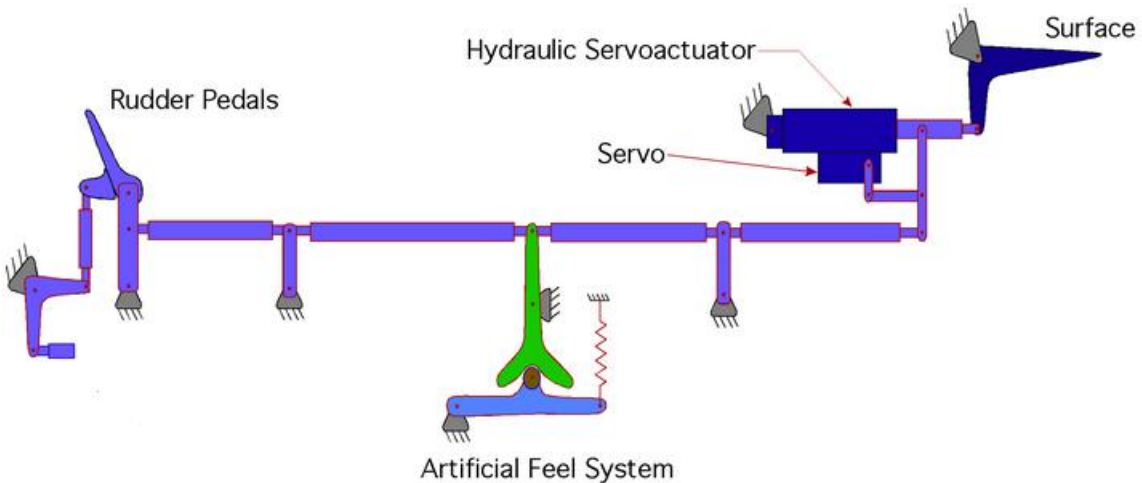


FIGURE 2.9 – Irreversible Flight Control System with hydraulic actuator Source: (DAEROSPACE, 2015)

2.3.1.2 Fly-by-wire Flight Control Systems

In fly-by-wire flight control systems, the mechanical link between the pilot input and the control surfaces are substituted by electrical signaling, therefore the name fly-by-wire. In this case, the pilot controls the aircraft motion and not the control surfaces angular position.

The pilot input are sent to a flight control electronics that generates commands to the aircraft flight control surfaces according to feedback received from aircraft sensors.

The cockpit controls translate pilot commands to electrical signals that are interpreted by the flight control system as aircraft attitude demands, which are translated into control surface position references based on flight control laws that take into account airspeed and other aircraft variables. Flight control surfaces reference positions are translated into actuator position commands and the actuator control loop sends a current command to the flight control actuator.

2.3.1.3 Flight Control Actuators

Hydraulic valves and filters, a hydraulic servo valve and a hydraulic actuator typically compose the flight control actuator for primary control surfaces. In modern flight control actuators, like the one shown in figure 2.10, the manifold and the piston are coupled being a single part number.



FIGURE 2.10 – F/A-18E/F Super Hornet rudder actuator. Source: (WOODWARD, 2015)

The servo valve has as main function to control the hydraulic flow into actuator's chambers. As it lets more flow to pass through one chamber, it forces the actuator piston to move and the actuator ram position will change. In figure 2.11, there is a hydraulic schematic of a typical flight control hydraulic actuator.

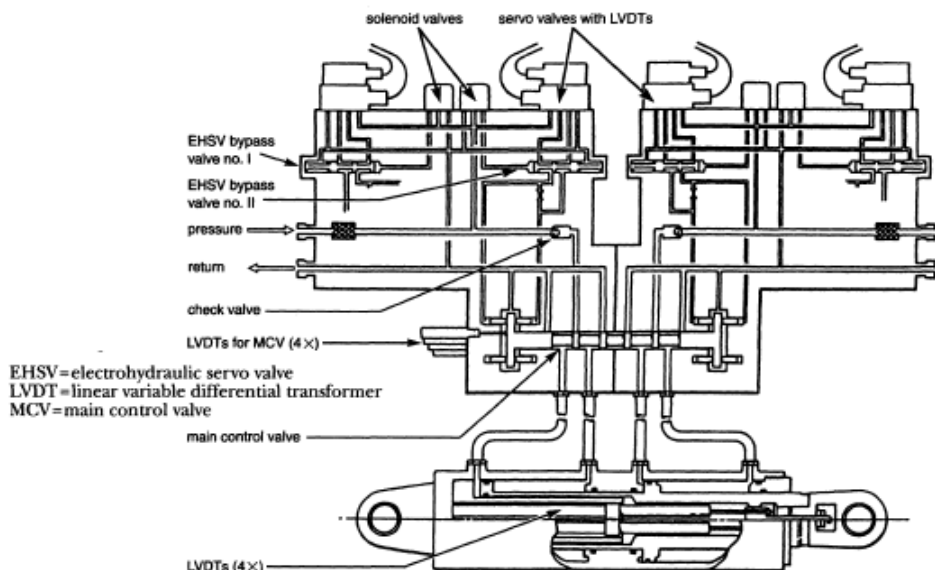


FIGURE 2.11 – Typical actuator using electrohydraulic servovalves - Dowty Aerospace. Source: (PRATT, 2000)

2.3.1.4 Hydraulic Actuator Dynamic Stiffness

From (PRATT, 2000), the ability of an actuator to resist an external oscillatory load is defined as dynamic stiffness, and it can be defined as the real part of the complex ratio between force and position (see equation 2.10), i.e. a measure of structural capability of a system to resist motion when submitted to an oscillatory force.

$$Z = K + jC \quad (2.10)$$

By installing the actuator in an adequate test rig, it is possible to measure dynamic stiffness characteristics. The test consists of applying a steady load to the actuator ram with an incremental oscillatory load at a range of frequencies and measuring the incremental ram displacement, relative to an inertial reference. The resulting ratio between the applied load and the ram displacement will be a complex number, its real part is known as dynamic stiffness and its imaginary part divided by the frequency is known as dynamic damping.

It is important that, during the test, the applied steady load shall be greater than the typical oscillatory load peak-to-peak amplitude to eliminate possible backlash that could influence the test. The steady load and oscillatory load values are determined by aeroelastic analysis. In this work, based on industry applications, the values adopted are 20% of the actuator's stall load for the steady load and 30% of the actuator's stall load for the peak-to-peak oscillatory load amplitude.

The hydraulic actuator must comply with dynamic stiffness and damping requirements to avoid control surface flutter. Those requirements can be translated into boundaries. Figure 2.12 shows typical boundaries based on aeronautic industry applications.

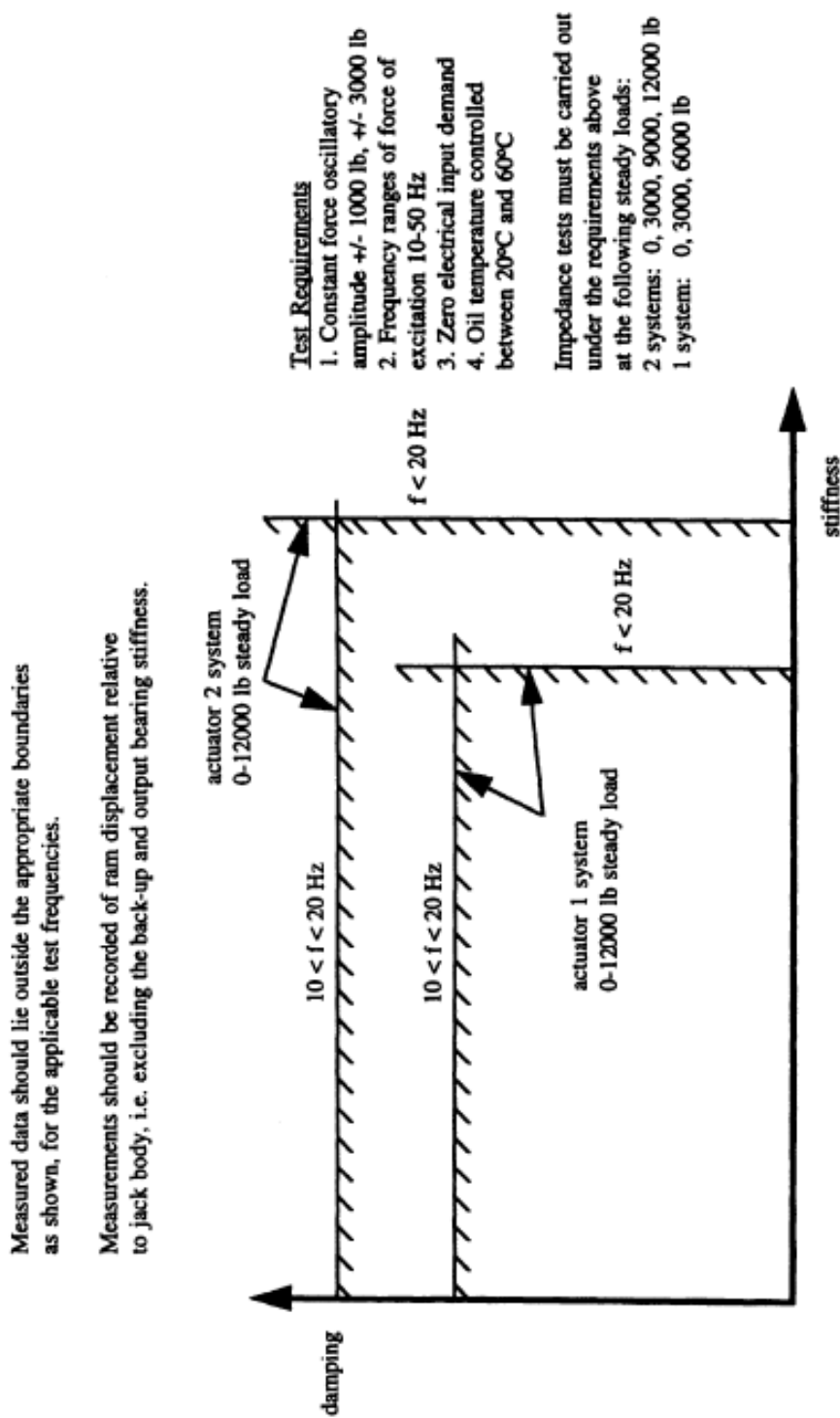


FIGURE 2.12 – Typical flight control actuator dynamic stiffness and damping boundaries.
Source:(PRATT, 2000)

At higher frequencies, due to the associated flutter criteria, the actuator system becomes critical as it contributes to provide stiffness to the control surface rotational mode to prevent flutter. Those margins must be met even if an actuation system failure occurs, e.g. hydraulic system failure, in those cases the actuator dynamic stiffness reduces, but it shall not fall below the required stiffness boundaries.

From (MERRITT, 1967), the transfer function of a hydromechanical position control servo is expressed by the block diagram below (figure 2.13), assuming a servovalve and piston combination with simple inertial load.

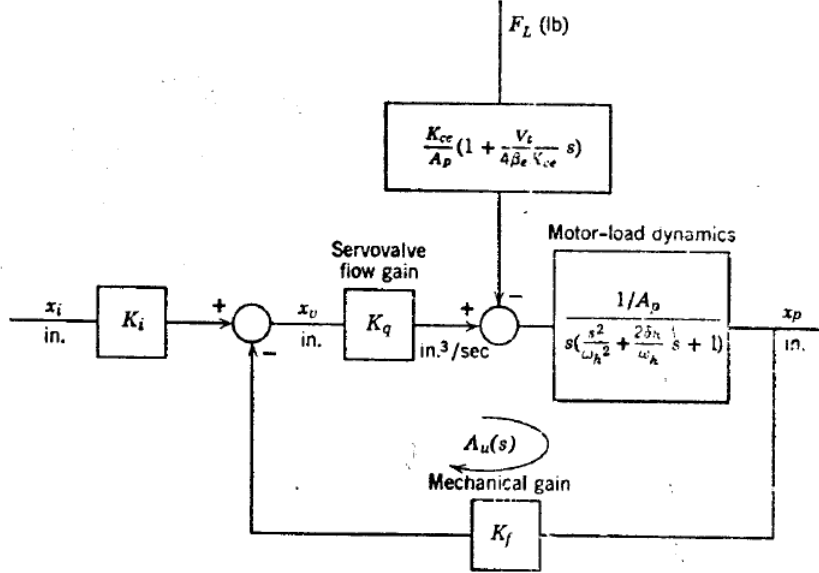


FIGURE 2.13 – Block diagram of hydromechanical position control servo.
Source:(MERRITT, 1967)

For this work, since its focus is on electro-hydraulic actuators, the piston position mechanical feedback (K_f) will be replaced by an electrical feedback (K_e), corresponding to the feedback gain of the piston position sensor. Also, the input gain will be considered as $K_i = 1$, since the piston command position will not be amplified. Therefore, the dynamic stiffness is obtained (MERRITT, 1967):

$$\frac{F_L}{x_p} = \frac{\left(\frac{s^3}{w_h^2} + s^2 \frac{2\delta_h}{w_h} + s + \frac{K_q K_e}{A_p} \right)}{\left(1 + s \frac{V_t}{4\beta_e K_{ce}} \right) \frac{K_{ce}}{A_p^2}} \quad (2.11)$$

where:

V_t : total volume of fluid under compression in both chambers;

M_t : total mass of piston and load referred to piston;

B_p : viscous damping coefficient of piston and load;

F_L : external load applied to the piston;

x_p : piston position;

A_p : piston area;

K_{ce} : total flow-pressure coefficient;

K_e : piston position sensor electrical feedback gain;

K_q : servovalve flow gain;

w_h : hydraulic natural frequency;

β_e : hydraulic fluid effective bulk modulus;

δ_h : hydraulic damping ratio.

As per (MERRITT, 1967), the hydraulic natural frequency and damping ratio are defined as:

$$w_h = \sqrt{\frac{4\beta_e A_p^2}{V_t M_t}} \quad (2.12)$$

$$\delta_h = \frac{K_{ce}}{A_p} \sqrt{\frac{\beta_e M_t}{V_t}} + \frac{B_p}{4A_p} \sqrt{\frac{V_t}{\beta_e M_t}} \quad (2.13)$$

To simplify equation 2.11, the cubic polynomial can be replaced by a linear and a quadratic factor:

$$\frac{F_L}{x_p} = \frac{-\frac{K_q K_e A_p}{K_{ce}} \left(\frac{s}{w_b} + 1 \right) \left(\frac{s^2}{w_{ne}^2} + \frac{2\delta_{ne}}{w_{ne}} s + 1 \right)}{\left(1 + s \frac{V_t}{4\beta_e K_{ce}} \right)} \quad (2.14)$$

where:

w_b : closed loop break frequency;

w_{ne} : closed loop natural frequency;

δ_{ne} : closed loop damping ratio.

For a closed loop position control hydraulic servo, w_b determines the position control servo bandwidth (MERRITT, 1967). Considering a low hydraulic damping ratio (δ_h) and

a low value for the ratio $K_q K_e A_p / w_h$, the following approximations can be assumed:

$$w_{ne} \approx w_h \quad (2.15)$$

$$w_b \approx K_q K_e A_p \quad (2.16)$$

$$2\delta_{ne} \approx 2\delta_h - \frac{K_q K_e A_p}{w_h} \quad (2.17)$$

It can be concluded that the servo actuator bandwidth is directly proportional to the flow gain coefficient (K_q), the piston area (A_p) and the electronic gain feedback (K_e). Thus, by increasing one of those factors, the servo actuator's bandwidth will increase.

From equation 2.14, the static gain of the transfer function can be obtained. Hence, the dynamic stiffness value for a step input is as follows:

$$\left. \frac{F_L}{x_p} \right|_{DCgain} = -\frac{K_q K_e A_p}{K_{ce}} \quad (2.18)$$

Thus, by increasing the actuator area it is possible to increase the dynamic stiffness for frequencies close to zero.

As the break frequencies (w_b and $\frac{4\beta_e K_{ce}}{V_t}$) are about the same value, their factor can effectively cancel, and the actuator minimal dynamic stiffness is obtained.

$$\left. \frac{F_L}{x_p} \right|_{min} = \frac{2\delta_{ne} K_q K_e A_p}{K_{ce}} \quad (2.19)$$

Therefore, by increasing the flow pressure coefficient (K_{ce}), the minimal dynamic stiffness of the system is reduced. Also, it can be observed that with a higher loop gain and for a bigger piston area, it is possible to increase the actuator minimal dynamic stiffness. Finally, the bulk modulus influence is identified by the presence of the δ_{ne} factor.

Using equations 2.12, 2.13, 2.17 and developing equation 2.19, it is obtained the minimal dynamic stiffness for a servo controlled linear hydraulic actuator:

$$\frac{F_L}{x_p}_{min} = K_q K_f \left(2\sqrt{\frac{\beta_e M_T}{V_T}} + \frac{B_p}{2K_{ce}} \sqrt{\frac{V_T}{\beta_e M_T}} \right) - \frac{K_q^2 K_f^2 A_p}{2K_{ce}} \sqrt{\frac{V_T M_T}{\beta_e}} \quad (2.20)$$

It can be concluded that the position control loop plays an important role in dynamic stiffness response. The hydraulic fluid bulk modulus and the actuator's piston area also have a large influence on dynamic stiffness.

3 Flight Control Actuator Design

According to (MERRITT, 1967), the term design is often associated with the analyses and engineering calculations necessary in the selection and sizing of hardware to create a component or a system.

This chapter is directed towards the design of an electro-hydraulic flight control actuator for primary control surfaces, and it aims to present its design process. The electro-hydraulic actuator design is an important part of the design of fly-by-wire systems.

The main objective in the following sections is to cover the design requirements and the actuator sizing specification. Materials and stress level will not be part of this approach.

3.1 Actuator Design Process

Typically, in the aeronautics industry, the flight control actuators design process starts with the control surface loads calculation. The maximum loads in the flight envelope, the limit loads, are the structures team input to size the control surface and the flight control team to size the structure of the electro-hydraulic actuator.

The aeronautics team is responsible to calculate the control surface operational hinge moments loads, which determine the minimum actuator output force.

Generally, the primary flight control surface actuator is attached to a fixed structure (wing, vertical or horizontal tail) and to a control surface, the movable structure. A representation of an actuator installation is presented in figure 3.1.

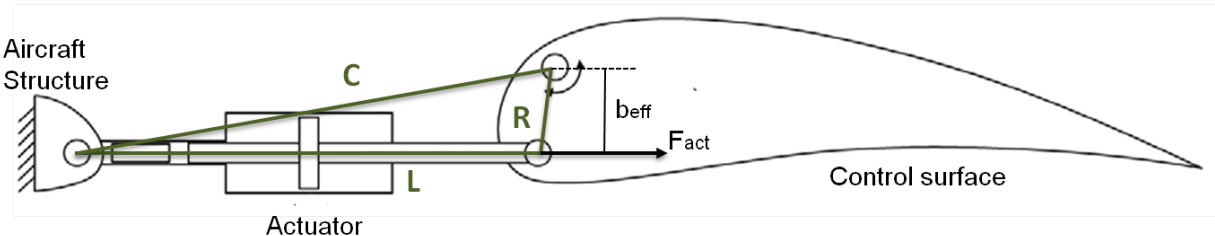


FIGURE 3.1 – Actuator installation and RLC triangle. Adapted from (CONSTANTINO, 2010)

The actuator installation determines an actuator kinematics, known as the RLC triangle. By convention, L is the actuator length, known as pin-to-pin distance, R is the horn radius and C is the distance between the anchorage point in the non-moveable surface and the anchorage point in the control surface, defining the RLC triangle, observed in figure 3.1.

Having the control surface loads and the actuator kinematics combined with the actuator performance requirements (exposed in next section), all the actuator design inputs are available and it is possible to obtain a first estimation of the actuator piston area.

Other important aspect to be considered in the design process is the actuator sealing choice. The (AS4716B, 2011) standard define the rod and piston elastomeric O-ring seals design criteria and dimensions for static and dynamic applications. The hydraulic flight control actuators shall be designed with dynamic sealing solutions. Figure 3.2 shows a balanced actuator and its components, including seals.

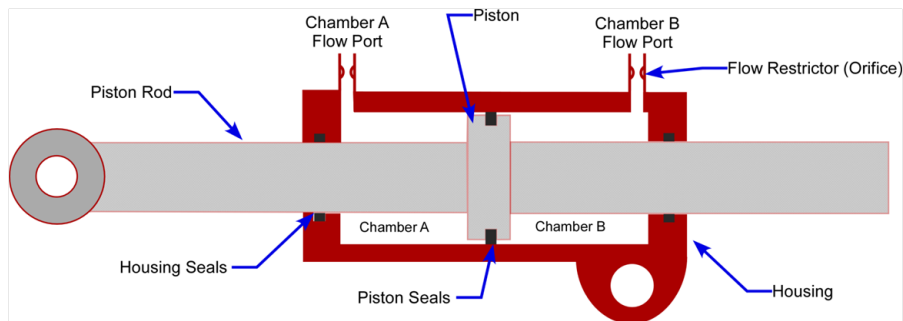


FIGURE 3.2 – Balanced hydraulic actuator, rod and piston seals. Source: (DAEROSPACE, 2015)

It is common practice in the aerospace industry to use standard seals dimensions (piston and rod seals) determining a final actuator area as close as possible to the estimated actuator piston area. The use of standard seals solutions is driven by maintainability and manufacturing costs aspects.

Figure 3.3 illustrates different aspects that influence the primary flight control actuator design.

3.2 Actuator Design Requirements

3.2.1 Flutter suppression requirements

The flight control designer needs to guarantee the compliance of the actuation system with aeroelastic stability requirements defined in the FAA Part 25 for transport category airplanes, exposed in annex A.

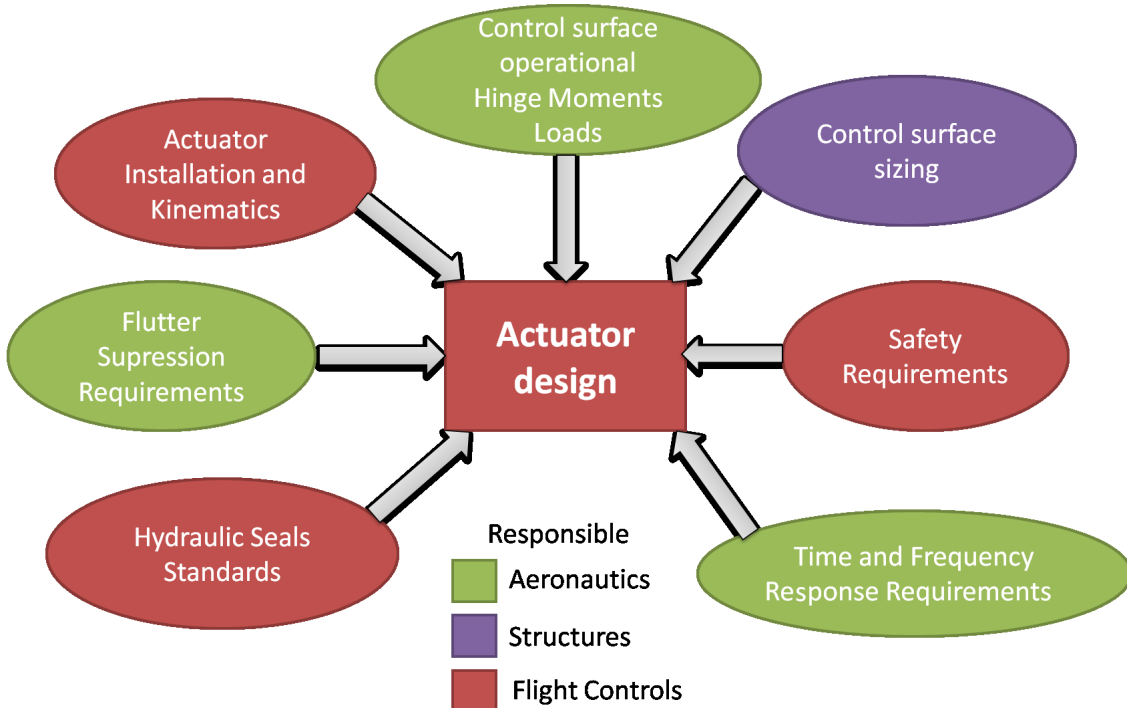


FIGURE 3.3 – Complete Primary Flight Control Actuator Design Process

Observing the regulation for flutter suppression in Annex A, it states that “the airplane must be designed to be free from aeroelastic instability for all configurations and design condition”. Since the flutter phenomenon is an aeroelastic dynamic instability, the aircraft must be designed to be flutter free.

In summary, to comply with flutter suppression requirements, the primary actuation system must guarantee that the control surface rotational mode does not couple with other aircraft structural modes.

The MIL-A-8870C is a military specification containing design requirements and criteria for the design and construction of aircraft to prevent flutter and other aeroelastic instabilities. This military specification states that the airplane shall be free from any aeroelastic instability in its entire flight envelope, as we observe in the following paragraph:

3.1.1 Aeroelastic stability.

All configurations of the airplane shall be free from any aeroelastic instability for all combinations of altitude and speed encompassed by the limit speed (V_L/M_L) versus altitude envelope enlarged at all points by the airspeed margin of safety. The airplane shall meet the following stability design requirements for both-normal and failure conditions:

- Airspeed margin: The equivalent airspeed, W_e , margin of safety shall be not less than 15 percent at all points on the V_L/M_L envelope of the airplane, both at constant Mach number, M, and separately, at constant altitude, (see Figure 3.4).

- b. Damping: The total (aerodynamic plus structural) damping coefficient, g , shall be not less than 3 percent ($g=0.03$) for any critical flutter mode for all altitudes and flight speeds from minimum cruising speeds up to V_L/M_L , (see Figure 3.5).

Also according to the MIL-A-8870C, “the interaction of the flight control system and the airplane structural modes shall be controlled to prevent any aeroservoelastic instability”. The aeroservoelastic stability “shall be met in all operational states of the flight control system (such as normal and failure states, degraded modes, and augmentation system on and off, if off is a design condition), and for the range of operating temperatures of the flight control system”. Figures 3.4 and 3.5 are extracted from MIL-A-8870C and illustrate the typical curves used in flutter suppression requirements definition.

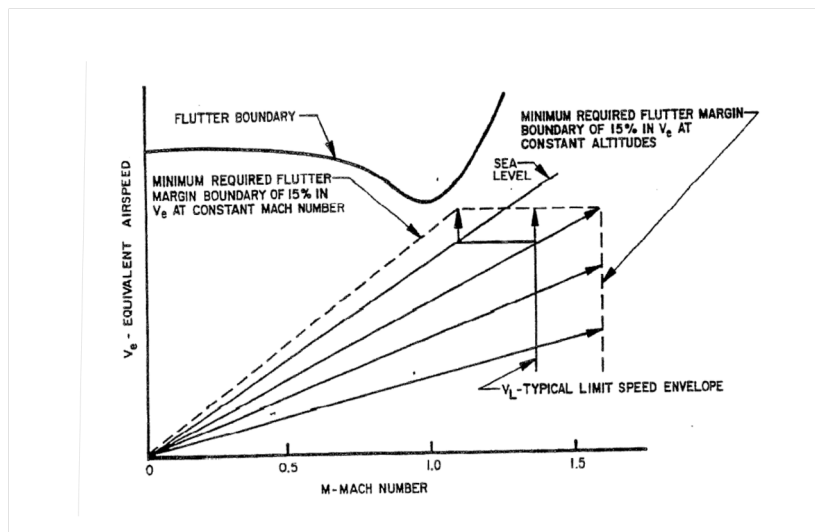


FIGURE 3.4 – Flutter requirements - airspeed margin. Source: (MIL-A-8870C, 1993)

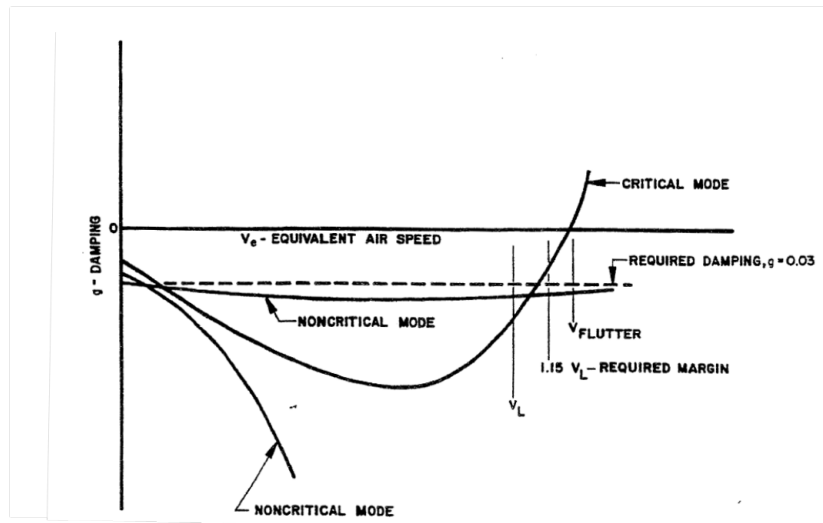


FIGURE 3.5 – Flutter requirements - damping coefficient. Source: (MIL-A-8870C, 1993)

The military specification MIL-A-8870C also approaches flutter analyses and actuator stiffness tests that should be met to prevent flutter phenomena.

3.2.1.1 Flutter Suppression Solutions

To comply with flutter suppression requirements the aeronautics industry usually adopts two well-known solutions:

1- Control surface mass balancing

This solution is based on changing the control surface mass distribution observed by the control surface hinge line. Changing the control surface static unbalancing moment (S.U.M.) accordingly will allow the decoupling between control surface rotational modes and the aircraft structural modes.

The change in the control surface vibration modes is made by adding mass to the control surface. It is possible to conclude that this solution has an undesirable consequence to aircraft design, as it increases control surface weight, harming aircraft's overall performance.

For purely mechanical flight control systems, control surface mass balance is the only possible solution to comply with flutter suppression requirements.

2- Dynamic stiffness and/or dynamic damping provided by the flight control actuator

This is the most common solution for hydraulically powered control surfaces. In this approach, the electro-hydraulic actuator is designed to guarantee a minimal dynamic stiffness and/or damping to comply with aeroelastic instability requirements.

As oscillatory external loads perturb the control surface, the actuation system damping and stiffness prevents the system vibration modes to approximate the flutter frequencies that may lead to catastrophic failures.

Even if an actuator loses its hydraulic source, in an active-active configuration, the actuation system must guarantee flutter suppression capability, as it is shown in the safety requirements section.

Generally, this solution leads to an increase in the actuator's piston area, increasing the hydraulic consumption, the actuator final volume and adding weight to the aircraft.

The actuator design based on this solution is presented in section 3.3.

This work will focus on the flutter suppression solution based on the actuator's dynamic stiffness.

3.2.2 Safety requirements

The control surface actuation system must guarantee the compliance with safety requirements based on the FAA Part 25 for transport category airplane. From those requirements, the actuation system must be designed to be free of assembly error, and it must guarantee a safe flight and landing after failures or jamming in the flight control surface.

Focusing in the analysis of one of the most important safety requirement, FAR 25.671 (exposed in Annex A):

25.671

- (c) The airplane must be shown by analysis, tests, or both, to be capable of continued safe flight and landing after any ...
 - (1) Any single failure
 - (2) Any combination of failures not shown to be extremely improbable ... or any single failure in combination with any probable failure

Analyzing 25.671(c)(1) and 25.671(c)(2) an aircraft, which adopts a flutter suppression solution based on the flight control actuator characteristics, needs to guarantee that the flutter suppression solution is still present after a single failure or a combination of not extremely improbable failures.

A single failure (25.671(c)(1)) is commonly a mechanical disconnection of the actuator from the movable control surface. This fact forces that even with only one active actuator, the control surface actuation system must guarantee the flutter suppression requirement. As it will be shown later in the text, the design to meet this requirement is done by a selection of an ensemble (actuator, control surface and fixed surface stiffness).

The 25.671(c)(2) approaches the combination of not extremely improbable failures, leading into two cases. In the first case (combination of any probable failures), the failures can be interpreted as a dual aircraft hydraulic system failure, or a dual electrical failure, or a hydraulic system with an electrical failure. In this failure scenario, the flight control solution for flutter suppression is similar to the one that will be presented in the next paragraph for the second failure case.

In the second case (combination of any single failure with any probable failure), the single failure is commonly the mechanical disconnection explained before and the probable failure typically is an aircraft hydraulic system loss. In this failure scenario, the flight control actuator does not have itself conditions to maintain a required stiffness for flutter suppression. Therefore, a spring pre-loaded valve is introduced in the actuation system. The spring pre-loaded valve is commanded by any hydraulic pressure variation, and when the pressure drops below a minimum value, the valve redirects the actuator's hydraulic

circuit connecting the extension and retraction chambers by an orifice that restricts the hydraulic flow. The presence of this orifice will cause a dynamic friction in the hydraulic flow resulting in a damping force ($F = -bV$) that will damp the actuation ensemble (control surface, actuator, fixed surface) movement, providing a backup flutter suppression solution that is based on damping in case of mechanical disconnection and a hydraulic system loss.

Another solution that comply with safety requirements and guarantees the flutter suppression functionality is the adoption of three actuator per surface powered by three different hydraulic sources. In this case, 25.671(c)(1) and 25.671(c)(2) are covered using only dynamic stiffness and the damping requirement is no longer necessary.

3.2.3 Actuator control loop requirements

For this work, as mentioned in chapter 2, the primary surface actuation system will be based on the rudder control surface. In recent flight control systems applications, the actuator is commanded by a closed control loop that must guarantee performance compliance in time and frequency domains. The flight mechanics group defines those performance requirements in order to guarantee a desired aircraft performance and handling qualities. In the following paragraphs, typical time and frequency domain's performance requirements for a rudder actuation system of a fly-by-wire aircraft are presented in the following sections (PRATT, 2000).

3.2.3.1 Time domain requirements

For a step input command, the actuator position control must guarantee:

1. Settling time $t_{ss} < 850\text{ms}$;
2. Steady state error $< 1\%$ of actuator full stroke;
3. Overshoot $< 10\%$ of actuator full stroke;
4. Average rate $> 32^\circ/\text{s}$;
5. Maximum rate $< 36^\circ/\text{s}$.

where the settling time t_{ss} is defined as the time for the response to reach and remain inside $\pm 2\%$ of its steady-state value y_s , or it is the smallest t_{ss} such that $|y(t) - y_s| \leq 0.02y_s$. The average rate is defined as the angular travel divided by the travel time between 15% and 85% of the steady-state value (y_s).

The rudder actuation system should be tested under the following conditions:

- a) Active-Disconnected configuration;
- b) Initial position = 0° ;
- c) Step amplitude = 30° ;
- d) Opposing hinge moment load varying linearly from 0 N.m to 3050 N.m;
- e) Maximum hydraulic supply pressure of 3000 psi;
- f) Maximum hydraulic return pressure of 150 psi;
- g) At $-40^\circ C$ ($-40^\circ F$) ambient temperature;
- h) At $-15^\circ C$ ($5^\circ F$) fluid temperature;

3.2.3.2 Frequency domain requirements

The stability margins of the rudder actuator's control loop must be:

- i Gain margin: at least 10.0 dB
- ii Phase margin: at least 45°

For the following conditions:

- a) active-disconnected configuration;
- b) measured from the surface angular position command in degrees provided at the actuator controller digital input to the Actuator Ram Position Feedback converted to surface angular position in degrees;
- c) for commands amplitudes of $+/- 0.5^\circ$;
- d) without the presence of aerodynamic load and backlash;
- e) for an actuator within nominal tolerances.

3.3 Flight Control Actuator design

A typical actuator/control surface system is represented in the figure 3.6, considering the control surface subjected to aerodynamic forces, the actuator will observe these loads and the surface inertia in its axis.

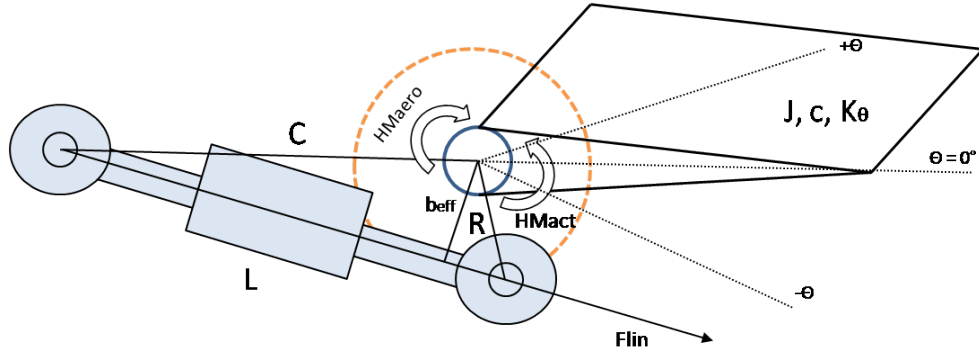


FIGURE 3.6 – Primary Flight Control Actuator and surface.

In figure 3.6:

R: the actuation radius, known as the horn radius, i.e., the distance between the hinge line and anchorage point of the actuator in the control surface;

L: the length of the actuator in the neutral position;

C: distance between the anchorage point in the non-movable surface and the anchorage point in the control surface;

b_{eff} : distance between the hinge point of the control surface and the actuator axial force, known as the effective arm;

J: control surface moment of inertia around the hinge line;

K_θ : rotational stiffness observed by the control surface;

c: viscous damping observed by the control surface;

$H M_{aero}$: aerodynamic hinge moment;

F_{lin} : forces in the actuator axis;

$H M_{act}$: hinge moment due to actuator output force.

3.3.1 Actuator Stall Load Requirement

The moment generated by the actuator observed by the control surface around the hinge line ($H M_{act}$) must be equal or greater than the maximum operational aerodynamic hinge moment $H M_{aero}$. This moment restriction, together with the RLC triangle, determines the actuator force (F_{act}) required to generate such actuator moment in the control surface.

Based on this information, it is possible, with equations 3.1, 3.2 and 3.3, to determine the required hydraulic actuator area ($A_{act,load}$).

$$F_{act} = \Delta P A_{act} \quad (3.1)$$

$$HM_{act} = F_{act} b_{eff} \geq HM_{aero} \quad (3.2)$$

$$A_{act} \geq \frac{HM_{aero}}{Pb_{eff}} \quad (3.3)$$

where:

ΔP - the differential pressure between the hydraulic actuator chambers

b_{eff} - the actuator effective arm

3.3.2 Actuation System Rotational Stiffness Requirement

Another criterion for a flight control hydraulic actuator sizing is to ensure a certain dynamic stiffness that would comply with flutter suppression requirements.

The hydraulic actuator should be designed to meet both linear (K_{lin}) and rotational (K_θ) stiffness requirements.

In the equilibrium condition, the aerodynamic hinge moment (HM_{aero}) is equal to the moment generated by the actuator (HM_{act}):

$$HM_{aero} = HM_{act} \quad (3.4)$$

where:

$$HM_{act} = F_{lin} b_{eff} \quad (3.5)$$

$$HM_{aero} = F_{lin} b_{eff} \quad (3.6)$$

From Hooke's law, the rotational stiffness and linear stiffness can be defined by equations 3.7 and 3.8, respectively:

$$K_\theta = \frac{HM_{aero}}{\theta} \quad (3.7)$$

$$K_{lin} = \frac{F_{lin}}{\Delta L} \quad (3.8)$$

where ΔL is the actuator's cylinder linear displacement and θ is the control surface angular position.

Replacing equations 3.7 and 3.8 into equation 3.6, we can observe the relation between rotational stiffness, linear stiffness and the effective arm (b_{eff}):

$$K_\theta = \frac{K_{lin}\Delta L b_{eff}}{\theta} \quad (3.9)$$

For small deflections, it is possible to consider $\Delta L = b_{eff}\theta$, and, in this case, the ratio between rotational and linear stiffness is equal to the effective arm squared:

$$\frac{K_\theta}{K_{lin}} = b_{eff}^2 \quad (3.10)$$

The control surface dynamics is represented by equation 3.11 and was obtained by the sum of the moments around the hinge line, as shown in chapter 2.

$$J\ddot{\theta}(t) + c\dot{\theta}(t) + K_\theta\theta(t) = \tau(t) \quad (3.11)$$

Applying Laplace transformation:

$$\frac{\Theta(s)}{\tau(s)} = \frac{\frac{1}{J}}{s^2 + \frac{c}{J}s + \frac{K_\theta}{J}} \quad (3.12)$$

Comparing the transfer function denominator with a second order characteristic equation ($s^2 + 2\xi\omega_n + \omega_n^2$) we have:

$$\omega_n^2 = \frac{K_\theta}{J} \quad (3.13)$$

$$2\xi\omega_n = \frac{c}{J} \quad (3.14)$$

The control surface actuation system must generate a moment that balances the control surface operational aerodynamic hinge moments and must resist to external oscillatory loads, based on the need to avoid control surface flutter.

The flutter occurrence is associated with high frequency oscillations and the actuation system rotational stiffness must suppress flutter phenomenon up to a certain frequency $f_{flutter}$, known as infinite stiffness frequency.

Thus solving equation 3.13 for K_θ , the primary control surface actuation rotational stiffness required to prevent flutter in a specific frequency ($f_{flutter}$) is defined as:

$$K_{\theta_{flutter}} = J(2\pi f_{flutter})^2 \quad (3.15)$$

3.3.3 Actuator Stiffness required for flutter suppression

The dynamic stiffness observed by the control surface is composed by the actuator stiffness (K_{act}), the control surface stiffness (K_L) and the anchorage surface stiffness (K_r), as seen in figure 3.7.

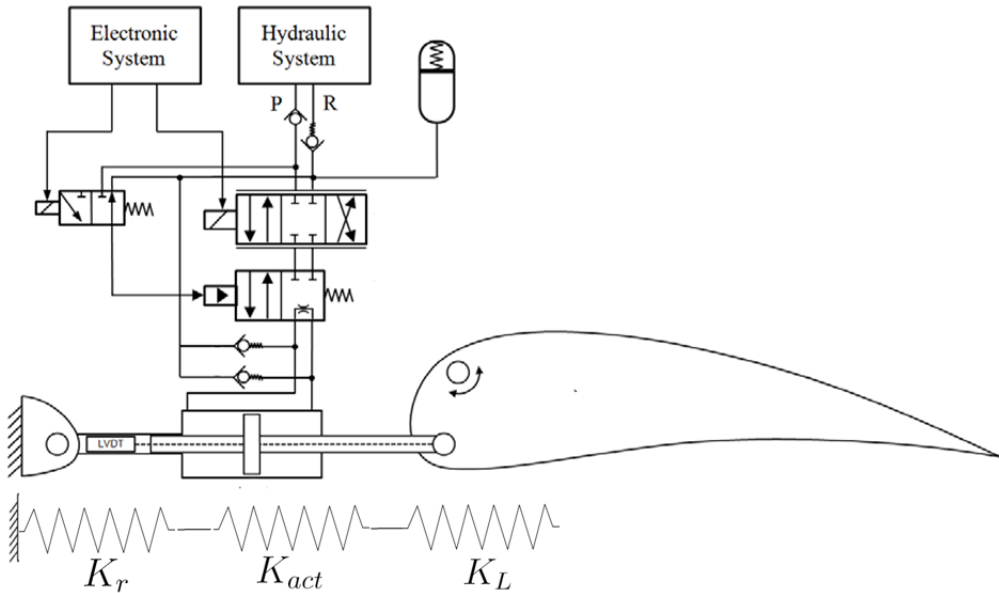


FIGURE 3.7 – Flight Control Actuator, Surface - stiffness components - adapted from (CONSTANTINO, 2010)

The equivalent linear dynamic stiffness (K_{lin}) is defined as:

$$\frac{1}{K_{lin}} = \frac{1}{K_r} + \frac{1}{K_L} + \frac{1}{K_{act}} \quad (3.16)$$

The structural stiffness K_{str} is defined:

$$\frac{1}{K_{str}} = \frac{1}{K_r} + \frac{1}{K_L} \quad (3.17)$$

As can be observed, the actuator (K_{act}) and structural stiffness (K_{str}) compose the equivalent linear dynamic stiffness (K_{lin}). To meet flutter suppression requirements, the actuation system must guarantee that the control surface linear stiffness K_{lin} is equal to

or greater than the equivalent control surface rotational stiffness transformed into a linear stiffness ($K_{\theta_{flutter_{lin}}}$) at the frequency $f_{flutter}$:

$$K_{lin} \geq K_{\theta_{flutter_{lin}}} \quad (3.18)$$

From equation 3.15:

$$K_{lin} \geq \frac{J(2\pi f_{flutter})^2}{b_{eff}^2} \quad (3.19)$$

Therefore, from equations 3.16 and 3.19, the required actuator stiffness for flutter suppression ($K_{act_{flutter}}$) is:

$$K_{act_{flutter}} >= \frac{1}{\frac{b_{eff}^2}{J(2\pi f_{flutter})^2} - \frac{1}{K_{str}}} \quad (3.20)$$

In addition, the actuator stiffness K_{act} is composed by the hydraulic fluid stiffness (K_{oil}) and the metallic stiffness K_{metal} , as shown in equation 3.21.

$$\frac{1}{K_{act}} = \frac{1}{K_{oil}} + \frac{1}{K_{metal}} \quad (3.21)$$

3.3.3.1 Actuator Oil Column Stiffness

The figure 3.8 represents an unbalanced piston with chamber areas A_1 and A_2 , Δx represents the piston displacement and S is the actuator stroke.

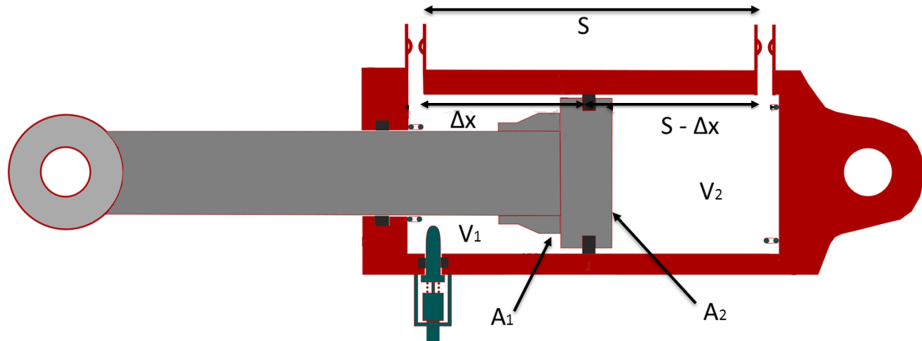


FIGURE 3.8 – Unbalanced piston - oil column stiffness. Adapted from: (DAEROSPACE, 2015)

The oil column stiffness (K_{oil}) is obtained in a similar way as the stiffness of a material with a Young modulus, where the stiffness is proportional to the area and inversely

proportional to the oil column length and the elasticity modulus is replaced by the fluid Bulk Modulus (β_{mod}):

$$K_{oil} = \beta_{mod} \left(\frac{A_1}{\Delta x} + \frac{A_2}{S - \Delta x} \right) \quad (3.22)$$

For a hydraulic actuator with balanced piston, the actuator chambers have equal areas $A_1 = A_2 = A$, replacing it in equation 3.22.

$$K_{oil} = \beta_{mod} \left(\frac{A}{\Delta x} + \frac{A}{S - \Delta x} \right) \quad (3.23)$$

The position δx where the oil column stiffness is minimum is obtained by using some basic calculus tools. With the first derivative of K_{oil} in relation to Δx , a critical point is found and if the second derivative, at this point, is positive, the critical point is a local minimum:

$$\frac{dK_{oil}}{d\Delta x} = \frac{A}{\Delta x^2} - \frac{A}{(S - \Delta x)^2} = 0 \quad (3.24)$$

$$\Delta x^2 = S^2 - 2S\Delta x + \Delta x^2 \quad (3.25)$$

$$\Delta x = \frac{S}{2} \quad (3.26)$$

$$\frac{d^2 K_{oil}}{d\Delta x^2} = \frac{A}{\Delta x^2} + \frac{A}{(S - \Delta x)^2} \quad (3.27)$$

Since the actuator area A and stroke S are both positively defined, substituting 3.26 in 3.27 yields:

$$\frac{d^2 K_{oil}}{d\Delta x^2} \Big|_{\Delta x = \frac{S}{2}} = \frac{10A}{S^2} > 0 \quad (3.28)$$

Thus, $\frac{S}{2}$ is a local minimum.

As conclusion, when the piston is at the half-stroke of a balanced actuator stroke S , called neutral position, the actuator's oil column stiffness is a minimum.

$$K_{oil@neutral} = \frac{4\beta_{mod}A}{S} \quad (3.29)$$

3.3.3.2 Actuator Metallic Part Stiffness

The actuator metallic part stiffness (K_{metal}) is 3 to 10 times greater than the column oil stiffness, depending on the actuator design and materials applied. Because of those values, it is not possible to neglect the K_{metal} in our work, thus a ratio between the column oil and actuator metallic part is defined as:

$$\frac{K_{metal}}{K_{oil}} = \lambda \quad (3.30)$$

3.3.3.3 Actuator Total Stiffness

From equations 3.21 and 3.30, the actuator stiffness (K_{act}) is

$$K_{act} = \frac{\lambda K_{oil}}{\lambda + 1} \quad (3.31)$$

From equations 3.29 and 3.31, conservative estimation for balanced actuator stiffness is obtained:

$$K_{act} = \frac{4\beta_{mod}A_{act}\lambda}{S(\lambda + 1)} \quad (3.32)$$

The actuator must be designed to have a K_{act} equal or greater than $K_{act_{flutter}}$:

$$K_{act} \geq K_{act_{flutter}} \quad (3.33)$$

Therefore, the required actuator area to meet flutter requirements is:

$$A_{act_{flutter}} \geq \frac{K_{act_{flutter}} S(\lambda + 1)}{4\beta_{mod}\lambda} \quad (3.34)$$

3.3.4 Actuator Stroke Estimation

The actuator stroke S is defined as:

$$S = L_e - L_r \quad (3.35)$$

where L_e is the actuator length in its extended position and L_r is the actuator length in its retracted position. Those positions are defined by the rudder's nominal surface deflection:

- i 30° trailing edge left, defining L_e ;
- ii 30° trailing edge right, defining L_e .

To calculate L_e and L_r , it will be used the law of cosines and sines, and the actuator installation kinematics defined by the RLC triangle. First, the actuator length (L) in its neutral position is used to obtain the angles α and β , as can be seen in figure 3.9.

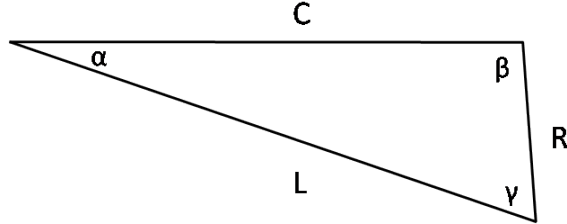


FIGURE 3.9 – Actuator in neutral position - RLC triangle

Using the law of cosines, it can be obtained α and β :

$$R^2 = C^2 + L^2 - 2CL \cos(\alpha) \quad (3.36)$$

$$L^2 = R^2 + C^2 - 2RC \cos(\beta) \quad (3.37)$$

Representing the actuator extended position (L_e) in figure 3.10 and applying the law of sines (3.38), L_e is easily found.

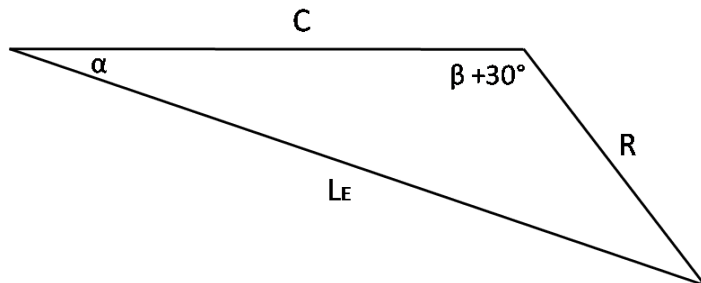


FIGURE 3.10 – Actuator in extended position - RLC triangle

$$\frac{L_e}{\sin(\beta + 30^\circ)} = \frac{R}{\sin(\alpha)} \quad (3.38)$$

Using the same methodology for the actuator retracted position, figure 3.11, L_r is obtained:

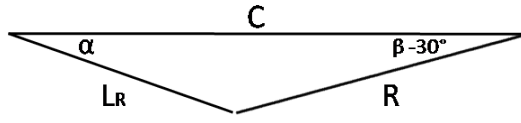


FIGURE 3.11 – Actuator in retracted position - RLC triangle

$$\frac{L_r}{\sin(\beta - 30^\circ)} = \frac{R}{\sin(\alpha)} \quad (3.39)$$

Having L_e and L_r , the actuator stroke S is obtained using equation 3.35.

3.4 Rudder flight control actuator design

This work will approach the design of a rudder actuation system of a fly-by-wire flight control system. In this section, it is aimed to present systematically the actuator design to guarantee compliance with the requirements presented previously.

First of all, the flight controls team together with the structure team define the actuator kinematics due to its installation in the aircraft, this data is presented in table 3.1.

TABLE 3.1 – Rudder Actuator Kinematics

Rudder Actuator Installation Kinematics	
R (mm)	173
L (mm)	505
C (mm)	529.7

Based on previous sections, having the actuator kinematics it is possible to obtain the RLC triangle angles (α , β and γ), the actuator extracted and retracted length (L_e and L_r) and the actuator stroke (S), as presented in table 3.2.

TABLE 3.2 – Rudder Actuator Design Results

Actuator Kinematics Design Results	
α (°)	19.06
β (°)	72.38
γ (°)	88.57
L_e (mm)	591.43
L_r (mm)	418.48
S (mm)	172.95

The structure team also provides to the actuator designer the control surface inertia (J) and stiffness (K_L), the backup structure stiffness (K_r). The aeroservoelasticity team provides the frequency of flutter ($f_{flutter}$) that the actuation system must protect and hydraulics team the hydraulic fluid equivalent bulk modulus (β_{mod}) as presented in table 3.3.

TABLE 3.3 – Rudder Actuation System Design Characteristics

Actuation System Characteristics	
J ($kg \cdot m^2$)	34
K_r (N/m)	$1.02 \cdot 10^8$
K_L (N/m)	$3.00 \cdot 10^7$
$f_{flutter}$ (Hz)	15
B_{mod} (ksi)	150

Having the kinematics and structure data along with the previously presented design requirements is possible to begin the rudder's actuator design.

3.4.1 Stall load compliance design

From the time domain requirement presented in section 3.2, it can be concluded that the actuator shall perform with an opposing hinge moment load of 3050 N.m, e.g., the actuator shall provide a hinge moment to the surface that must be equal or greater than the maximum control surface operational hinge moment load.

Therefore, considering that the hydraulic system provides a maximum pressure difference (δP) between actuator chambers of 2850 psi and equations 3.1, 3.2 and 3.3, the actuator area to meet time domain requirements must be:

$$A_{act_load} \geq 1.630 \text{ in}^2 \quad (3.40)$$

3.4.2 Flutter suppression compliance design

Based on the presented data in table 3.3 and in the equation 3.20, the rudder actuator required stiffness for flutter suppression $K_{act_{flutter}}$ is:

$$K_{act_{flutter}} \geq 1.79 \cdot 10^7 \text{ N/m} \quad (3.41)$$

Considering a conservative approach in which the actuator metal part stiffness (K_{metal}) is equal to the actuator's oil column stiffness (K_{oil}), consequently $\lambda = 1$, it is possible to deduce, using equation 3.34, the actuator piston area that complies with the stiffness requirement ($A_{act_{flutter}}$) is:

$$A_{act_{flutter}} \geq 2.319 \text{ in}^2 \quad (3.42)$$

3.4.3 Final actuator design

Having different actuator areas to meet different requirements, the actuator designer shall choose the greater piston area. So, from equations 3.40 and 3.42, the final piston area is:

$$A_{act_{flutter}} = 2.319 \text{ in}^2 \quad (3.43)$$

To conclude the actuator design, it is necessary to have the piston and rod diameter that give the final actuator area:

$$A_{act} = \frac{\pi}{4}(PistonD^2 - RodD^2) \quad (3.44)$$

where $PistonD$ and $RodD$ are the piston and rod diameters, respectively.

The piston and rod diameter in aerospace applications are determined by its standard dynamic seals defined in (AS4716B, 2011). Thus, it is important to choose a rod and piston seal configuration that determine an area as close as possible to the actuator design area.

Once determined the seal configuration, the actuator final design is presented in table 3.4.

TABLE 3.4 – Actuator Design

Actuator Preliminary Design	
Piston Seal number	328
Rod Seal number	221
Actuator area (A_{act})	2.329 in ²

The actuator final design will be confirmed by simulation using the model presented in next chapter and the compliance with performance and flutter suppression requirements will be evaluated. The table 3.5 presents the final actuator design margins from requirements.

TABLE 3.5 – Preliminary Actuator compliance with design requirements

Actuator Design Margin			
Design parameter	Requirement	Design	Margin (%)
Stall load (lbf)	4545.57	6638.05	46.03
$K_{act}(N/m^2)$	$1.79 \cdot 10^7$	$1.80 \cdot 10^7$	0.56

4 Model Construction

This chapter aims to develop a mathematical model of a flight control electro-hydraulic actuator and to describe the hydraulic actuation system model implemented in this work. In addition, it presents the validation of the actuator design from previous chapter against performance and flutter suppression requirements.

4.1 Flight Control Actuator Nonlinear Model

This section presents the nonlinear model of the electro-hydraulic actuator implemented in this work, which has its hydraulic schematic presented in figure 4.1.

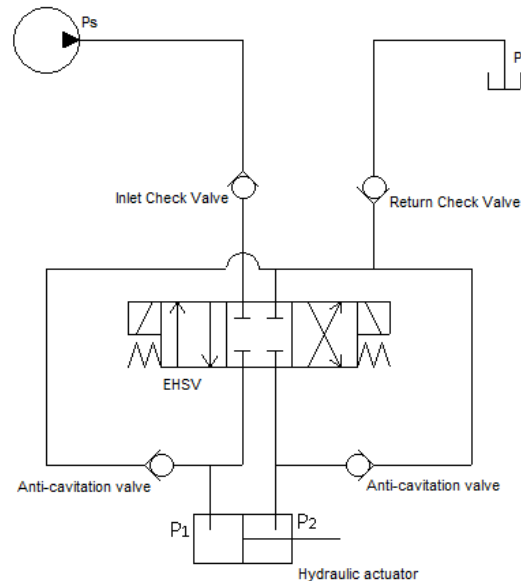


FIGURE 4.1 – Actuator Hydraulic Schematic

For the performance and dynamic stiffness analysis, the actuator will be considered in its normal operation. Thus, for the check valves modelling, see (CONSTANTINO, 2010).

The actuator servo valve considered in this work is a two-stage four-way electro-hydraulic servo valve, represented in figure 4.2.

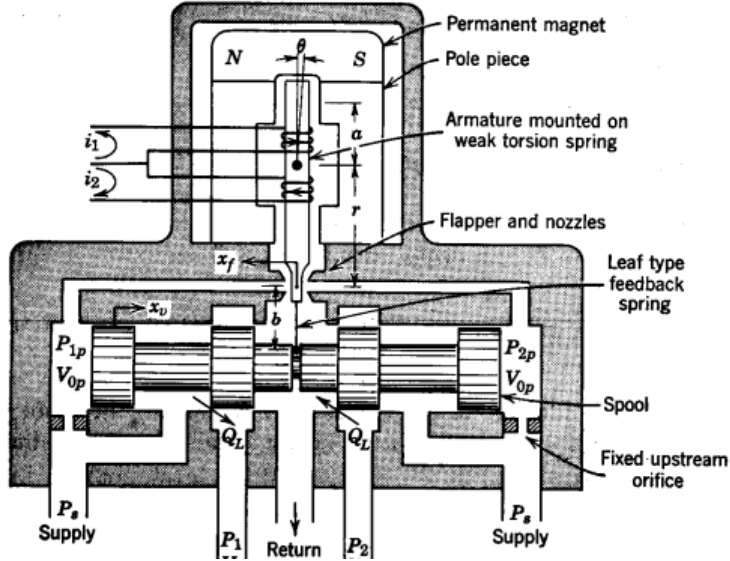


FIGURE 4.2 – Schematic of a two-stage electrohydraulic servovalve with force feedback and a flapper nozzle system as first stage (THAYER, 1965)

The first stage is a flapper-nozzle system, which consists of a torque motor and a flapper nozzle. When a current is inserted in the EHSV, an electromagnetic field is generated through the solenoid and reacting with the permanent magnetic field produce a torque force on the flapper causing a flapper displacement.

Moving the flapper, it directs the hydraulic flow to one side of the EHSV second stage spool, which will increase the pressure in one side of the spool and will make the spool move to the opposite direction of the flapper displacement until the feedback spring force balances the flapper torque.

Therefore, the first stage of the electro-hydraulic servovalve (EHSV) is responsible for piloting the EHSV spool. Hence, based on a current command (i) the EHSV 1st stage determine a spool position (x_v), represented by the equation 4.1 obtained from (THAYER, 1965):

$$\ddot{x}_v = \frac{1}{A_s K_r} (K_i K_2 w_{n_e}^2 i - 2\xi_e w_{n_e} A_s K_r \dot{x}_v - A_s K_r w_{n_e}^2 \dot{x}_v - K_2 K_w w_{n_e}^2 x_v) \quad (4.1)$$

where:

x_v : EHSV 1st stage spool position

w_{n_e} : EHSV 1st stage natural frequency

ξ_e : EHSV 1st stage damping ratio

A_s : EHSV spool end area

K_r : EHSV flapper-armature gain

K_l : EHSV 1st stage torque motor gain

x_v : EHSV spool displacement

i : EHSV current

K_2 : hydraulic amplifier flow gain

K_w : feedback wire stiffness

Using the flow continuity equation, which relates the net flow into a container to the internal fluid pressure and volume, the hydraulic actuator chambers pressures (P_1 and P_2) dynamics can be obtained as follows:

$$\dot{P}_1 = \frac{\beta(P_1, T)}{V_1(x_p)}(Q_1 - A_p \dot{x}_p - Q_{ep1} - Q_{ip}) \quad (4.2)$$

$$\dot{P}_2 = \frac{\beta(P_2, T)}{V_2(x_p)}(A_p \dot{x}_p - Q_{ep2} + Q_{ip} - Q_2) \quad (4.3)$$

The $\beta(P_1, T)$ and $\beta(P_2, T)$ are the fluid bulk modulus which are function of the chamber pressure and the fluid temperature (T), and the actuator chambers volume (V_1 and V_2) are linear function of the piston position (x_p):

$$V_1(x_p) = V_{01} + A_p x_p \quad (4.4)$$

$$V_2(x_p) = V_{02} - A_p x_p \quad (4.5)$$

where:

x_p : the piston position

A_p : the piston area

V_{01} : Chamber 1 initial volume

V_{02} : Chamber 2 initial volume

The resulting flows due to external leakage are represented by Q_{ep1} and Q_{ep2} and the internal leakage between chambers by Q_{ip} , and they are represented as follows:

$$Q_{ep1} = C_d A_{ext} \sqrt{\frac{2P_1}{\rho}} \quad (4.6)$$

$$Q_{ep_2} = C_d A_{ext} \sqrt{\frac{2P_2}{\rho}} \quad (4.7)$$

$$Q_{ip} = C_d A_{int} \sqrt{\frac{2(P_1 - P_2)}{\rho}} \quad (4.8)$$

where:

C_d : Discharge coefficient

A_{int} : internal leakage equivalent area

A_{ext} : external leakage equivalent area

Q_{ip} : Internal leakage between chambers

Q_{ep_1} : External leakage on chamber 1

Q_{ep_2} : External leakage on chamber 2

Q_1 and Q_2 represent the resulting flow from the EHSV second stage to each actuator chamber.

Q_1 is the difference between the flow from the connecting path between P_s and P_1 and the flow from the connecting path between P_1 to P_t for an EHSV spool position greater than the EHSV overlap ($x_v \geq x_{ov}$). Hence, the following equation¹ can be obtained, where $K_{CD} = C_d \sqrt{\frac{2}{\rho}}$:

$$Q_1 = K_{CD} \sqrt{P_s - P_1} (x_v x_w + A_{leak}) - K_{CD} \sqrt{P_1 - P_t} A_{leak} \quad (4.9)$$

Q_2 is the difference between the flow from the connecting path between P_2 to P_t and the flow from the connecting path between P_s to P_2 for an EHSV spool position greater than the EHSV overlap ($x_v \geq x_{ov}$). Hence, the following equation can be obtained, where $K_{CD} = C_d \sqrt{\frac{2}{\rho}}$:

$$Q_2 = K_{CD} \sqrt{P_2 - P_t} (x_v x_w + A_{leak}) - K_{CD} \sqrt{P_s - P_2} A_{leak} \quad (4.10)$$

¹According to (MERRITT, 1967), and considering a valve with the spool centered, the leakage flows can be considered as laminar (proportional to a linear orifice differential pressure) for a new valve, and becomes turbulent flows (proportional to a square root orifice differential pressure) as abrasive materials in the fluid erode the orifices edges for in service valves . In this work, it was maintained the turbulent flow assumption by (CONSTANTINO, 2010), however the laminar flow leakage may be considered for some cases.

For $x_v \leq -x_{ov}$, Q_1 and Q_2 equations are as follows:

$$Q_1 = K_{CD} \sqrt{P_S - P_1} A_{leak} - K_{CD} \sqrt{P_1 - P_T} A_{leak} + K_{CD} \sqrt{P_1 - P_T} x_v x_w^{-1} \quad (4.11)$$

$$Q_2 = K_{CD} \sqrt{P_2 - P_T} A_{leak} - K_{CD} \sqrt{P_S - P_2} A_{leak} + K_D \sqrt{P_S - P_2} x_v x_w^{-1} \quad (4.12)$$

where:

x_{ov} : EHSV second-stage overlap

x_{width} : EHSV second-stage orifice area width

x_{length} : EHSV second-stage orifice area length

A_{leak} : EHSV second-stage leakage

P_s : Supply pressure

P_t : Return pressure

ρ : fluid density

Finally, the net force acting on the actuator piston can be obtained by multiplying the piston area (A_p) by the differential pressure across the piston ($P_1 - P_2$). By applying the Newton's second law, the piston dynamics is represented as follows:

$$m_p \ddot{x}_p + B_p \dot{x}_p + K_p x_p + F_L = A_p (P_1 - P_2) \quad (4.13)$$

where:

m_p : piston mass

B_p : viscous damping coefficient

K_p : load coefficient

F_L : external load

4.2 Flight Control Actuation System Simulation Model

This section intends to present an overview of the model developed in this work, which is based on (CONSTANTINO, 2010) that presents a model of a fly-by-wire and hydraulic powered flight control actuation system with an active-active configuration, focusing on

the analysis of the force-fight generated on the actuators due to oscillatory failures. The model is constructed using MatLab/Simulink.

The flight control actuator nonlinear model developed in the previous section is part of the Flight Control Actuation system model that will be described in this section, and is shown in figure 4.3.

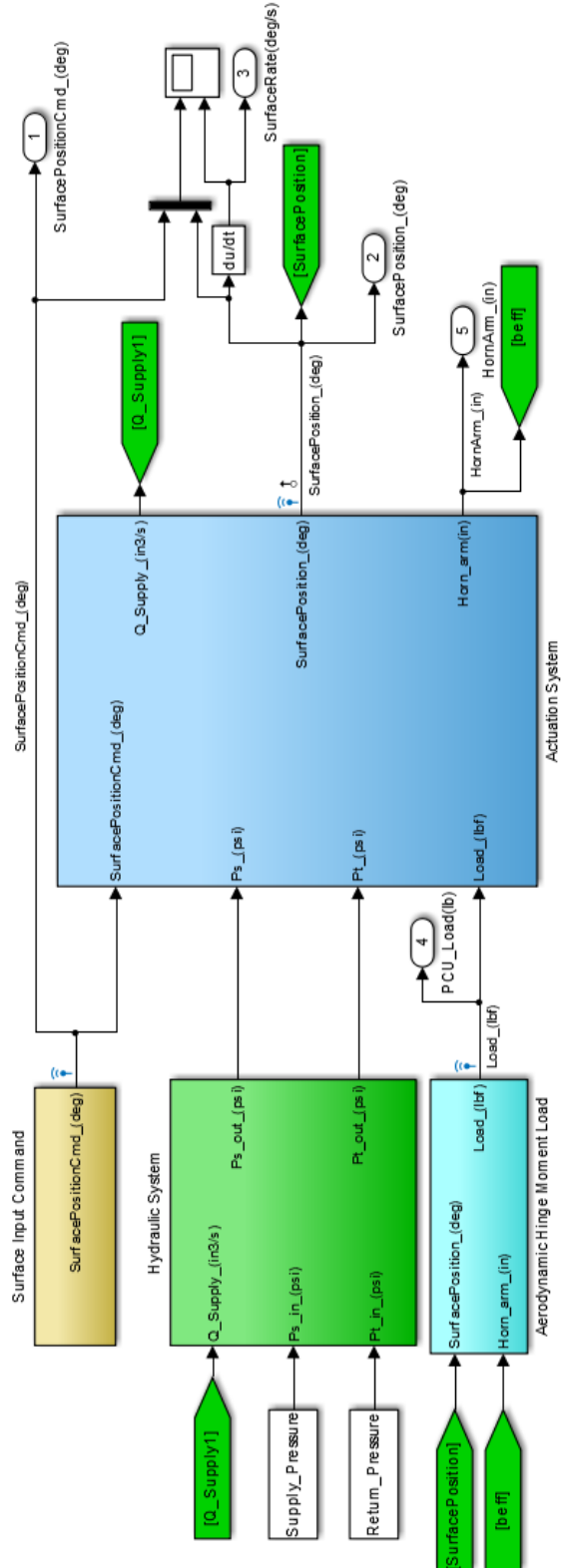


FIGURE 4.3 – Hydraulic Actuation System Model overview

As illustrated in figure 4.3, it is possible to divide the Flight Control Hydraulic Actuation System in:

- i Surface Input Command
- ii Aerodynamic Hinge Moment Load
- iii Hydraulic System
- iv Actuation System

The Surface Input Command subsystem block allow the configuration of an input command to the actuator in degrees, it can be a sine wave, a step, a constant or a square wave.

The Aerodynamic Hinge Moment Load subsystem block allow the configuration of the load applied to the actuator, it can simulate a hinge moment load varying linearly with the surface angle, a constant hinge moment or a sine wave.

The model, presented in figure 4.3, will be described in details in the following sections.

4.2.1 Hydraulic System

The Hydraulic System, shown in figure 4.4, is responsible to model the hydraulic system supply pressure line and return pressure line. Based on a fixed displacement pump that controls the stagnation pressure of the pump line, the Hydraulic System model also takes into account the aircraft hydraulic losses, due to the line flow and tube losses, and the hydraulic fluid inertia.

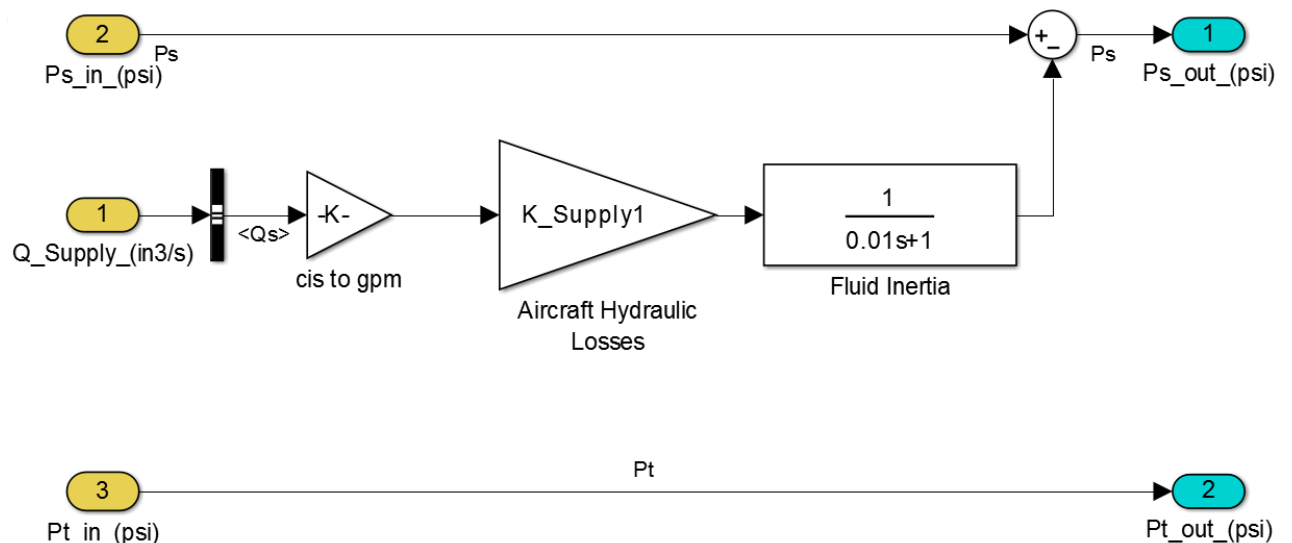


FIGURE 4.4 – Hydraulic System Model

4.2.2 Actuation System Model

The Actuation System is divided into Electronics System, Actuator and Surface Kinematics, as illustrated in figure 4.5.

4.2.2.1 Electronics System

The actuator electronics system, shown in figure 4.5, represents the electronic signal processing and the actuator's position control loop.

The signal processing consists of an analog-to-digital converter and is necessary because the actuator electronic system is considered as a digital processor and the pilot input signal (control surface desired angle) and the actuator's feedback sensors (piston position, servo valve's spool position and chambers differential pressure) are considered analog signals.

The position control loop implements a simple proportional controller that commands the servovalve input current according to the error between the control surface commanded position and the feedback position.

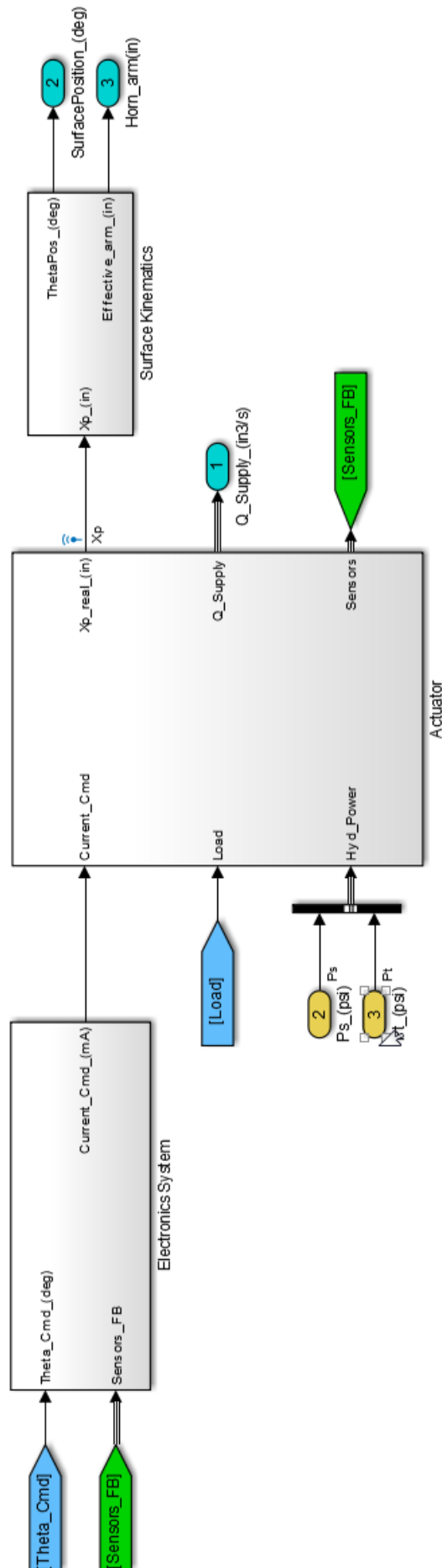


FIGURE 4.5 – Actuation System Model

In addition, there is a digital-to-analog converter, which converts the control loop digital signal to the actuator's servo valve into an analog signal. The actuator electronic subsystem block can be seen in figure 4.6.

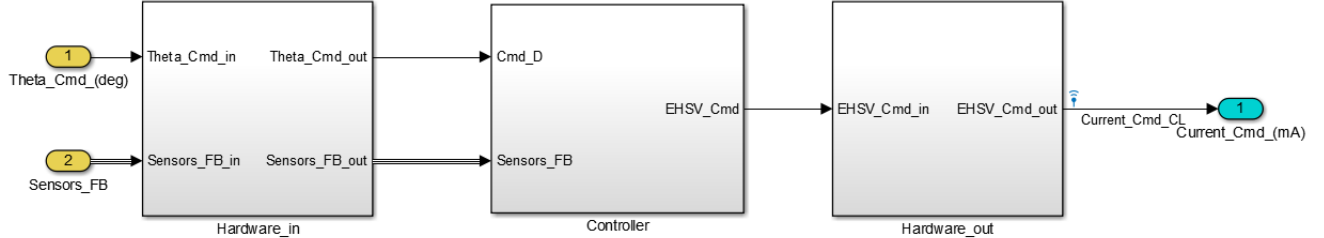


FIGURE 4.6 – Actuator Electronics System Model

4.2.2.2 Electro-hydraulic Actuator

The nonlinear model developed in the previous section has its implementation described in the following paragraphs.

The actuator subsystem block implements the actuator piston dynamics (equation 4.13), the valves dynamics that allow a safer and proper operation of the hydraulic actuator and the sensors dynamics, as it is shown in figure 4.7.

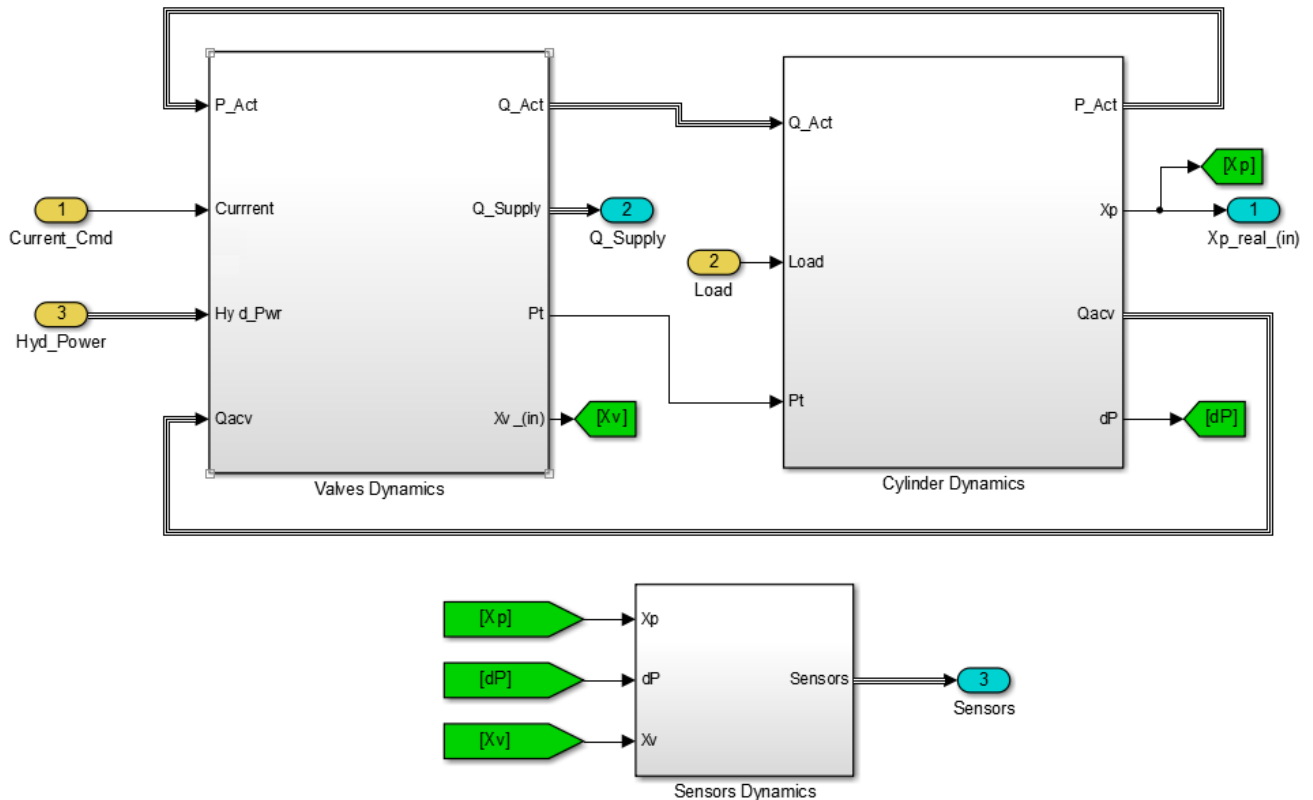


FIGURE 4.7 – Actuator Model

The valves dynamics model represents the inlet check valve, the return check valve and the servo valve dynamics.

The check valves present in this model are poppet-style valves used to prevent a returning flow from the actuator to the supply and return hydraulic system lines.

The servo valve considered is an EHSV - Electro Hydraulic Servo Valve commanded by an electric current. It controls the hydraulic flow between supply and return paths and the hydraulic actuator's chambers.

The valves models can be observed in figure 4.8.

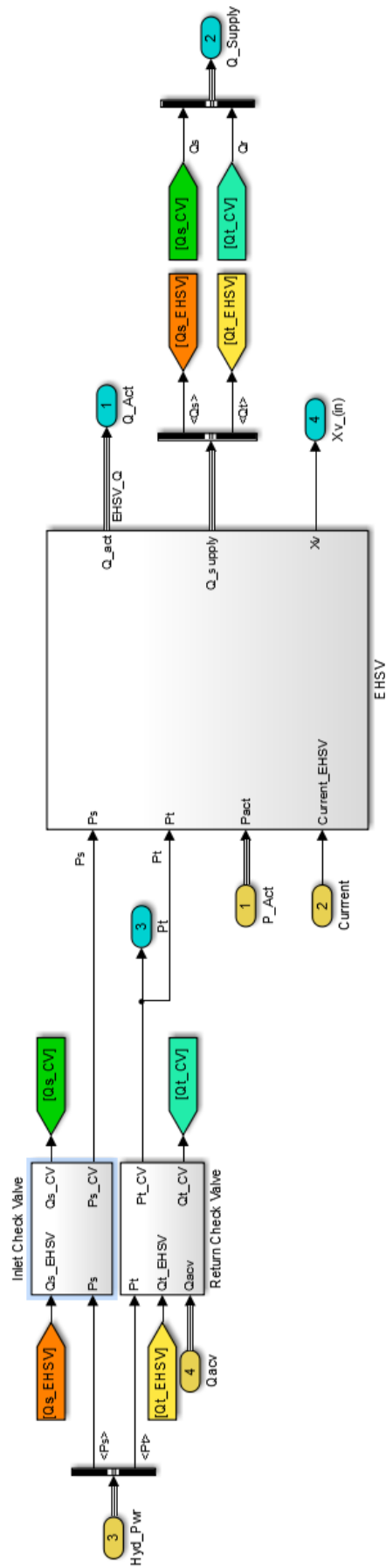


FIGURE 4.8 – Actuator Model - Valves Dynamics

The cylinder dynamics model, shown in 4.9, represents the fluid dynamics subsystems models the actuator chambers pressures dynamics (equations 4.2 and 4.3), and the piston dynamics implements equation 4.13.

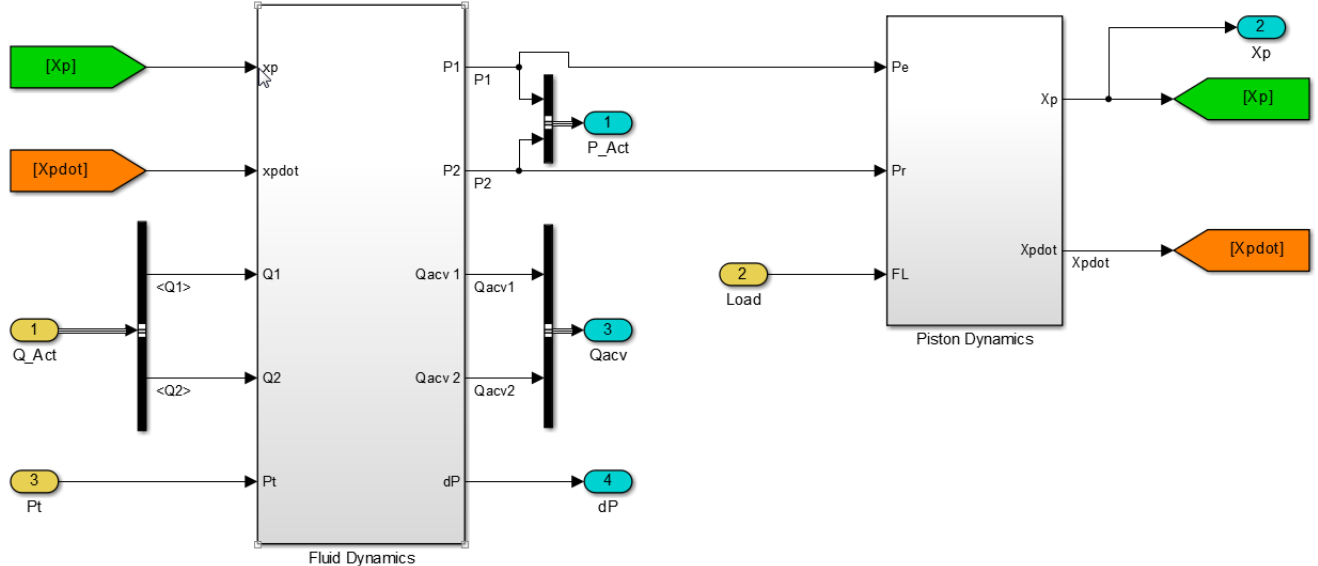


FIGURE 4.9 – Actuator Model - Cylinder Dynamics

For valves, cylinder and fluid dynamics details see (CONSTANTINO, 2010).

There are three sensors in the actuator model, as illustrated in figure 4.10. Those sensors measure the piston position (x_p), the differential pressure in actuator chambers (Δp) and the servo valve spool position (x_v). They represent typical sensors present in fly-by-wire actuators industry applications. All of them are LVDT (Linear Variable Differential Transformer) type and will be described in the next section.

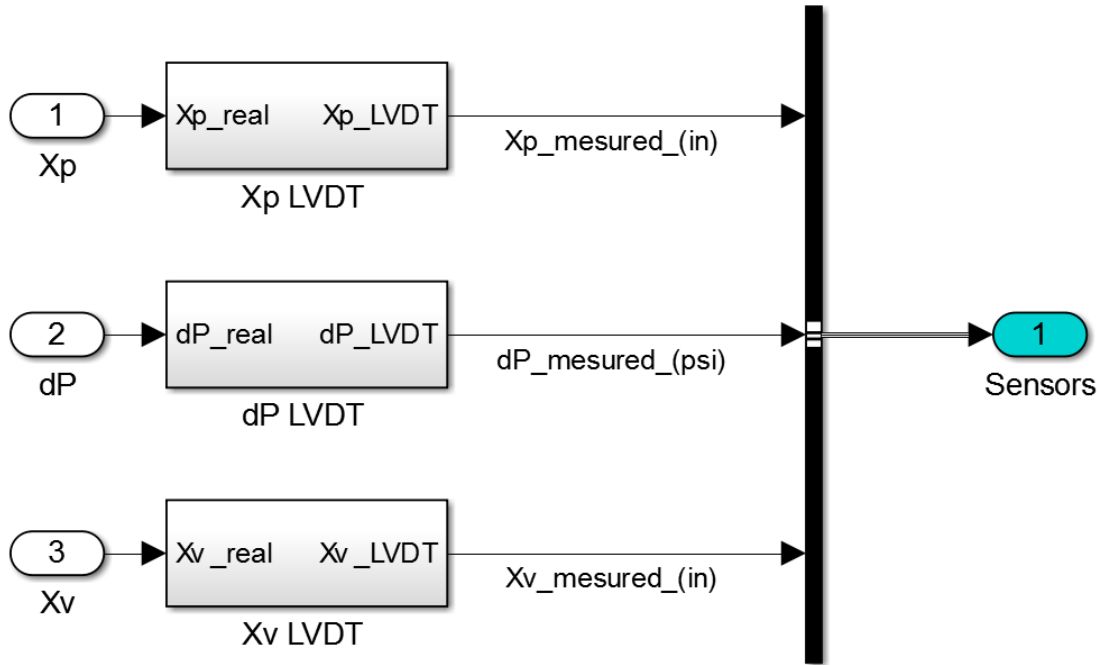


FIGURE 4.10 – Actuator Model - Sensor Dynamics

4.2.2.3 Surface Kinematics

The surface kinematics block is responsible for modelling the actuator kinematics. It represents the control surface position based on the actuator kinematics; it does not consider the control surface rotational dynamics. For an increment in the piston ram position the surface block transforms it in a control surface angular position, as shown in figure 4.11

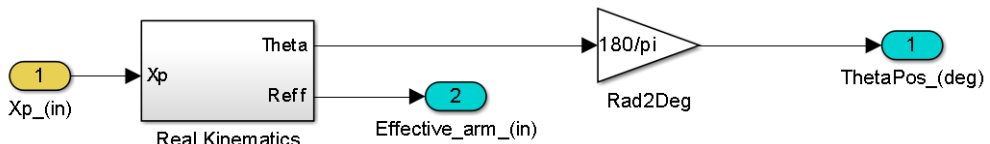


FIGURE 4.11 – Surface Kinematics Model

4.3 Flight Control Actuation System Model Modifications

In order to bring (CONSTANTINO, 2010) model to meet this study needs and to construct a new Flight Control Actuator model, some modifications were implemented and will be described in this section.

4.3.1 Surface simplification

The surface rotational dynamics model developed in (CONSTANTINO, 2010) is not an interest to this study, since the focus is not to analyze control surface force-fight, but the actuator performance and design. Thus, the surface kinematics is sufficient to represent the control surface. The aerodynamic forces and perturbations will be represented as linear forces applied directly to the actuator piston.

Therefore, the surface block was simplified to a surface kinematics block, as can be observed in figure 4.11.

4.3.2 Fluid Bulk Modulus Variation

In (CONSTANTINO, 2010), the Bulk Modulus is considered a non-variable parameter and is maintained as a constant during the entire simulation. In order to take into account the Bulk Modulus variation, shown in chapter 2, some modifications were performed to accommodate pressure, temperature and entrained air effects.

The Bulk Modulus variation was implemented according to the SAE Aerospace Information Report - AIR 1362 Rev B, which presents data on hydraulic fluids.

This SAE information report also presents different test data of Bulk Modulus variation due to pressure and temperature for different hydraulic fluid.

The hydraulic fluid chosen to have its properties represented in this work is the AS1241, Type IV, Class 1, which is a common fluid in aerospace industry applications.

The modified model can be observed in figure 4.12.

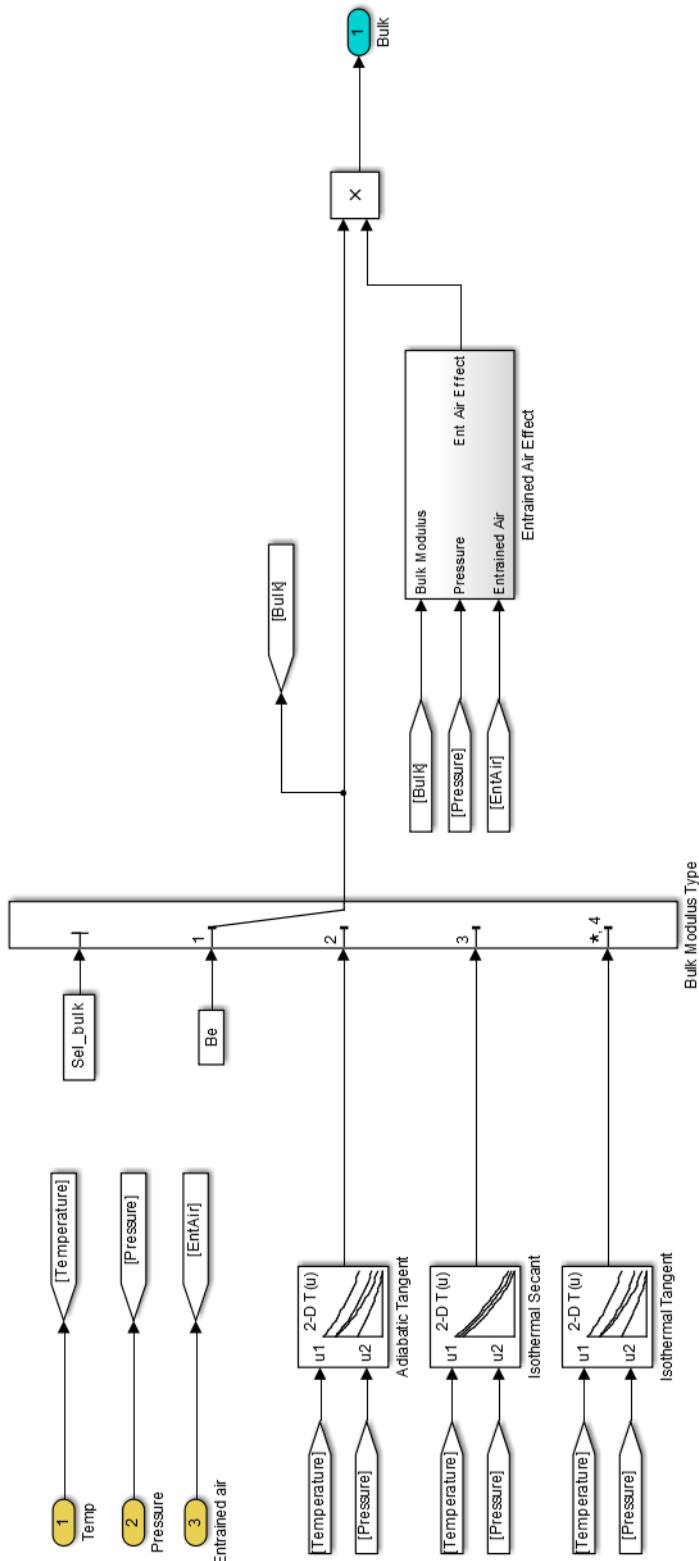


FIGURE 4.12 – Bulk Modulus modifications

As it is possible to realize, the Bulk Modulus can be configured in four different settings:

- i Constant;

- ii Adiabatic Tangent;
- iii Isothermal Secant;
- iv Isothermal Tangent.

4.3.2.1 Entrained Air Effect on Bulk Modulus

In hydraulic systems, it is common to have a mixture of fluid and air during normal operation in hydraulic lines. Consequently, some fluid properties may present changes when mixed with air.

The compressibility of the fluid changes due to entrapped air, therefore the effective Bulk Modulus of the fluid-air mixture β_M is different from the fluid only Bulk Modulus β_{oil} .

Consider the following representation of an actuator's chamber in figure 4.13.

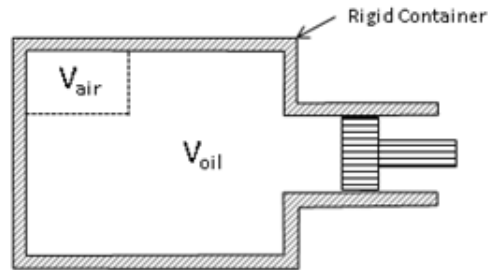


FIGURE 4.13 – Actuator chamber with fluid and air. Source: (RABIE, 2009)

The total volume of the actuator's chamber is given by:

$$V_M = V_{oil} + V_{air} \quad (4.14)$$

where:

- a) V_M is the total chamber volume, considering the mixture of air and fluid;
- b) V_{oil} is the fluid volume;
- c) V_{air} is the air volume.

Considering a small displacement of the piston, the chamber volume variation will be:

$$dV_M = dV_{oil} + dV_{air} \quad (4.15)$$

For small variation of pressure and volume, the equivalent tangent bulk Modulus for the system is defined as:

$$\beta_M = -V_M \frac{dp}{dV_M} \quad (4.16)$$

In the same way, the tangent bulk modulus for fluid and air are:

$$\beta_{oil} = -V_{oil} \frac{dp}{dV_{oil}} \quad (4.17)$$

$$\beta_{air} = -V_{air} \frac{dp}{dV_{air}} \quad (4.18)$$

Replacing 4.16, 4.17 and 4.18 in 4.15:

$$-V_M \frac{dp}{\beta_M} = -V_{oil} \frac{dp}{\beta_{oil}} - V_{air} \frac{dp}{\beta_{air}} \quad (4.19)$$

Rearranging:

$$\frac{1}{\beta_M} = \frac{V_{oil}}{V_M} \frac{1}{\beta_{oil}} + \frac{V_{air}}{V_M} \frac{1}{\beta_{air}} \quad (4.20)$$

Assuming that the air volume is negligible comparable to the total air-fluid mixture volume ($V_M \approx V_{oil}$):

$$\frac{1}{\beta_M} = \frac{1}{\beta_{oil}} + \frac{V_{air}}{V_M} \frac{1}{\beta_{air}} \quad (4.21)$$

Thus, the effect of the entrained air (EA) in the fluid bulk modulus can be represented as:

$$EA = \frac{\beta_M}{\beta_{oil}} = \frac{1}{1 + \frac{V_{air}}{V_M} \frac{\beta_{oil}}{\beta_{air}}} \quad (4.22)$$

Now, it is necessary to define V_{air} and β_{air} .

The air at atmospheric pressure undergoes a transformation process to mix with fluid in the actuator chamber. This process can be represented as an isothermal or adiabatic process.

In an isothermal process, the temperature of a system remains constant, but there are heat exchanges during the process. Generally, it occurs when the system pressure changes slowly in order to allow the temperature change to be compensated by heat exchanges.

For an isothermal process, the product of the pressure and volume is equal to a constant (K_{iso}), thus, the transformation from point 1 to 2 of a p x V isothermal curve can be expressed by:

$$p_1 V_1 = p_2 V_2 = K_{iso} \quad (4.23)$$

Considering the entrained air undergoing an isothermal process:

$$p_0 V_{air0} = p V_{air} = K_{iso} \quad (4.24)$$

where:

- a) p_0 is the atmospheric pressure;
- b) V_{air0} is the air volume in the chamber at atmospheric pressure;
- c) p is the chamber pressure;
- d) V_{air} is the air volume at chamber pressure.

Thus, rearranging 4.24, V_{air} is given by:

$$V_{air} = \frac{p_0}{p} V_{air0} \quad (4.25)$$

Deriving 4.25 for $\frac{dp}{dV_{air}}$:

$$\frac{dp}{dV_{air}} = -\frac{K_{iso}}{V_{air}^2} \quad (4.26)$$

Substituting in 4.18:

$$\beta_{air} = V_{air} \frac{K_{iso}}{V_{air}^2} = \frac{p V_{air}}{V_{air}} = p \quad (4.27)$$

Replacing 4.25 and 4.27 in 4.22:

$$\frac{\beta_M}{\beta_{oil}} = \frac{1}{1 + \frac{V_{air0} p_0 \beta_{oil}}{V_M p^2}} \quad (4.28)$$

In an adiabatic process, there is no heat exchange between the system and its surrounding, and the system temperature varies during the transformation process. Generally, it occurs for fast changes in the system pressure in order that no heat exchange occurs during the process.

For an adiabatic process, the product of the pressure and volume to the power of the adiabatic index is equal to a constant, thus the transformation from point 1 to 2 considering a $p \propto V$ adiabatic process can be expressed by:

$$p_1 V_1^\gamma = p_2 V_2^\gamma = K_{ab} \quad (4.29)$$

Considering the entrained air undergoing an adiabatic process:

$$p_0 V_{air0}^\gamma = p V_{air}^\gamma = K_{ab} \quad (4.30)$$

where:

- a) p_0 is the atmospheric pressure;
- b) V_{air0} is the air volume in the chamber at atmospheric pressure;
- c) p is the chamber pressure;
- d) V_{air} is the air volume at chamber pressure.

Thus, V_{air} is:

$$V_{air} = \left(\frac{p_0}{p}\right)^{\frac{1}{\gamma}} V_{air0} \quad (4.31)$$

Deriving 4.31 for $\frac{dp}{dV_{air}}$:

$$\frac{dp}{dV_{air}} = -\gamma \frac{K_{ab}}{V_{air}^{\gamma+1}} \quad (4.32)$$

Substituting in 4.18:

$$\beta_{air} = V_{air} \gamma \frac{K_{ab}}{V_{air}^{\gamma+1}} = \gamma \frac{p V_{air}^\gamma}{V_{air}^\gamma} = \gamma p \quad (4.33)$$

Replacing 4.31 and 4.33 in 4.22:

$$\frac{\beta_M}{\beta_{oil}} = \frac{1}{1 + \frac{V_{air0} p_0^{\frac{1}{\gamma}} \beta_{oil}}{V_M p^{\frac{1}{\gamma}} \gamma p}} \quad (4.34)$$

The effect of the entrained air is implemented in the bulk modulus model for both isothermal and adiabatic process method and is presented in figure 4.12.

4.3.3 Electro-hydraulic servovalve - EHSV

The electro-hydraulic servovalve first stage from (CONSTANTINO, 2010) model was modified to allow the use of EHSV industry parameters. This change will increase the model flexibility to evaluate different off-the-shelf EHSV drivers.

The first stage servo valve implemented in this work was derived from (THAYER, 1965), which presents the typical parameters for a Moog 31 series servo valve and considers the following assumptions:

1. all nonlinearities can either be approximated by linear dynamic effects, or can be neglected;
2. fluid compressibility and viscosity effects can be neglected;
3. negligible load pressure;
4. the force necessary to move the spool are small with respect to the driving force available, thus differential pressure across the spool is negligible during dynamic conditions and spool mass, friction, flow forces, other spool force effects can be neglected;
5. the armature/flapper can be represented as a simple lumped parameter model;
6. motions of the flapper smaller than the spool motions;
7. an ideal current source is used in the system;
8. perturbations conditions can be applied to hydraulic amplifier orifice characteristics.

The resulting electro-hydraulic servo valve model is a third order system that can be represented by the diagram in figure 4.14.

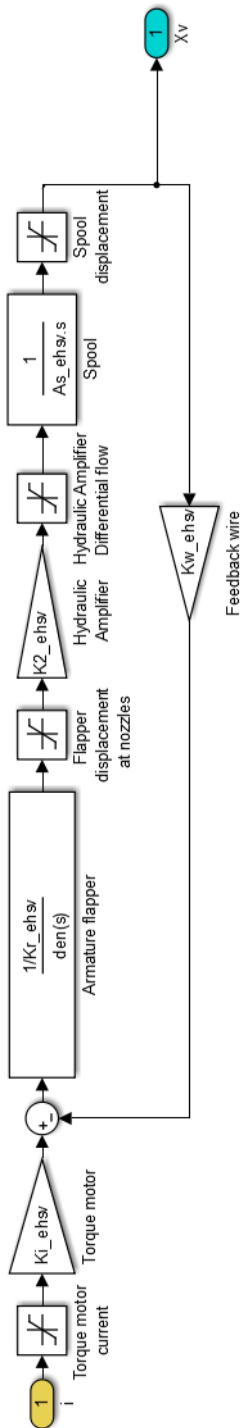


FIGURE 4.14 – EHSV 1st Stage Moog model valve in Simulink

The EHSV first stage frequency response can be seen in figure 4.15. As can be observed, the phase margin is infinite, as its gain response does not cross 0 dB. The gain margin is approximately 65 dB at 733.5 Hz, as expected from (THAYER, 1965), which model has the EHSV first stage natural frequency around 730 Hz. The bandwidth of the EHSV 1st stage is around 166 Hz.

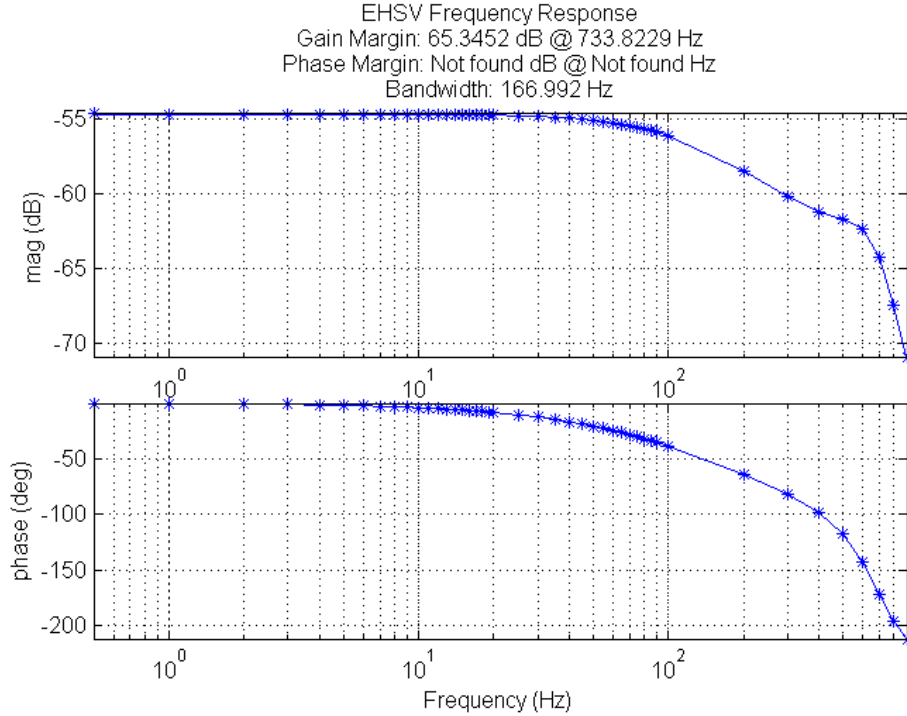


FIGURE 4.15 – Simulated EHSV 1st Stage Frequency Response

The EHSV 1st stage frequency response was performed following the frequency tests described in (ARP490F, 2008). The EHSV input was set to an oscillatory current with an amplitude of 10% of the maximum EHSV current and a frequency sweep from 0.1 Hz to 750 Hz was performed. The output observed for the EHSV frequency response was the EHSV spool position.

The ratio between EHSV spool position and EHSV input current give us the EHSV frequency response. It is important to highlight that the EHSV supply pressure was maintained constant and the EHSV was disconnected from the actuator.

The EHSV's second stage used in this work is the same as the one implemented in (CONSTANTINO, 2010), it is a four-way directional flow control valve. The EHSV second stage is responsible for evaluating the flow through each path of the EHSV for a given spool position. There are five paths in the EHSV second stage, as illustrated in figure 4.16:

1. Path 1: Between the supply line and the actuator's chambers 1;
2. Path 2: Between the actuator chamber 2 and the return line;
3. Path 3: Between the actuator chamber 1 and the return line;
4. Path 4: Between the supply line and the actuator's chambers 2;
5. Path 5: Between the supply line and return line.

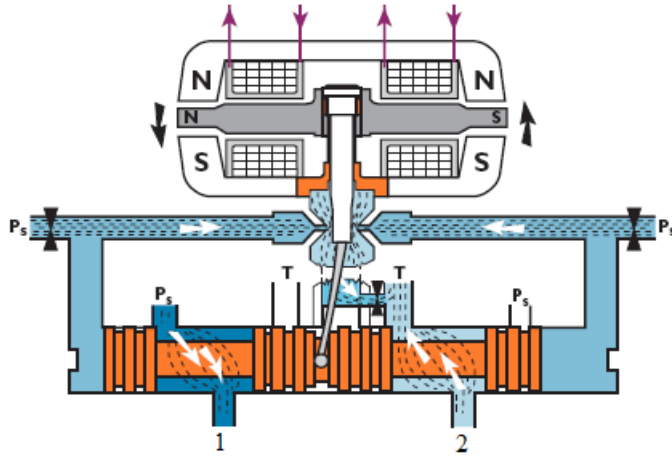


FIGURE 4.16 – Schematic of a two-stage electrohydraulic servo valve with force feedback and a flapper nozzle system as first stage [adapted from Moog]

To comply with performance requirements, it was necessary to increase of the EHSV flow gain by expanding the EHSV slot, as it will be discussed in section 5.1.

4.3.4 Seal Friction

Seals are used in hydraulic systems to prevent loss of hydraulic fluid. In an electro-hydraulic actuation system, dynamic sealing solutions must be applied to mitigate leakages and to the system performance during normal operation. The sealing solution presents an inherent drawback that is the presence of friction forces, which act against piston movements reducing the actuator performance.

According to FAR 25.1309 requirement, “the aeroplane systems and associated components, considered separately and in relation to other systems, must be designed so that any catastrophic failure condition is extremely improbable, and does not result from a single failure”. Normally, the design with redundant piston and rod seals is a solution to mitigate that a single (and latent) simple failure in one of these components could lead to a catastrophic failure condition - as a severe external leakage. However, sealing redundancy contributes to penalize the actuator performance, as mentioned before. Thus, it is necessary to characterize and to take into account the effect of the seals friction forces in the actuator model.

There are different possible sealing configurations and seals formats for flight control actuator. In this work, it will be used O-ring type seals under the following configuration: two seals for piston, two seals for the rod with one backup seal, one piston backup seal and one scrapper seal.

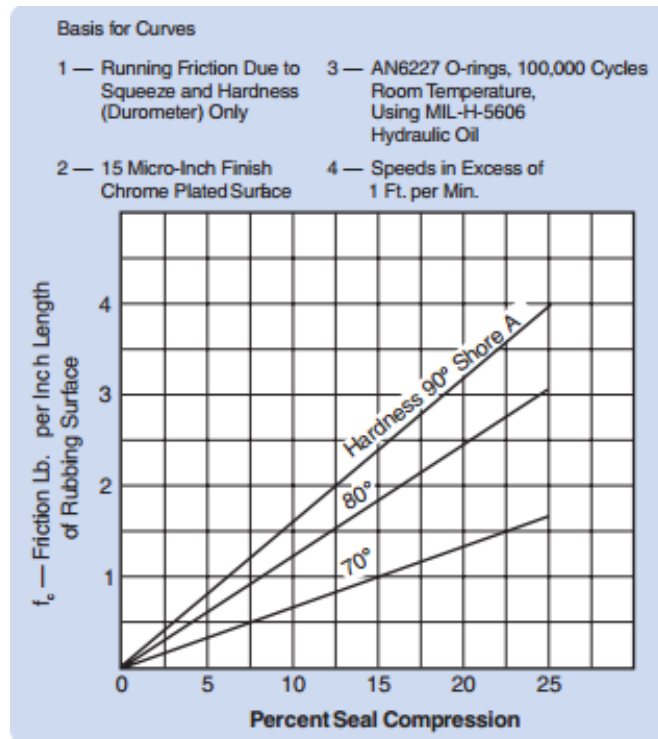


FIGURE 4.17 – Friction due to O-ring seal compression and hardness. Source:(PARKER, 2007)

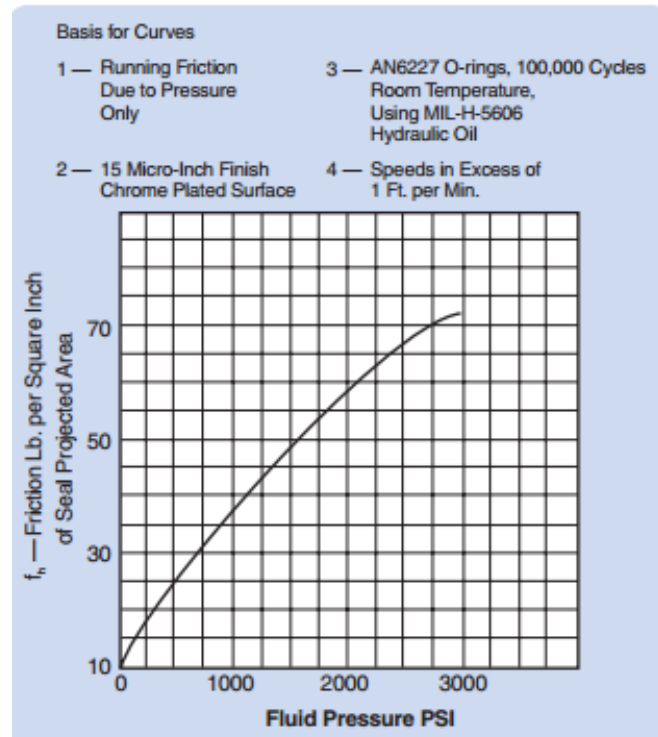


FIGURE 4.18 – Friction due to fluid pressure. Source:(PARKER, 2007)

Friction force due to dynamic sealing applications varies:

- i with the actuator's chambers pressures;
- ii with seal hardness;
- iii with seal compression.

as it is possible to observe in figures 4.17 and 4.18.

From (PARKER, 2007), it is possible to estimate the friction force generated by O-ring dynamic seals using the following formulas:

For actuator's piston:

$$F_C = f_c L_p \quad (4.35)$$

$$F_H = f_h A_p \quad (4.36)$$

$$F_f = F_C + F_H \quad (4.37)$$

For actuator's rod:

$$F_C = f_c L_r \quad (4.38)$$

$$F_H = f_h A_r \quad (4.39)$$

$$F_f = F_C + F_H \quad (4.40)$$

where:

A_p – projected area of seal for piston groove applications;

A_r – projected area of seal for rod groove applications;

f_c – Friction coefficient due to O-ring compression from figure 4.17;

f_h – Friction coefficient due to fluid pressure from figure 4.18;

L_p – length of seal rubbing surface in inches for piston groove applications;

L_r – length of seal rubbing surface in inches for rod groove applications

F_C – Total friction due to seal compression;

F_H – Total friction due to hydraulic pressure on the seal;

F_f – Total seal friction force;

In the hydraulic actuation system model, it is possible to observe the implementation of friction force due to the presence of dynamic seal in figure 4.19.

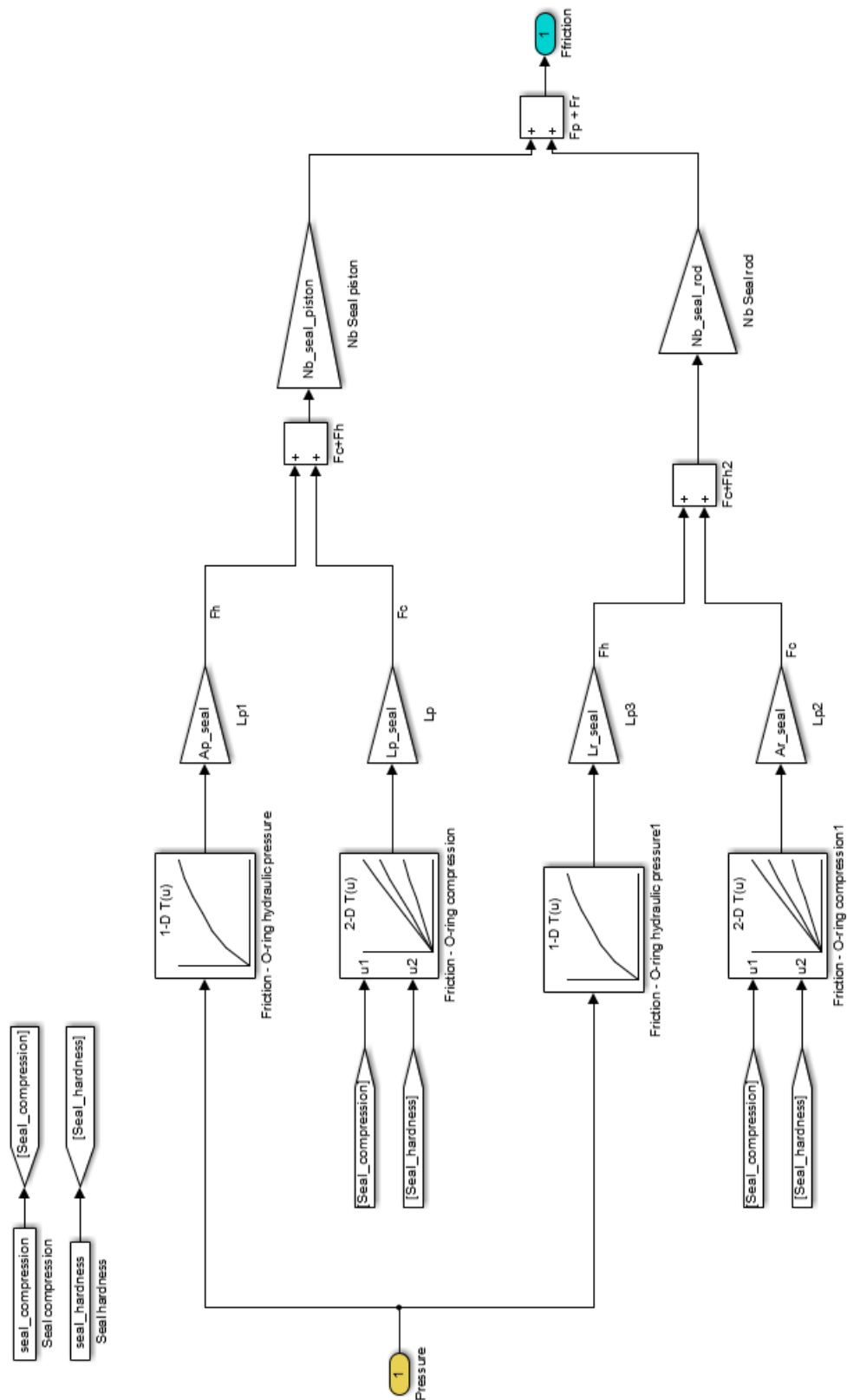


FIGURE 4.19 – Friction force implementation for piston and rod groove applications

4.3.4.1 Friction force and Stribeck effect

According to (YANADA *et al.*, 2014), the seal friction force (F_{fs}), which was derived previously, must take into account the fact that during normal operation the seal friction decreases as function of the piston velocity according to the following equation:

$$F_{fr} = F_{fs} \operatorname{sign}(\dot{x}_p) e^{\left(\frac{\dot{x}_p}{s_c}\right)} \quad (4.41)$$

where F_{fr} is the resulting friction force, x_p is the piston position, \dot{x}_p is the piston velocity, F_{fs} is the Parker O-ring estimate friction force and s_c is the Stribeck coefficient.

The Stribeck effect takes into account that the friction force between two lubricated surfaces decreases as function of velocity. In a hydraulic actuator, when the piston moves the hydraulic fluid enters between the seal and the piston surfaces creating a fluid film. The greater the velocity, the thicker is the lubricating fluid film.

Two different friction-modelling approaches are implemented in the model:

- i the Stribeck effect combined Parker O-ring friction force estimation (equation 4.41);
- ii the Parker O-ring friction force estimation.

In the first approach, due to the unstable numerical estimation of friction forces caused by nonlinearities encountered close to piston's neutral position, it was included a hysteresis effect in the piston velocity. Figure 4.20 illustrates the friction force time stamp for a zero current command in to the actuator with and without hysteresis in the piston velocity. It is possible to conclude that including the hysteresis, the friction estimation noise is reduced.

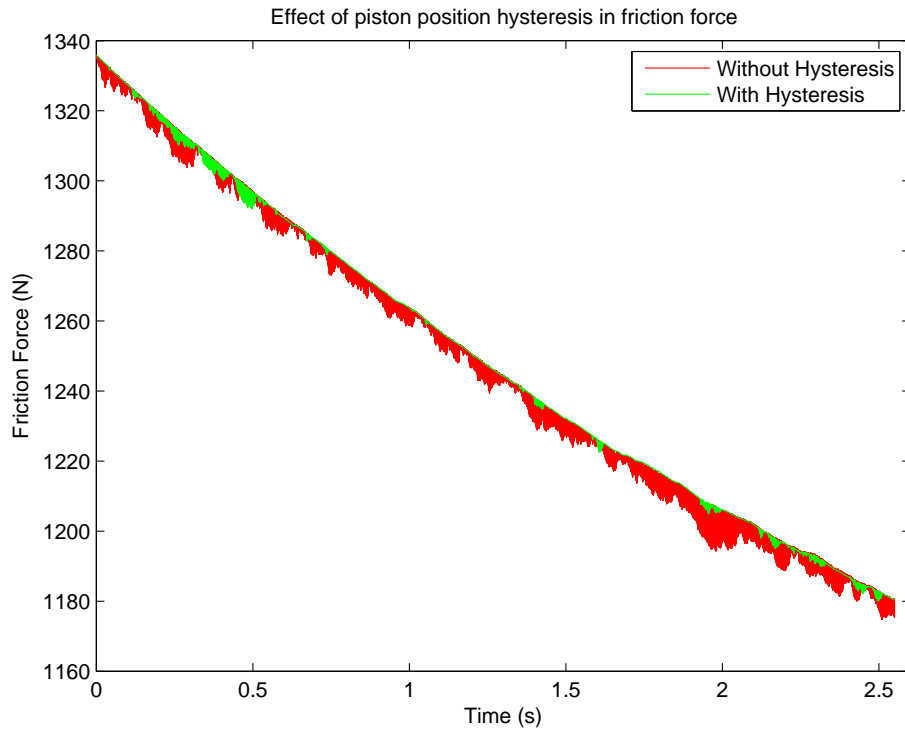


FIGURE 4.20 – Friction force implementation for piston and rod groove applications

4.3.5 Position Control Loop

The position control loop implemented in the model receives from the analog-digital converter the required surface position in degrees and the sensors feedback signals, listed:

- i Piston Position (x_p);
- ii EHSV spool position (x_v);
- iii Differential pressure between actuators chambers (Δp).

The surface command pass through a saturation block that limits the command rate to prevent aggressive surface commands. The rate limited surface command is converted from degrees to a linear reference command, based on the actuator-surface kinematics. This linear reference position command is compared to the actuator piston position obtained by the feedback of the piston position sensor, and it enters into a discrete PID controller, which generates a current command to the EHSV that pilots the hydraulic actuator.

From (THAYER, 1965), the EHSV current command is limited in -10 mA and 10 mA, due to EHSV first stage specification.

The position control loop is shown in figure 4.21.

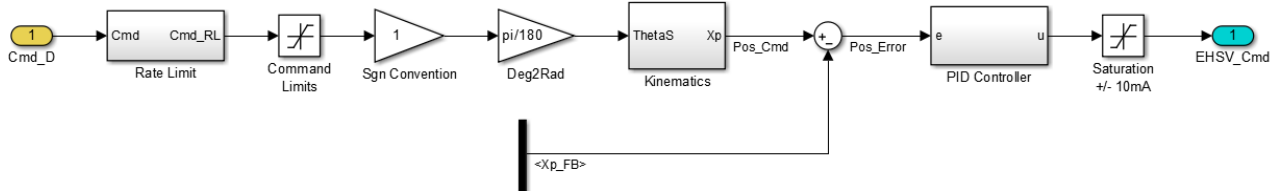


FIGURE 4.21 – Actuator Position Control Loop with piston position feedback

In a first approach, the discrete PID controller will be configured as a proportional controller, and the inclusion of derivative and integral gains will be evaluated regarding the actuator's time response, frequency response and dynamic stiffness. For the results presented in this chapter, the proportional gain value is fixed in 40 mA/in , which will be later explained in chapter 5.

4.3.6 Inlet Check Valve

The inlet check valve's function in hydraulic actuators is to prevent a returning flow to the hydraulic system. This valve is usually placed between the hydraulic supply pressure line and the EHSV. The type of inlet check valve implemented in the model can be seen in figure 4.22.

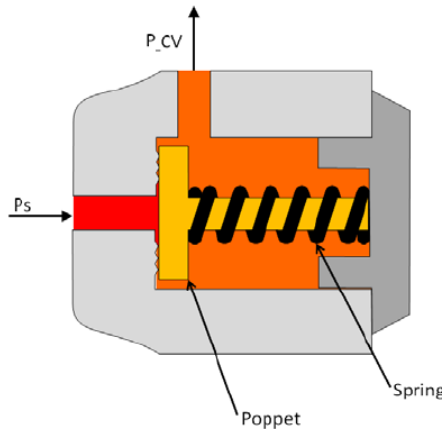


FIGURE 4.22 – Inlet check valve. Source:(CONSTANTINO, 2010)

The inlet check valve will release the flow through the valve only after the inlet pressure (P_s), applied to the valve poppet's area, results in a force greater than the force applied by the remaining pressure inside the valve (P_{cv}) plus the force applied by the loaded spring.

In order to meet performance requirements, the inlet check valve's poppet area was increased to allow less pressure drop and to guarantee a higher flow to the EHSV inlet port.

The new inlet check valve was chosen from the catalog of Lee Company (LEECO, 2009), the LO-LOHM poppet-style check valve of 0.500 in was chosen, because it is a high flow gain check valve and operates with a nominal inlet pressure of 3000 psi and stands system peak pressures up to 4050 psi.

4.3.7 Sensors

The sensors modelled in this work are all LVDT (Linear Variable Differential Transformer) type. LVDTs are linear displacement transducers known for its robustness and are widely applied in the aerospace industry.

LVDT is a type of electrical transformer that consist of a primary winding centered between a pair of identical secondary windings, composing a coil assembly, this part is known as the stationary part of the sensor. The moving part of the LVDT is a ferromagnetic core and it is attached to the object which position is to be measured. An LVDT cutaway is illustrated in figure 4.23.

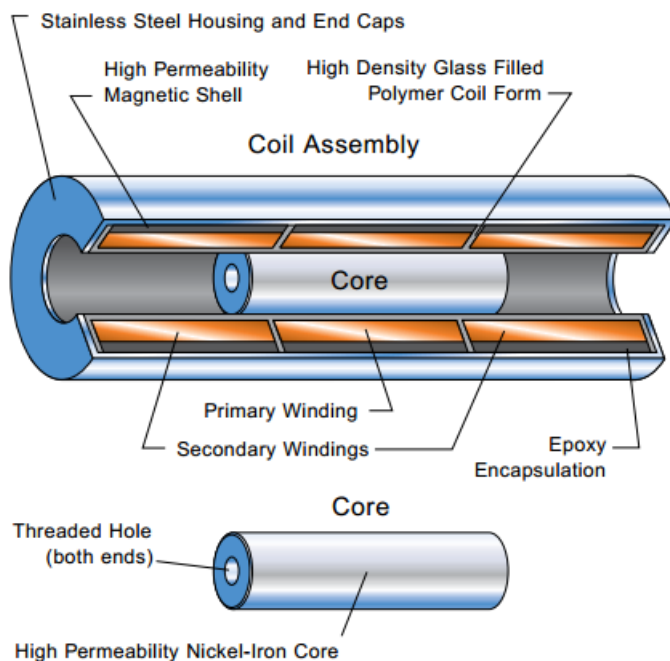


FIGURE 4.23 – Cutaway view of a typical LVDT sensor. Source: (MACROSENSORS, 2015)

An AC voltage excites the LVDT's primary winding, and it results in an induced differential AC voltage between its two secondary windings. Moving the ferromagnetic core within the primary and secondary windings will cause the secondary output voltage and phase to change, making possible to identify not only the position of the core, but also the direction of the core displacement. One of the key assets of LVDTs is that the moving core do not have any electrical contact with the stationary assembly part, what

contributes to high reliability and robustness for this type of sensors.

In this work, the actuator is instrumented with sensors to measure:

- i Piston Position (x_p);
- ii EHSV spool position (x_v);
- iii Differential pressure between actuators chambers (Δp).

To model the LVDTs in this work, it was used basic data from aerospace industry off-the-shelf sensors, particularly from (MACROSENSORS, 2015). The general specifications for the LVDTs implemented in this work are:

- i Linearity error: 0.1% – 0.25% of full range output
- ii Bandwidth 250Hz
- iii Hysteresis error < 0.01%

The linearity error will vary with the LVDT core position, achieving a maximum at the extremes and a minimal at neutral position, as shown in figure 4.24.

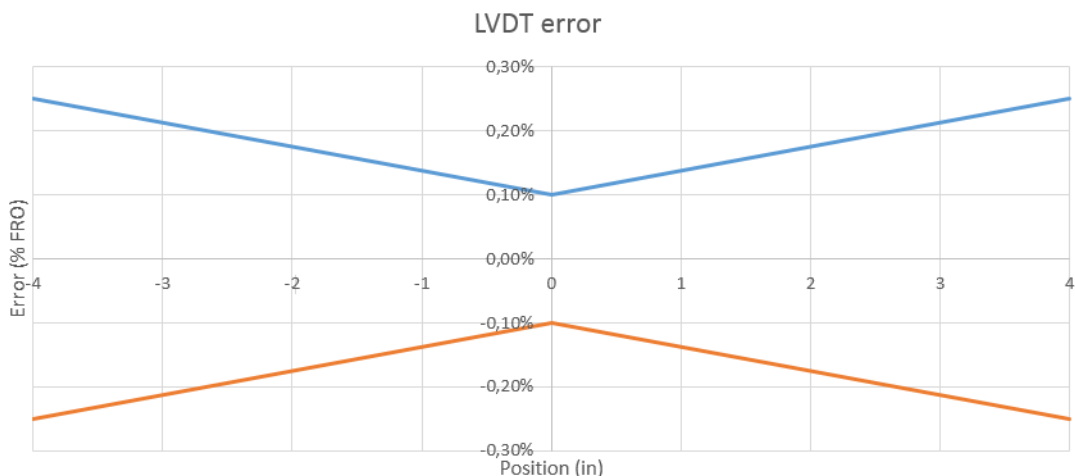


FIGURE 4.24 – LVDT error - for a LVDT range of + / – 4in

The final LVDT model can be seen in figure 4.25.

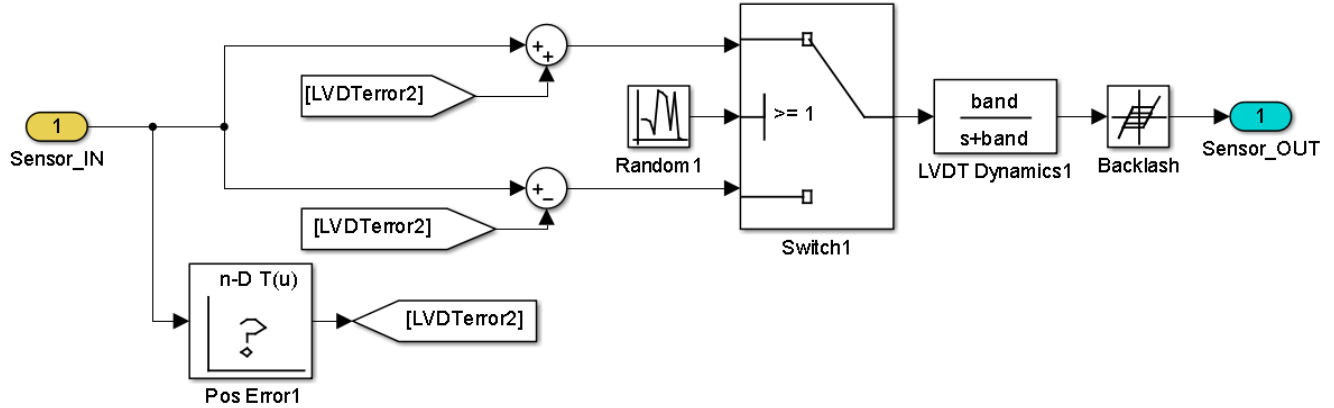


FIGURE 4.25 – LVDT model implemented

4.4 Model results and design requirements compliance

A step response, a frequency response and a dynamic stiffness test were simulated in order to validate the flight control actuator's model and evaluate the compliance of the designed actuator with performance and flutter suppression requirements.

4.4.1 Time response

A step input from 0 to 30 degrees was simulated in the rudder actuation system designed in previous chapter under the time response requirements conditions. It was used a simple proportional controller. Figure 4.26 shows the result obtained.

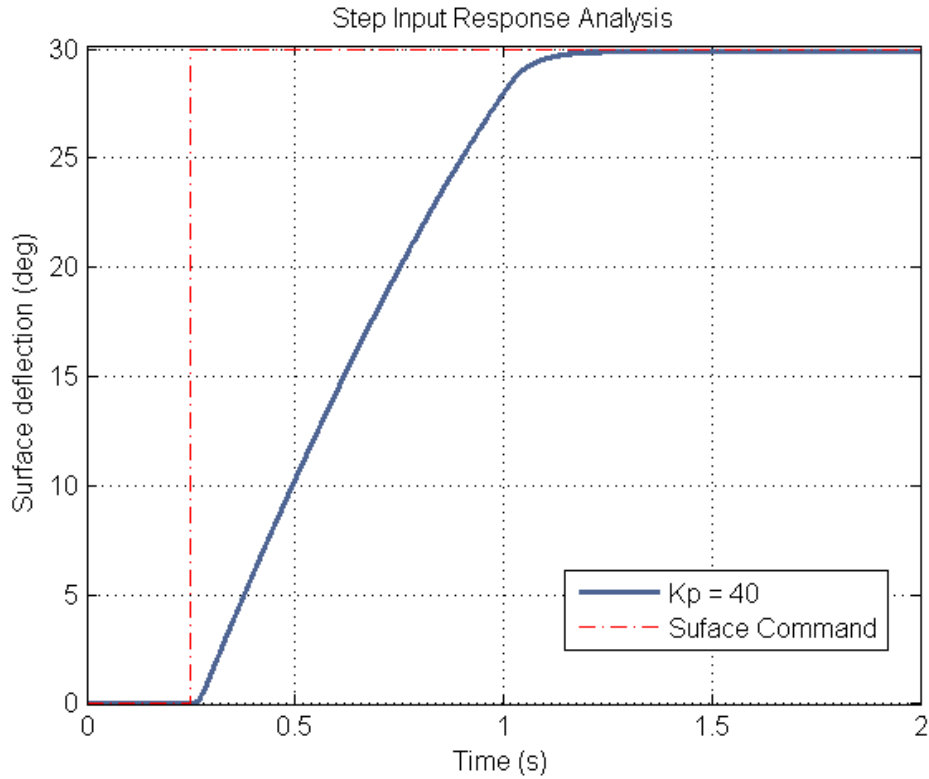


FIGURE 4.26 – Step Response - proportional controller gain $K_p = 40 \text{ mA/in}$

The compliance with time domain performance requirements are shown in table 4.1. As can be observed from table 4.1, the designed actuator comply with all time response requirements with a proper margin.

TABLE 4.1 – Rudder Actuator Design - Time Response Requirements Compliance

Actuator Design Validation - Time Response			
Design parameter	Requirement	Simulation	Status (%)
Settling time (ms)	< 850	690	PASS
Steady State error (%)	< 1	0.17	PASS
Overshoot (%)	< 10	0.0	PASS
Minimum Average rate (\circ/s)	> 32	34.94	PASS
Maximum Average rate (\circ/s)	< 36	34.94	PASS

In figure 4.27, it is possible to observe the instantaneous surface rate, the piston position, the applied aerodynamic hinge moment load and the friction force. The friction force is consistent to the expected behavior due to the Stribeck effect that was modelled: the friction force decays when the piston start moving, and increases when the piston stops.

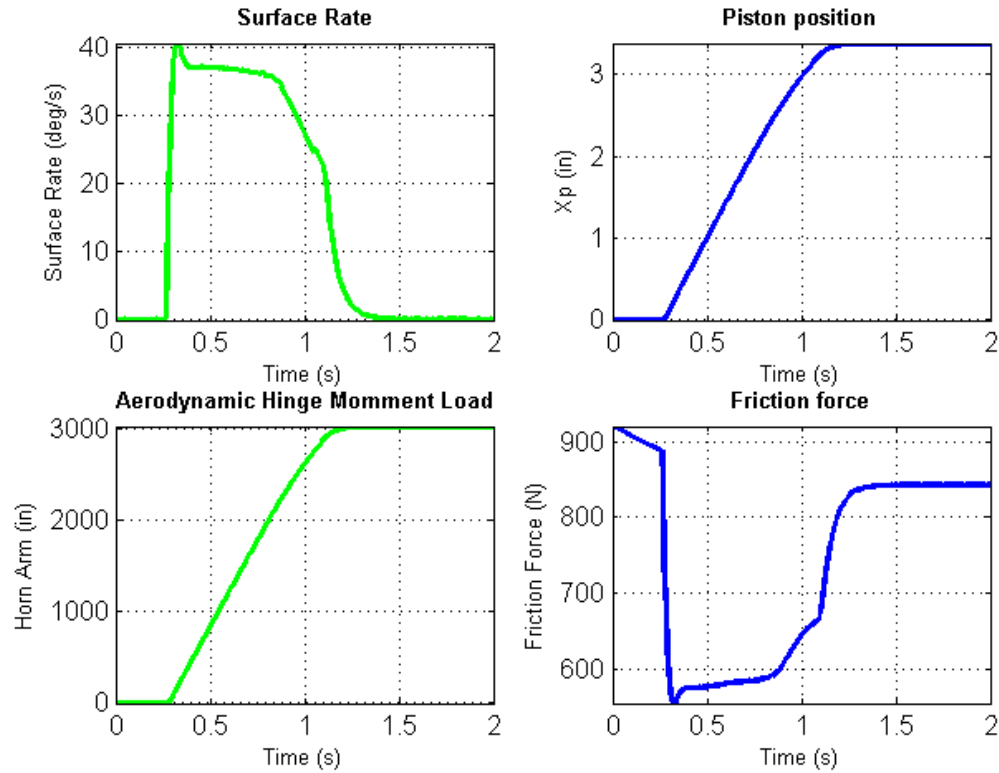


FIGURE 4.27 – Step Response - Overview

Figure 4.28 gives an overview of the actuator's oil column dynamic stiffness, which has an expected behavior (per chapter 3 results): it is greater at the piston final position and smaller at piston neutral position.

Also, the bulk modulus variation can be analyzed in figure 4.28, the pressure in the extension chamber grows, increasing the fluid bulk modulus in this chamber, a result expected as seen in chapter 2.

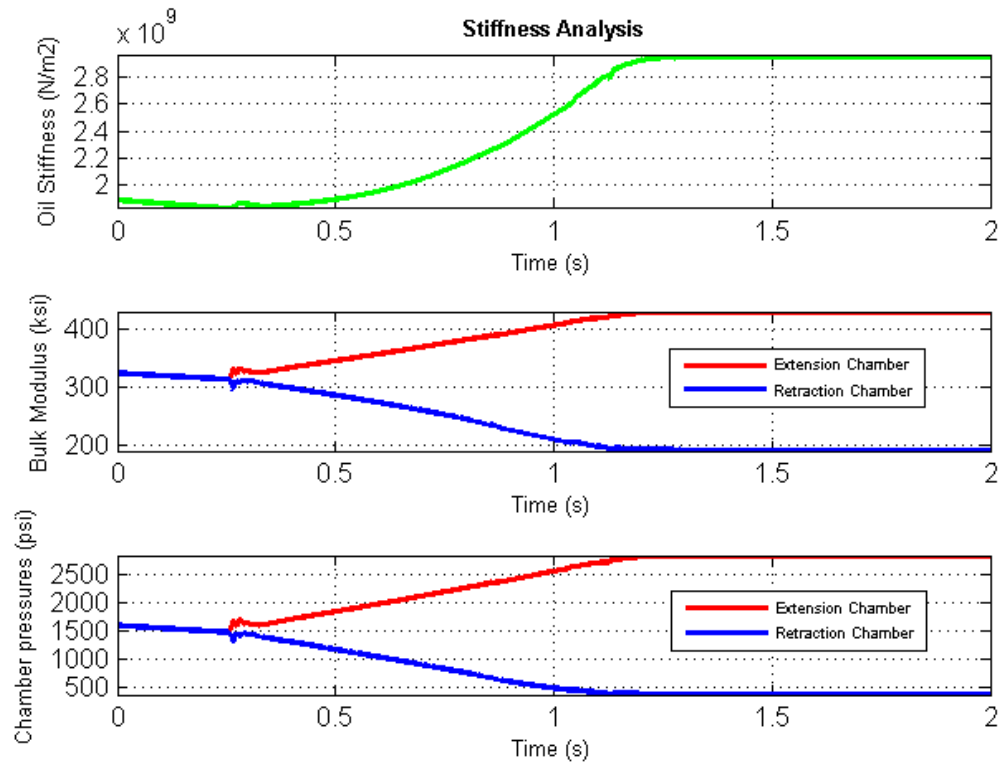


FIGURE 4.28 – Step Response - Stiffness Analysis

The EHSV behavior can be analyzed in figure 4.29, the EHSV spool position and the current command reach their maximum value during the actuator extension, as expected. The chambers flows are around 2 to 4 gpm during the actuator extension period and are in the expected range from EHSV design (later illustrated in chapter 5).

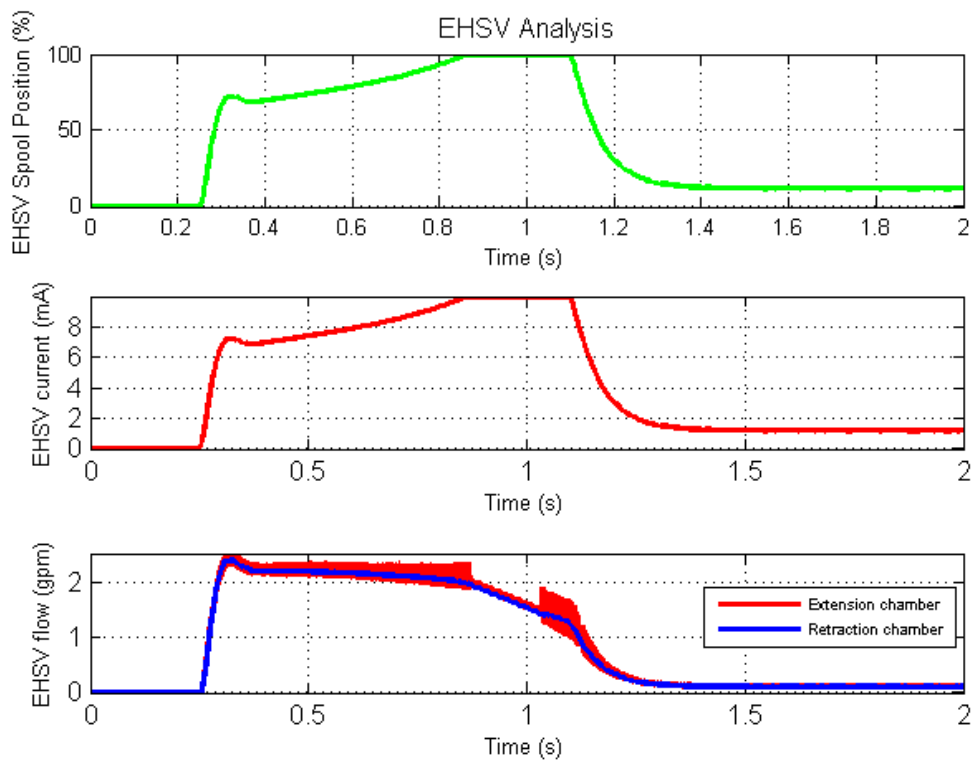


FIGURE 4.29 – Step Response - EHSV Analysis

4.4.1.1 Actuator Loaded Rate Capability

To better characterize the actuator performance, it is interesting to have its loaded rate capability. Therefore, it was applied constant linear compression loads to the actuator with different current step inputs in the EHSV. The surface average rate obtained for each condition is graphically represented in figure 4.30.

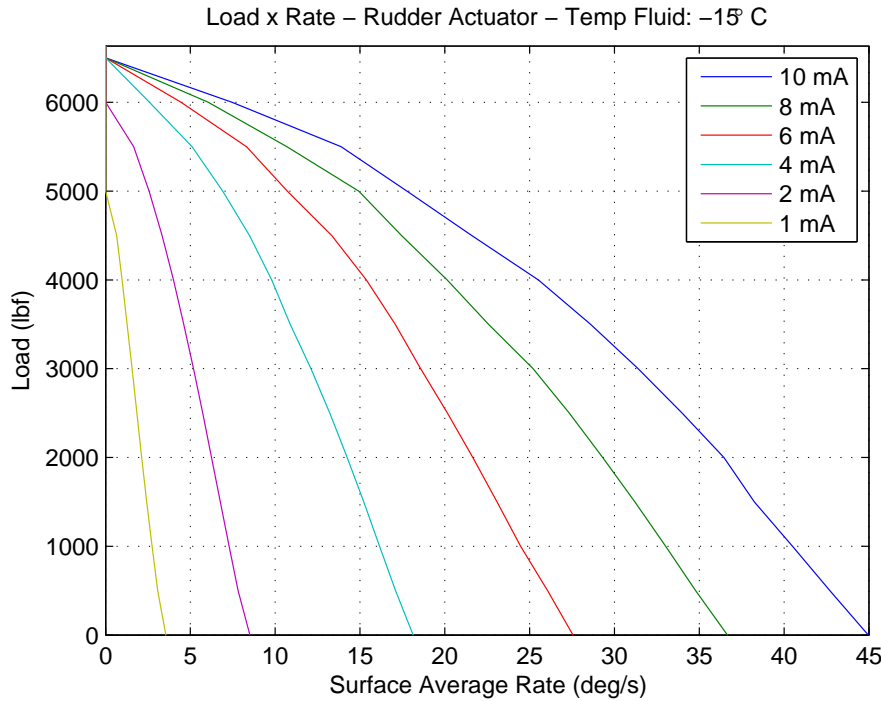


FIGURE 4.30 – Linear Load x Surface Rate

From 4.30, it can be observed that the maximum actuator no loaded rate determine an average surface rate around 45 deg/s. In addition, it can be concluded that the actuator stall load is around 6600 lbf.

4.4.2 Frequency Response

For the rudder flight control actuator frequency response, the results are presented in table 4.2 and can be seen in figure 4.31.

TABLE 4.2 – Rudder Actuator Design - Frequency Response Requirements Compliance

Actuator Design Validation - Frequency Response			
Design parameter	Requirement	Simulation	Status
Gain margin (dB)	≥ 10	17.04	PASS
Phase margin ($^\circ$)	≥ 45	inf	PASS

The actuator gain margin achieved in simulation is well above the requirement. For the phase margin, the simulated actuator's frequency response gain does not cross the 0 dB; therefore, it has an infinite phase margin. It is possible to conclude that the actuator is stable and has a 6.59 Hz of bandwidth, which is a typical value found in the industry for an actuator of the same size.

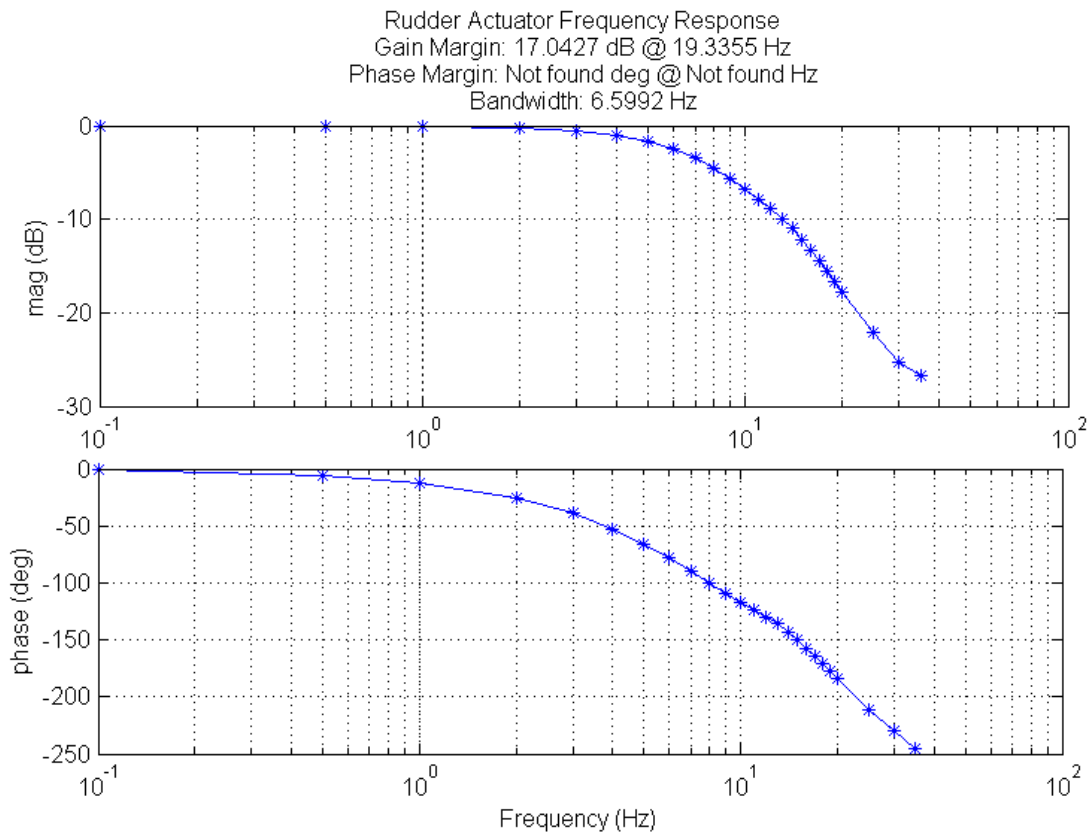


FIGURE 4.31 – Rudder actuator's frequency response for different fluid temperatures

4.4.3 Dynamic Stiffness

A dynamic stiffness simulation was ran to evaluate the actuator design compliance with flutter suppression requirement, the results are shown in figure 4.32.

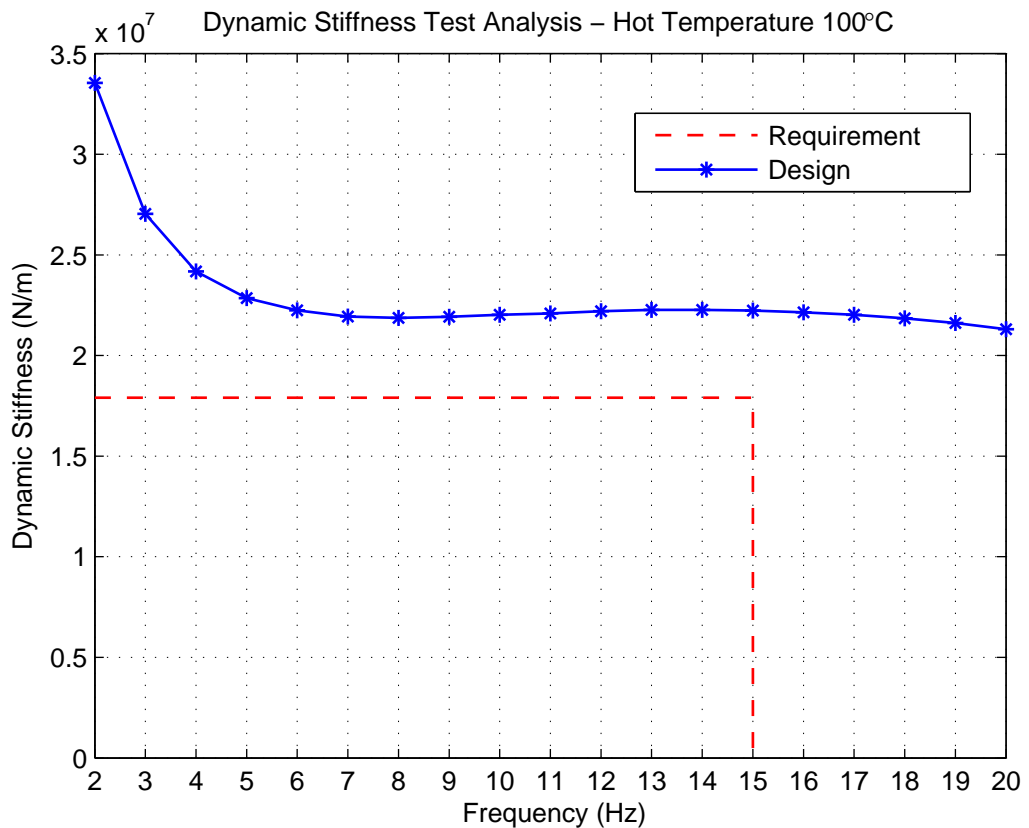


FIGURE 4.32 – Dynamic Stiffness test in hot temperature - compliant with requirement

It can be concluded that the actuator dynamic stiffness exceeds the required dynamic stiffness value for the infinite stiffness frequency of 15 Hz. Thus, it is possible to guarantee that, during normal actuator operation, there will be no coupling between the rudder control surface rotational mode and the aircraft aeroelastic modes. The designed rudder hydraulic actuation system comply with flutter suppression requirements.

5 Control Strategies

This chapter presents different control strategies adopted to enhance the actuator dynamic stiffness and comply with time and frequency response requirements.

5.1 Parametric Study

This section presents a parametric study performed with the help of the model developed in chapter 4. The main goal of this section is to characterize the influence of the EHSV size and proportional controller gain on dynamic stiffness, time response and frequency response of a flight control actuator. In addition, it will be evaluated the influence of the control loop update rate and the actuator's internal leakage in the dynamic stiffness response.

5.1.1 EHSV second stage size

The effect of the EHSV's output flow in the performance response of the actuator is analyzed in this section. The actuator's position controller is set as a simple proportional gain ($K_p = 40mA/in$, this value will be explained in next section).

The EHSV output flow was controlled by changing the EHSV's second stage slot size, increasing the slot width size (X_{width}), the flow gain delivered from the EHSV to the actuator's chambers increases. Figure 5.1 shows the EHSV flow gain output to a ramp current input (from -10 mA to +10 mA) for different EHSV slot's width (X_{width}). As can be seen, if the EHSV slot is increased, its output flow gain increases.

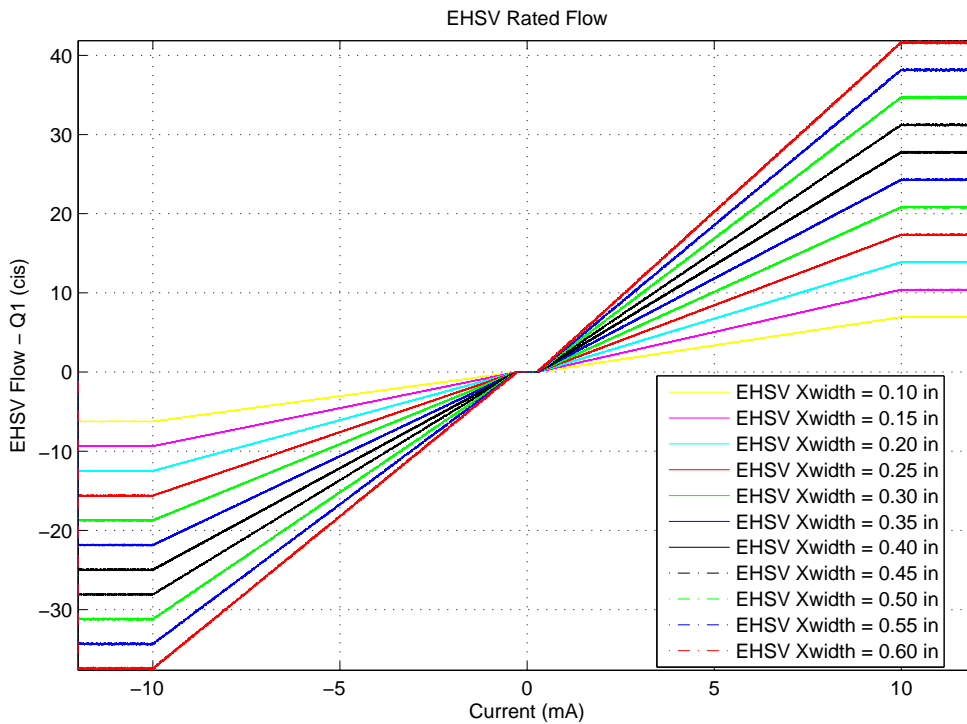


FIGURE 5.1 – EHSV flow output x EHSV current

The actuator's step response is presented in figure 5.2. As expected, increasing the EHSV flow gain leads to a faster time response with a higher average surface rate and in some cases leads to an overshoot, as it can be observed in table 5.1. After a certain EHSV's second stage slot size, the time responses performance becomes very similar, as it can be seen in figure 5.2, this is due to the actuator's stall load capability, determined by the piston area.

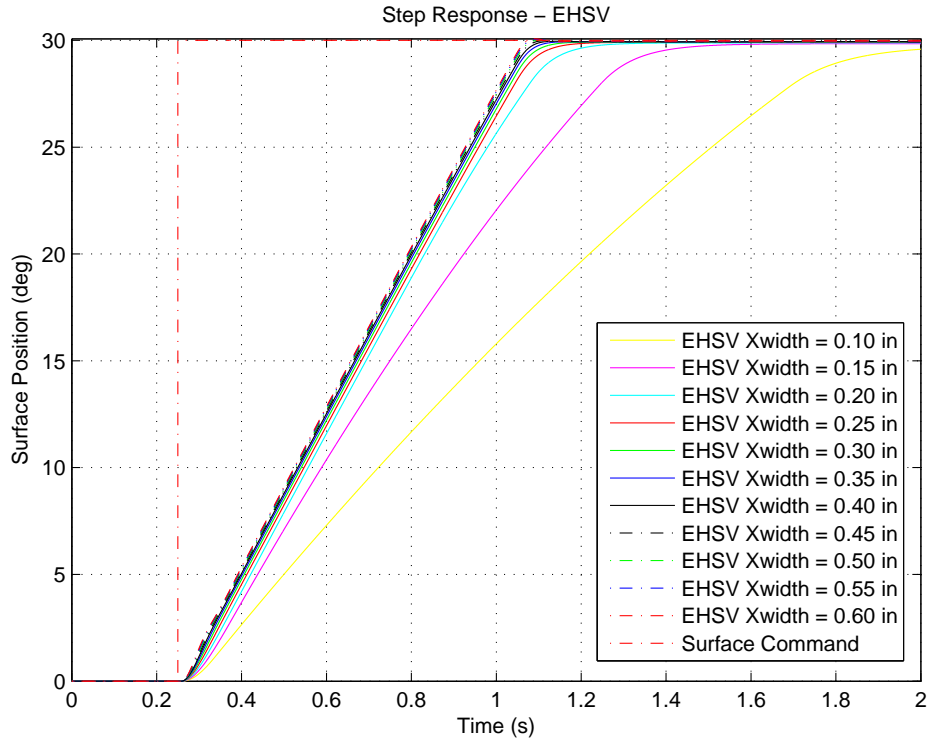


FIGURE 5.2 – Time response for different EHSV flow output

TABLE 5.1 – Rudder Actuator Design - Time Response Requirements Compliance EHSV study

EHSV slot size - Time Response Performance						
Design parameter	Requirement	0.10in	0.20in	0.40in	0.60in	
Settling time (ms)	< 850	1531	690	568	550	
Steady State error (%)	< 1	0.35	0.18	0.09	0.06	
Overshoot (%)	< 10	0.0	0.0	0.0	0.2	
Minimum Average rate (<i>deg/s</i>)	> 32	18.37	34.94	37.07	37.38	
Maximum Average rate (<i>deg/s</i>)	< 36	18.37	34.94	37.07	37.38	

The actuator frequency response is also influenced by the EHSV's slot size as it is shown in figure 5.3. Increasing the EHSV slot size leads to a frequency response resonant peak. In addition, the actuator's bandwidth increases.

The resonance peaks in the gain response reflect a underdamped EHSV response caused by the increasing of its output flow gain. Thus, from table 5.2, the actuator gain and phase margin decreases and the bandwidth increases while increasing the EHSV size.

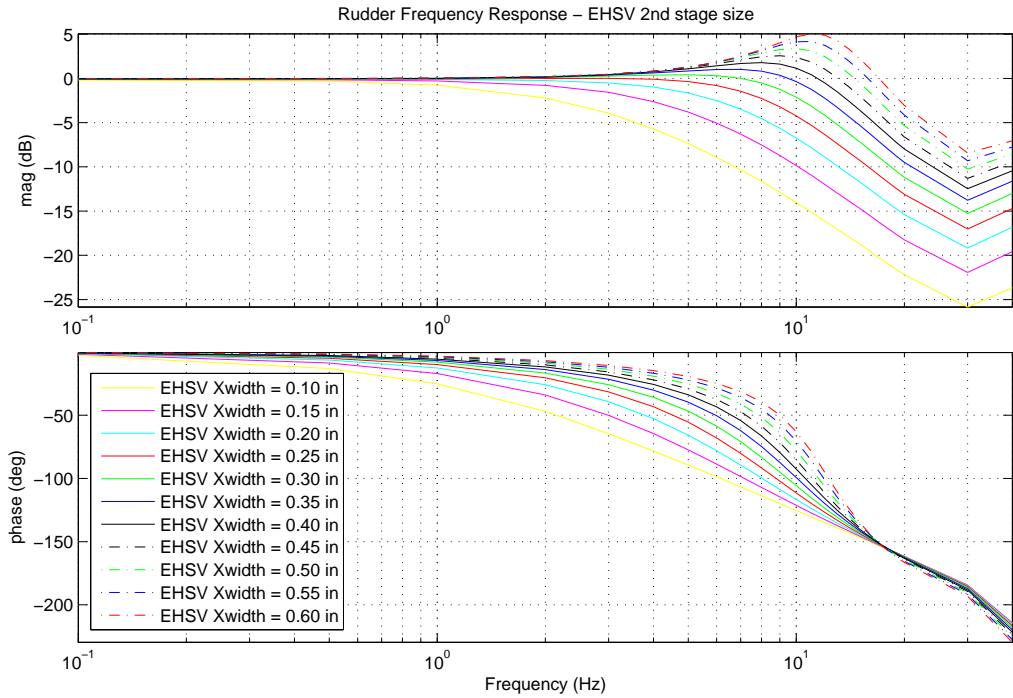


FIGURE 5.3 – Frequency Response for different EHSV flow output

TABLE 5.2 – Rudder Actuator Design - Frequency Response Requirements Compliance EHSV study

EHSV slot size - Frequency Response Performance					
Design parameter	Requirement	0.10in	0.20in	0.40in	0.60in
Gain margin (dB)	≥ 10	25.15	18.38	10.98	5.78
Phase margin (deg)	≥ 45	<i>inf</i>	<i>inf</i>	70.11	29.90
Bandwidth (Hz)	<i>None</i>	2.57	6.60	14.47	19.97

From figure 5.4, it is observed that as the EHSV's second slot size increases, the actuator's dynamic stiffness response begins to decay after a certain EHSV slot size until it violates the dynamic stiffness design requirement.

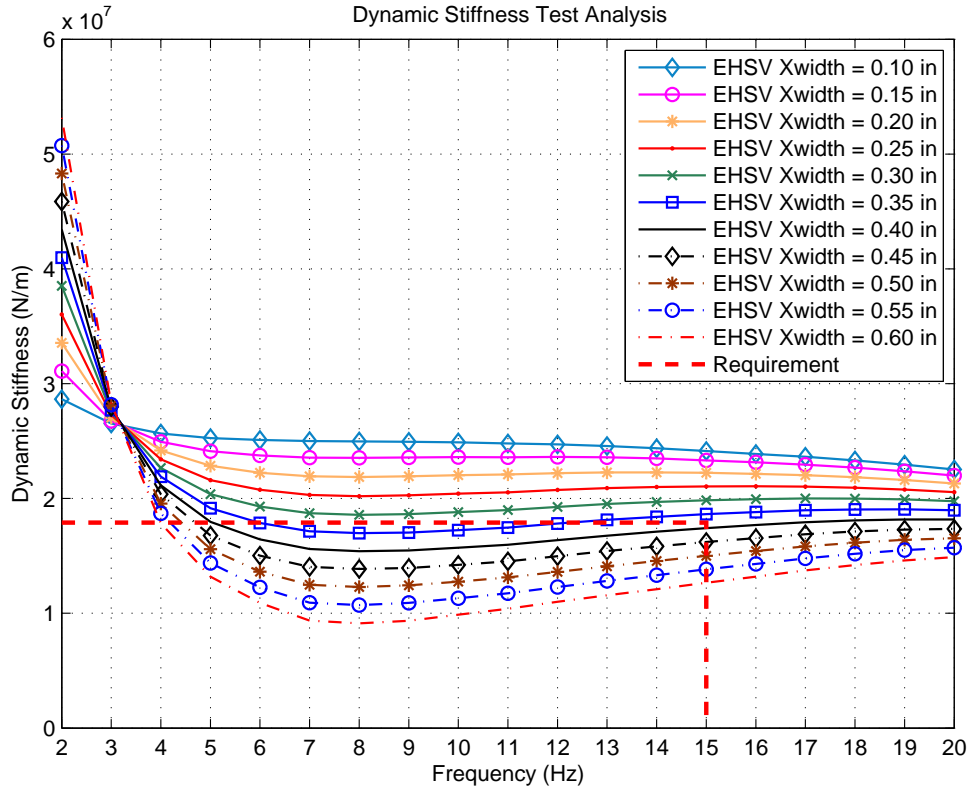


FIGURE 5.4 – Dynamic Stiffness for different EHSV flow output

Comparing figures 5.4 and 5.3, it is possible to realize that after an EHSV second stage slot size, the actuator's frequency response begins to present resonance gain peaks, which correspond to the minimum actuator's dynamic stiffness.

It can be concluded that increasing the EHSV's output flow can bring benefits to the actuator performance, but after a certain output flow value the benefits for time response and frequency response are not so significant and the actuator dynamic stiffness begins to decrease and violates the dynamic stiffness design requirement.

Regarding the EHSV slot size, it was chosen the EHSV slot width of 0.20 in. The main reason is that it determines a good actuator performance for time and frequency response and the actuator's dynamic stiffness response still exceeding the requirement with a comfortable margin.

5.1.2 Proportional Controller

The proportional controller implemented in this work can be represented by equation 5.1.

$$u(t) = K_p e(t) = K_p(r(t) - y(t)) \quad (5.1)$$

The control signal (u) is proportional by a gain (K_p) to the error (e) between the command position signal ($r(t)$) and the feedback piston position sensor signal ($y(t)$). As the position control loop implemented is a digital control loop, the controller implemented is represented by equation 5.2, a discrete version of equation 5.1.

$$u[n] = K_p e[n] \quad (5.2)$$

where $e[n]$ is the error discrete-time signal at time instant n and $u[n]$ is the control discrete-time signal value at time n . Moreover $n = kT_s$, where k is a positive natural number and T_s is the control loop sampling time.

The parametric study in this section consists of varying the proportional control gain K_p and analyzing the actuator's dynamic stiffness, time and frequency response. The control loop update rate is kept at 500 Hz, and the EHSV slot width (X_{width}) is 0.20 in.

From figure 5.5, the actuator's step response becomes faster as the controller gain is increased. After a certain gain, the proportional gain effect is not so important to the actuator's time response, because the actuator has reached its maximum rate capability.

As presented in table 5.3, augmenting the proportional control gain will increase the average rate response, up to a maximum value determined by the actuator's physical properties and non-linearities (e.g., saturations, stall load capability).

The settling time value decreases while augmenting the K_p gain and the same decreasing effect is observed by the steady state error.

Therefore, for low proportional gain values, the actuator time response is not compliant with its time design requirements, but after a certain gain value, it is always compliant.

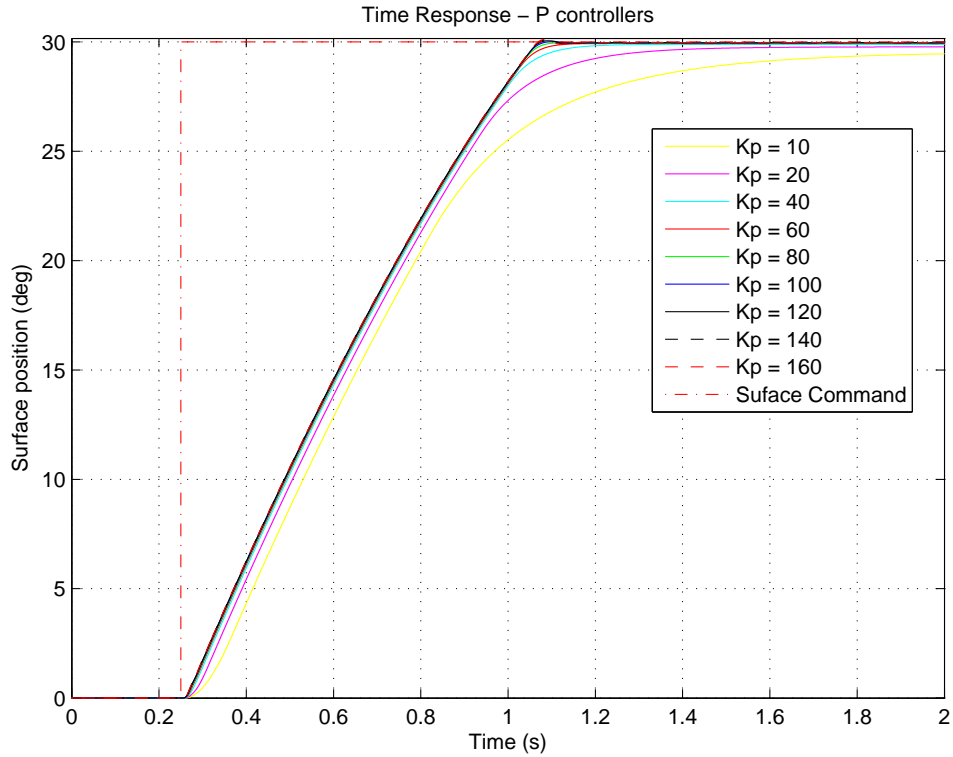


FIGURE 5.5 – Time Response for different proportional gains

TABLE 5.3 – Rudder Actuator Design - Time Response Requirements Compliance P controller

Kp gain controller - Time Response Performance						
Design parameter	Requirement	10	40	80	120	160
Settling time (ms)	< 850	1670	690	629	618	613
Steady State error (%)	< 1	0.68	0.18	0.09	0.06	0.05
Overshoot (%)	< 10	0.0	0.0	0.0	0.0	0.0
Minimum Average rate (deg/s)	> 32	29.33	34.94	35.17	35.24	35.24
Maximum Average rate (deg/s)	< 36	29.33	34.94	35.17	35.24	35.24

The proportional action can be better observed while performing a step response for a lower reference command without external load, as shown in figure 5.6. Overshoots are observed for high proportional gains, while for low proportional gains an unexpected steady-state error is identified. This steady-state error is explained by the deadband nonlinearity from the EHSV spool overlap that leads the EHSV to do not deliver flow to the actuator chambers for small values of current command, so even if with a steady-state error, the controller action is suppressed by the EHSV deadband zone.

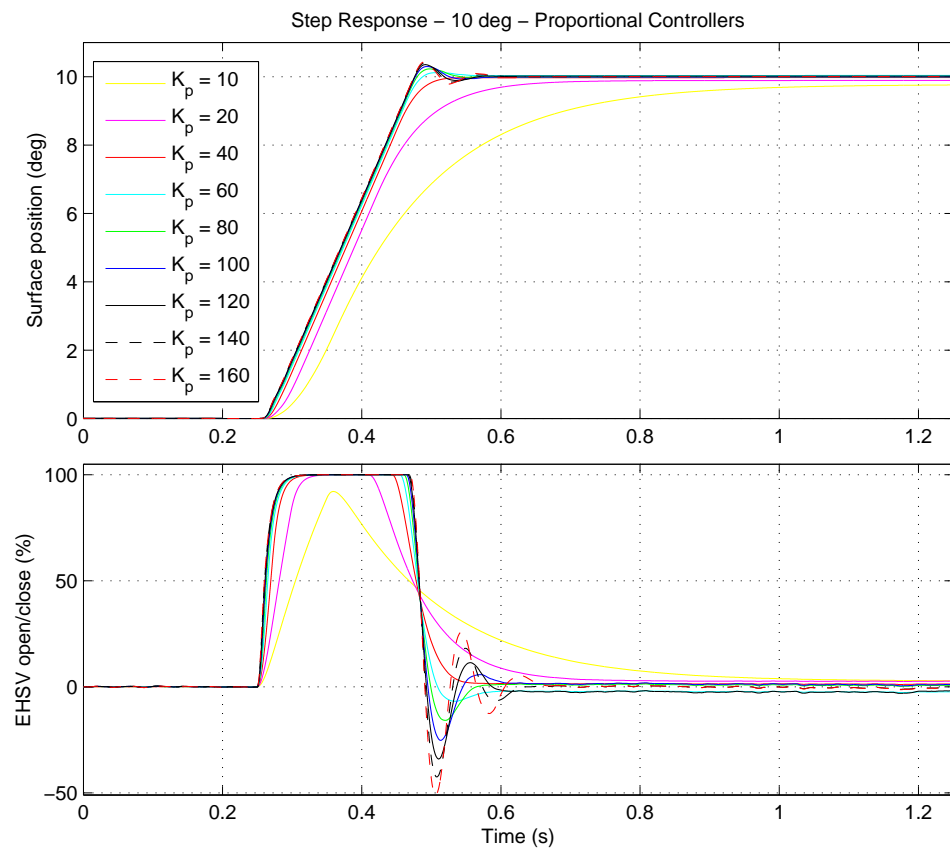


FIGURE 5.6 – Step Response for different proportional gains

As K_p gain increases, the actuator frequency response gain increases and starts to present resonance peaks after certain K_p value and the phase of the actuator frequency response shifts to the right. The results are shown in figure 5.7.

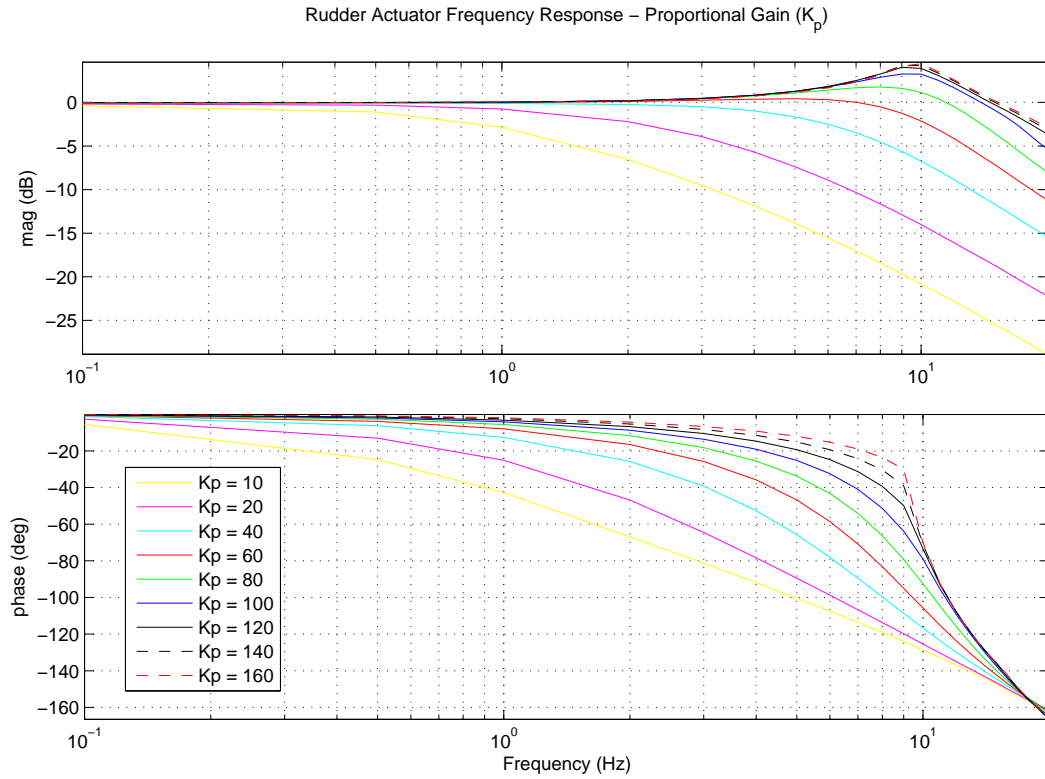


FIGURE 5.7 – Frequency Response for different proportional gains

From table 5.4, it is possible to observe that the gain margin decreases as the proportional gain increases, the same decreasing effect is observed in the phase margin. The actuator's bandwidth starts at low values, and as K_p is increased, the bandwidth increases. Those effects together with the gain resonance peaks prove that the actuator's response becomes faster and less stable as the controller proportional gain is increased.

TABLE 5.4 – Rudder Actuator Design - Frequency Response Requirements Compliance P controller

K _p gain controller - Frequency Response Performance						
Design parameter	Requirement	10	40	80	120	160
Gain margin (dB)	≥ 10	32.02	18.38	10.98	6.11	4.40
Phase margin (deg)	≥ 45	<i>inf</i>	<i>inf</i>	70.11	46.46	42.34
Bandwidth (Hz)	<i>None</i>	1.15	6.60	14.47	19.05	20.50

Figure 5.8 shows the dynamic stiffness response for different proportional control gains. It is possible to observe that increasing the K_p gain determines a decrease of the actuator's dynamic stiffness response after a frequency around 4 Hz and the actuator violates the requirement for proportional control gains higher than 120 mA/in. From 0 to 4 Hz, the dominant effect is the friction effect and a faster actuator control loop will improve the

performance in this range of frequencies.

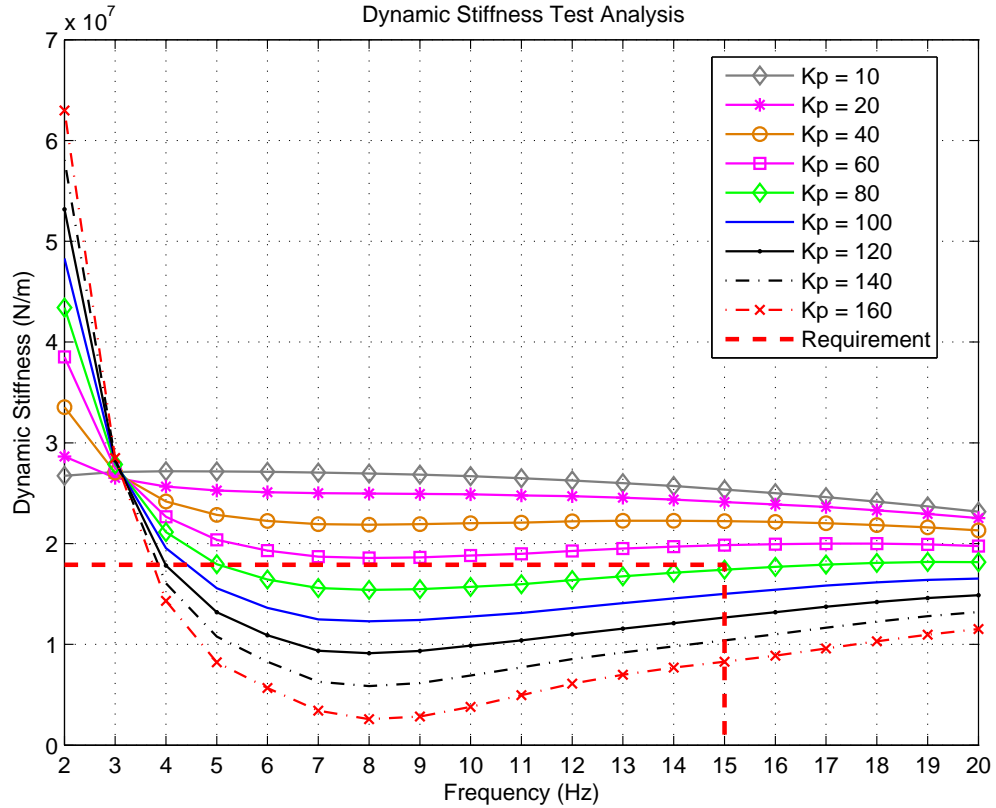


FIGURE 5.8 – Dynamic Stiffness test for different proportional gains

It can be concluded that a higher K_p gain brings benefits to the actuator performance, especially for time and frequency response. However, after a certain gain value, the benefits for time response and frequency response are not so significant and the actuator's dynamic stiffness begins to decrease and violates flutter suppression design requirement.

Thus, the position control loop with a $K_p = 40 \text{ mA/in}$ and an EHSV slot width of 0.20 in determines an actuator performance that comply with time and frequency response with certain margin. In addition, the actuator's dynamic stiffness exceeds its requirement with a comfortable margin. Consequently, this proportional gain value and EHSV size will be maintained for further analysis.

5.1.3 Control loop update rate study

With the growing reliability of electronic components and the decreasing cost of digital devices, the aerospace industry has begun to adopt digital technologies, and the actuator's control loop is typically implemented in a digital device. Thus, it is important to determine the influence of the control loop's update rate in the actuator's dynamic stiffness response.

Figure 5.9 shows the dynamic stiffness of an actuator with a proportional digital position control loop ($K_p = 40mA/in$) for different control loop update rate.

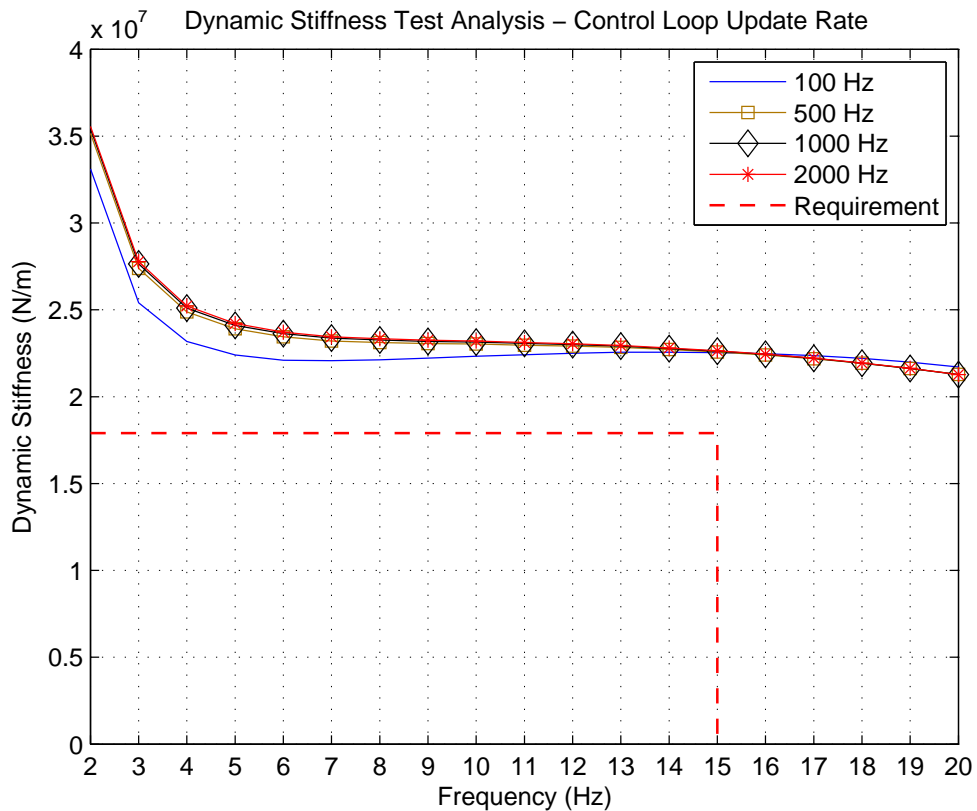


FIGURE 5.9 – Dynamic Stiffness Response for different control loop's update rates

As it is possible to observe in figure 5.9, increasing the control loop update rate helps to increase the actuator's dynamic stiffness up to 15 Hz, approximately. Above this frequency, the update rate increase determines a dynamic stiffness decrease. For control loop's update rates above 500 Hz, the influence of this parameter in the dynamic stiffness response is minimal.

It can be concluded that even if the control loop update rate is increased, which in theory would determine a faster control response, the actuator's dynamic stiffness does not always increase: for all control loop update rates simulated, after a certain frequency, there is a limiting effect that does not allow a dynamic stiffness enhancement.

At 15 Hz, from the EHSV slot size study, the actuator's frequency response (EHSV slot size .20 in), shown in figure 5.3, presents a phase delay around 120 deg. This fact can explain why a faster control loop will not determine a better actuator's dynamic stiffness response in all frequencies.

Thus, those results help to identify that the EHSV has a major influence in the actuator's dynamic stiffness and that influence is greater than the update rate of the position

control loop.

5.1.4 Internal Leakage

The internal leakage between the hydraulic actuator's chambers is present during normal operation of hydraulic actuation systems. Hence, it is important to determine its influence in the actuator's dynamic stiffness.

A common failure in hydraulic actuation systems is the actuator's seal failure. This failure will contribute to increase the internal leakage between the actuator's chambers. Typically, this kind of failure needs to be considered in the actuator's safety analysis, since it will affect the actuator performance and safety.

The influence of the internal leakage in the actuator dynamics stiffness is shown in figure 5.10.

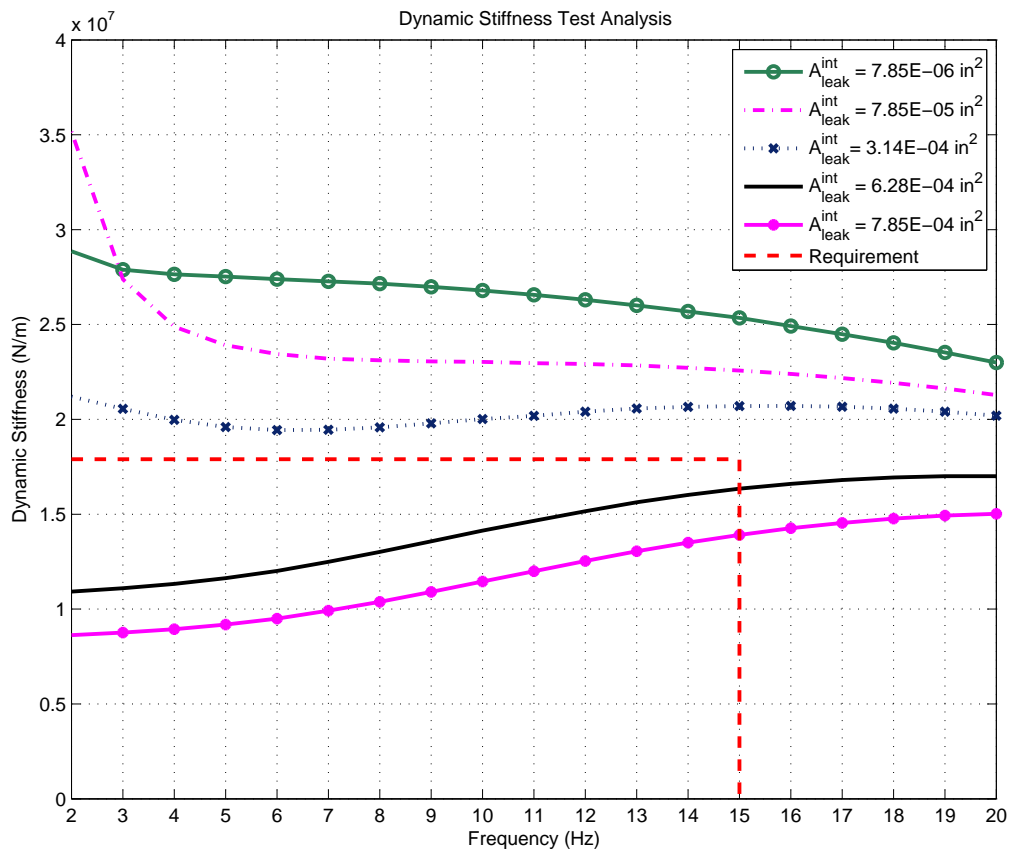


FIGURE 5.10 – Dynamic Stiffness Response for different internal leakage values

As it can be observed, the internal leakage growth will help to diminish the overall actuator dynamic stiffness, and determine a major degradation at frequencies up to 20

Hz. In addition, it can be concluded that if an actuator were constructed with small internal leakage, it would bring benefits for its dynamic stiffness, as it would have an overall increase.

Thus, a hydraulic seal failure may determine non-compliance with flutter suppression requirement, which could lead to a catastrophic failure.

5.2 Control Strategies

In this section, different position control strategies will be presented and the actuator's time response, frequency response and dynamic stiffness will be evaluated.

5.2.1 Classic Controllers

The classic control strategy adopted in this work is based on the classic PID controller (ASTROM; MURRAY, 2009), which the proportional, integral and derivative actions are summed in a parallel configuration. This control strategy is represented by equation 5.3.

$$u(t) = K_p e(t) + K_i \int_0^t e(\tau) d\tau + K_d \frac{de(t)}{dt} \quad (5.3)$$

where $u(t)$ is the continuous-time control signal, $e(t)$ is the feedback error signal, K_p represents the proportional gain, K_i corresponds to the integral gain and K_d is the derivative gain.

Applying the Laplace transform in equation 5.3, the PID controller is represented as follows:

$$U(s) = \left(K_p + \frac{K_i}{s} + K_d s \right) E(s) \quad (5.4)$$

where $U(s)$ and $E(s)$ are the laplace-transform of control and error feedback signals.

Since the actuator control loop in aeronautics industry applications is typically implemented in a digital device, PID controller shall be transformed into a digital PID controller. For the transformation from continuous to discrete PID controller, it was chosen the Tustin or bilinear approximation, which yields the mapping between continuous-time and discrete-time systems (ASTROM; WITTENMARK, 1997).

The Tustin transformation relates the s-domain with the z-domain by equation 5.5.

$$s \longleftrightarrow \frac{2}{T_s} \frac{z - 1}{z + 1} \quad (5.5)$$

where T_s is the discrete system sample time.

Therefore, substituting 5.5 into 5.4 give us:

$$U(z) = \left(K_p + K_i \frac{T_s}{2} \frac{z+1}{z-1} + K_d \frac{2}{T_s} \frac{z-1}{z+1} \right) E(z) \quad (5.6)$$

Figure 5.11 represents the implemented structure in the actuator model. The main difference from the theoretical discrete PID (equation 5.6) is the discrete derivative substituted by a digital high-pass filter. The discrete derivative was implemented as high-pass digital filter to have a smooth derivative, not generating noisy control signals. Equation 5.7 illustrates this implementation:

$$U(z) = \left(K_p + K_i \frac{T_s}{2} \frac{z+1}{z-1} + K_d \frac{N}{1 + N \frac{T_s}{2} \frac{z+1}{z-1}} \right) E(z) \quad (5.7)$$

where N is the high-pass filter coefficient.

Also, the anti-windup structure was added to the controller model implemented as seen in figure 5.11. The integrator windup is a nonlinear phenomenon that occurs because the system operating in a certain condition may have the control variable reaching the actuator limits. When it occurs, the actuator saturates and corresponds to an open-loop situation. While the error is non-zero, the integral action will build up to compensate, becoming very large and inducing large transients in the system response.

The anti-windup technique is used to prevent an integral windup. The anti-windup structure adopted is the back calculation strategy (ASTROM; MURRAY, 2009). This strategy consists of decreasing the integral term of the PID controller when the control variable surpass the actuator limits, as observed in figure 5.6. In the flight control actuator implementation, when the actuator controller current command sent to the EHSV (control variable) is greater than the EHSV current limit (actuator saturation), the integral term is decreased avoiding large transients in the actuator response.

Figure 5.11 illustrates the discrete PID controller implemented in this work.

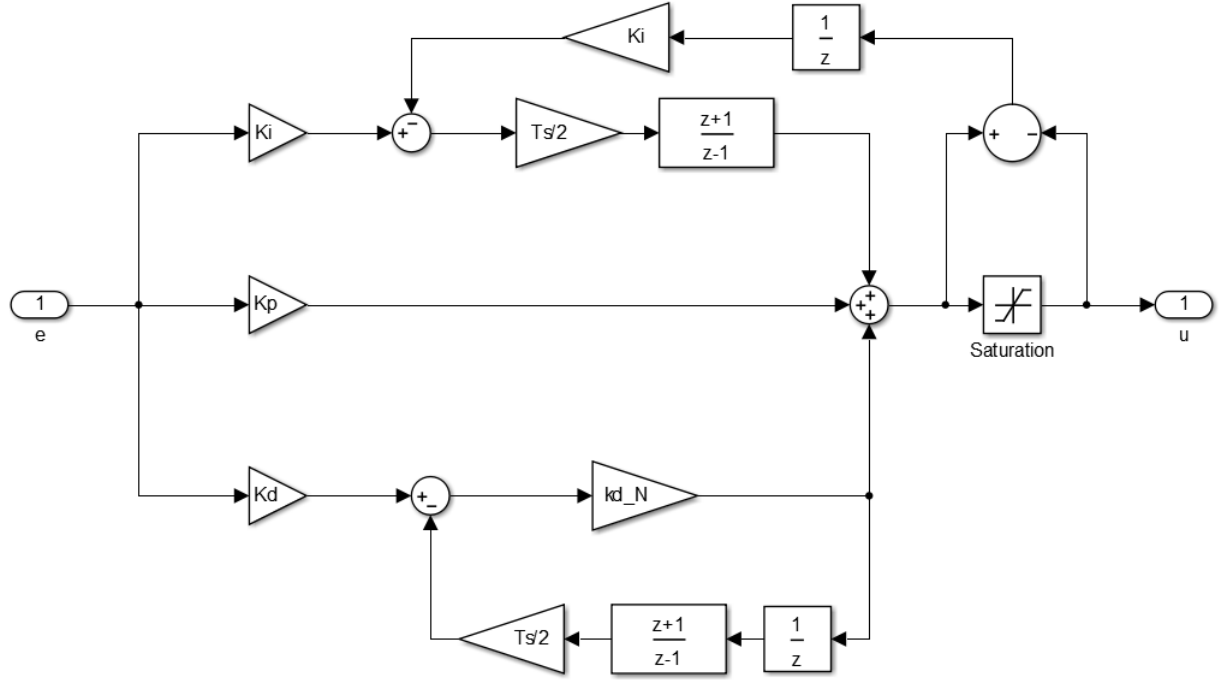


FIGURE 5.11 – Discrete parallel PID implementation

The sampling frequency ($F_s = \frac{1}{T_s}$) adopted for the actuator control loop is 500 Hz. The parallel implementation brings to the model the flexibility to implement different controllers by simply adjusting gains, e.g. pure proportional (P), proportional and integral (PI), proportional and derivative (PD) and proportional-derivative and integral (PID) controllers.

5.2.1.1 Proportional Integral (PI) Controller

The proportional integral controller was implemented using the previously described discrete PID controller (figure 5.6) and bringing the derivative gain K_d to zero.

The main objective is to investigate the effect of the controller integral term in the actuator performance, thus the proportional gain K_p was maintained at $40mA/in$ and the integral gain K_i was varied.

Figure 5.12 shows the actuator step response for different controller integral gains. As expected, the integral action acts to eliminate the steady-state error, as observed per table 5.5. In addition, the integral gain increase does not have major influence in the other time response requirements.

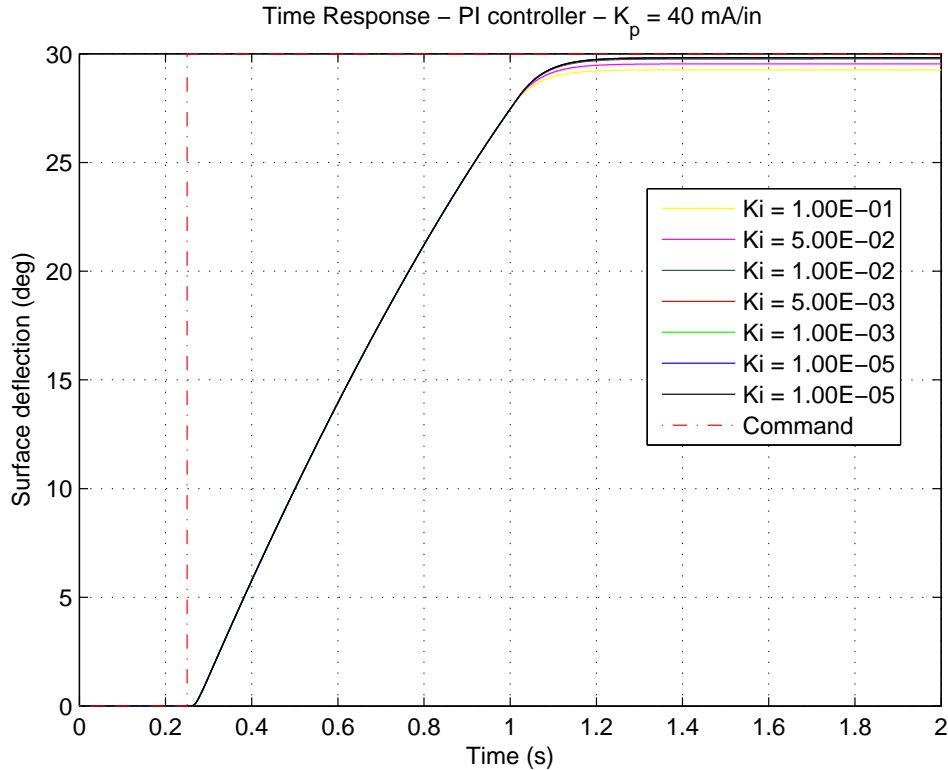


FIGURE 5.12 – Time Response for different integral gains

TABLE 5.5 – Rudder Actuator Design - Time Response Requirements Compliance PI controller

PI controller - K_i variation - Time Response Performance						
Design parameter	Requirement	$1E - 1$	$5E - 2$	$1E - 3$	$1E - 4$	$1E - 5$
Settling time (ms)	< 850	712	710	709	709	709
Steady State error (%)	< 1	0.31	0.29	0.27	0.27	0.27
Overshoot (%)	< 10	0.0	0.0	0.0	0.0	0.0
Minimum Average rate (deg/s)	> 32	34.45	34.45	34.45	34.45	34.45
Maximum Average rate (deg/s)	< 36	34.45	34.45	34.45	34.45	34.45

The integral action for a lower step reference command and no external load can be observed in figure 5.13. The integral action inserts a pole at the origin in the system root-locus plan, and for a type-1 system (plant with inherent integral action) this does not bring any benefit for step command tracking. As it can be seen, for high integral gains the response rising time becomes smaller and it tends to eliminate the error by smoothly ramping the surface position.

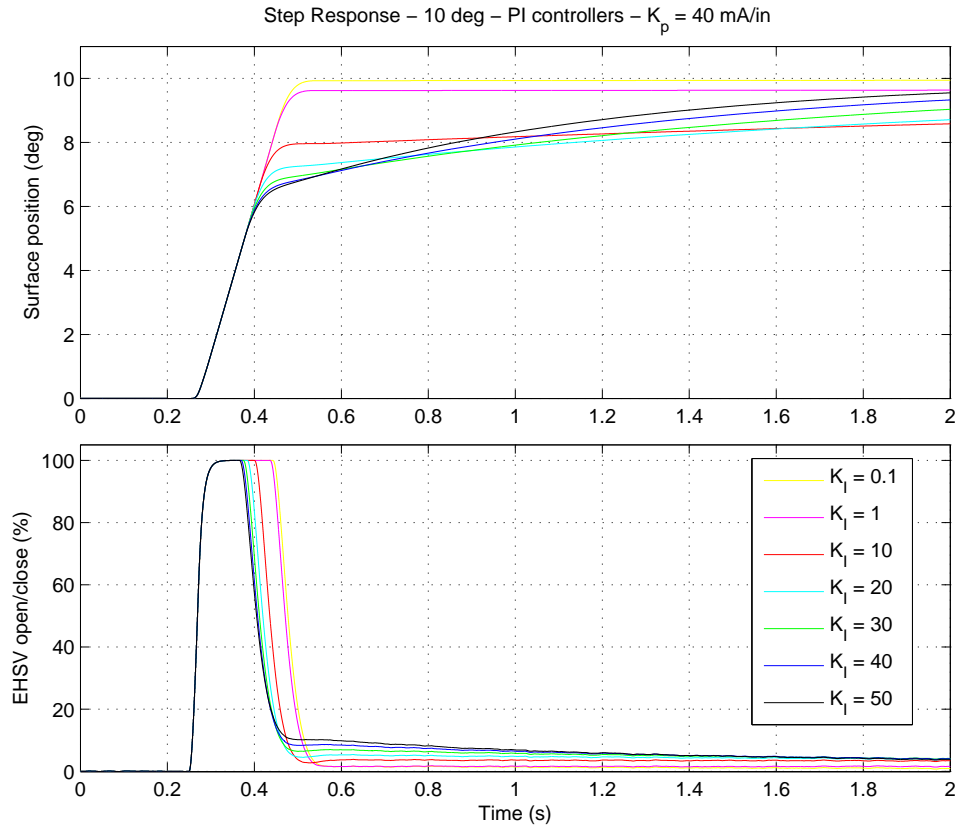


FIGURE 5.13 – Step Response for different integral gains

The actuator frequency response for different controller integral gains is shown in figure 5.14 and table 5.6 summarizes the frequency response performance results. As K_i is reduced the gain margin, phase margin and bandwidth do not present any change.

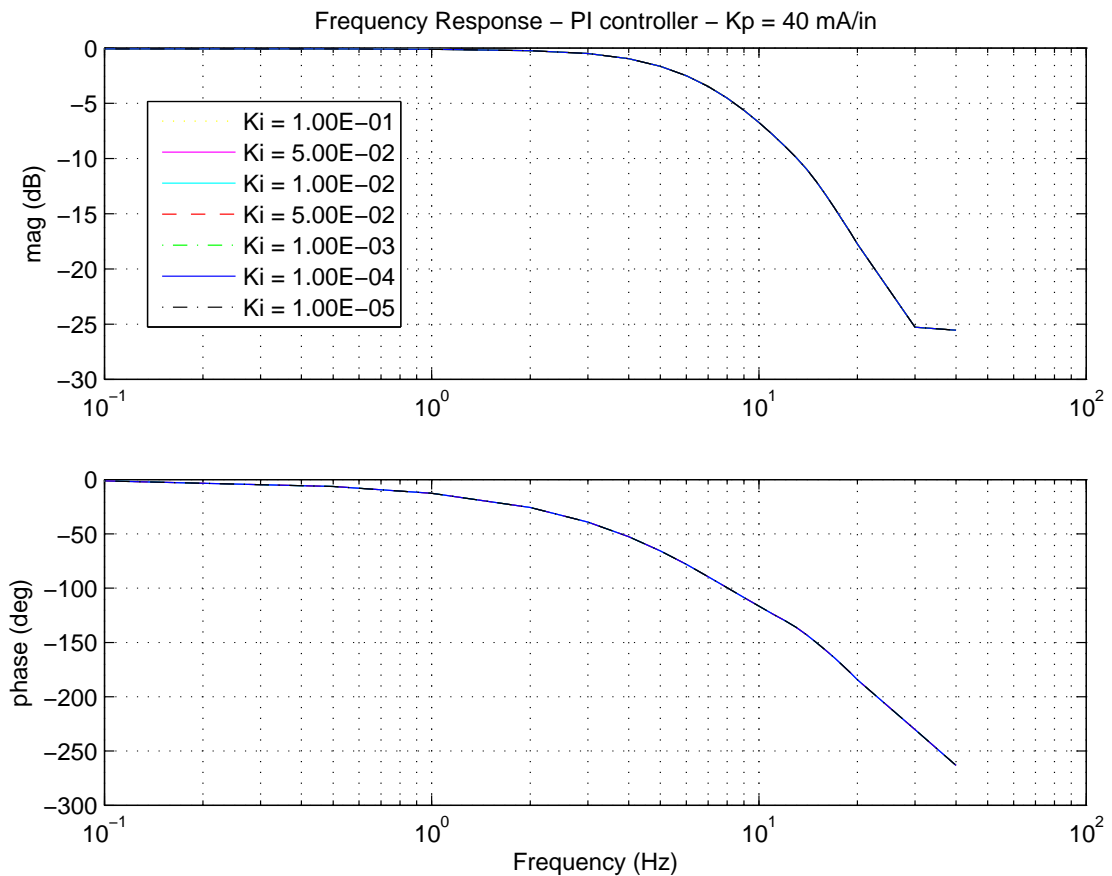


FIGURE 5.14 – Frequency Response for different integral gains

TABLE 5.6 – Rudder Actuator Design - Frequency Response Requirements Compliance PI controller

PI controller - K_i variation - Frequency Response Performance			
Design parameter	Requirement	$1E - 1$	$1E - 5$
Gain margin (dB)	≥ 10	22.33	22.33
Phase margin (deg)	≥ 45	inf	inf
Bandwidth (Hz)	<i>None</i>	5.51	5.52

The dynamic stiffness effect of varying controller integral gain is not so significant as shown in figure 5.15.

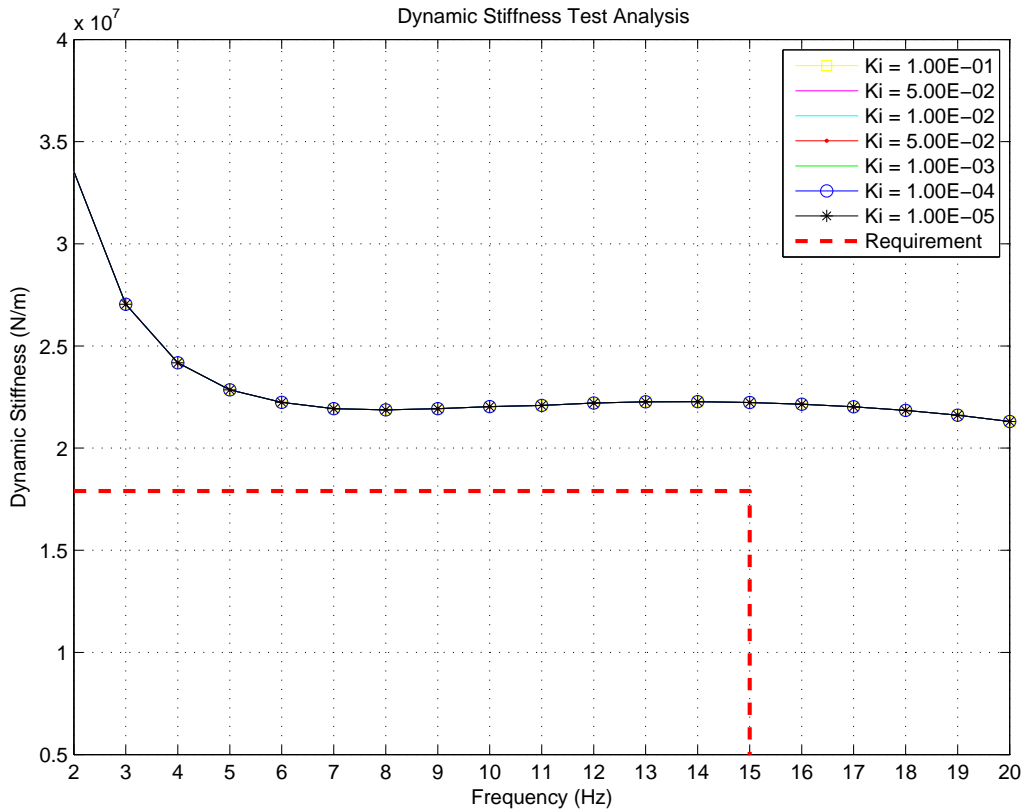


FIGURE 5.15 – Dynamic Stiffness test for different integral gains

As has been noted, the time response steady-state error suffers major influence by the controller integral action. For the frequency response and actuator's dynamic stiffness, the integral gain does not have major influence in their performance. This can be explained by the masking effect of non-linearities represented in the model, such as the current command saturation and the servo valve's flow output limit. Due to those saturations, the integral action is limited and cannot have a full performance in this application.

5.2.1.2 Proportional Derivative (PD) Controller

The proportional derivative controller was implemented using the previously described discrete PID controller (figure 5.6) and bringing the integral gain K_i to zero. The derivative action can be interpreted as providing the controller a linear prediction over the time K_d of the error feedback.

From figure 5.16, the actuator step response becomes more damped, as the derivative gain (K_d) is increased. This is an expected behaviour, because increasing the derivative action means to increase the system damping. However, when the derivative gain becomes too large, it is expected that its error prediction capability gets worst(ASTROM; MURRAY, 2009).

From table 5.7, it is possible to observe a degradation in the actuator time response as the derivative gain is increased: the settling time increases, the steady state error increases and the surface average rate decays.

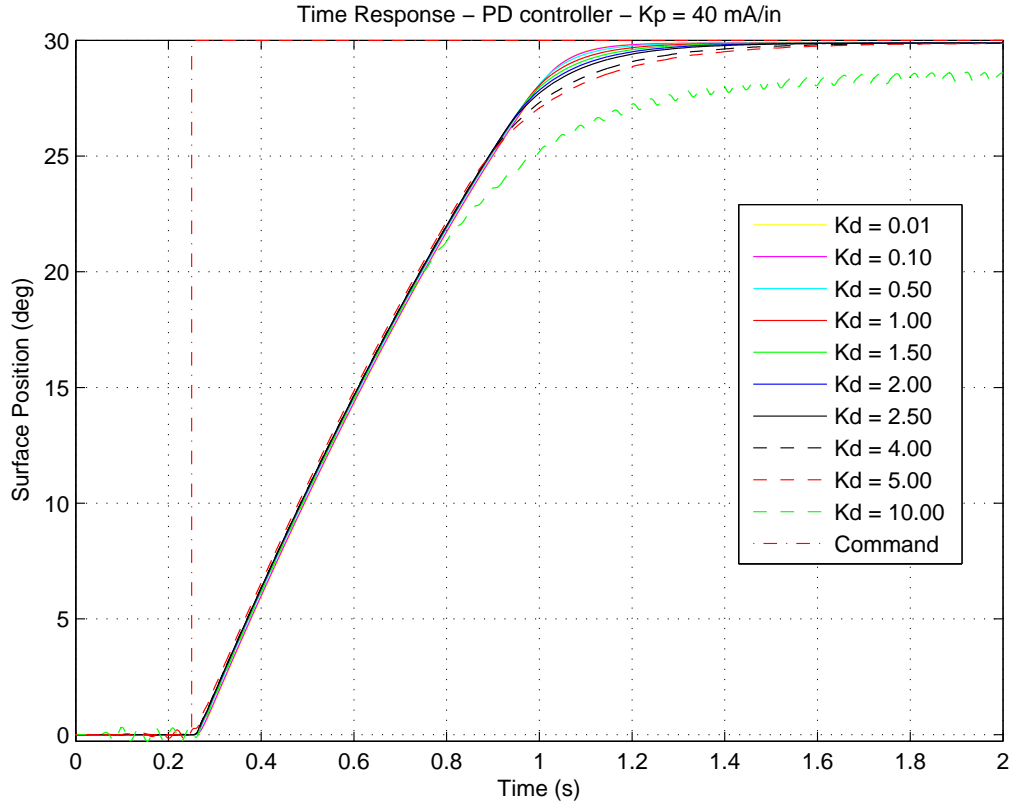


FIGURE 5.16 – Time Response for different derivative gains

TABLE 5.7 – Rudder Actuator Design - Time Response Requirements Compliance PD controller

PD controller - K_d variation - Time Response Performance						
Design parameter	Requirement	0.01	0.5	1.5	2.5	10
Settling time (ms)	< 850	690	711	758	807	inf
Steady State error (%)	< 1	0.17	0.17	0.18	0.18	1.42
Overshoot (%)	< 10	0.0	0.0	0.0	0.0	0.0
Minimum Average rate (deg/s)	> 32	34.94	34.85	34.65	34.50	34.54
Maximum Average rate (deg/s)	< 36	34.94	34.85	34.65	34.50	34.54

The derivative action is observed in for a lower step reference command with no external load in figure 5.17. It can be concluded that for high derivative gains the actuator system damping increases and the step response becomes slower, however there is no steady-state error observed.

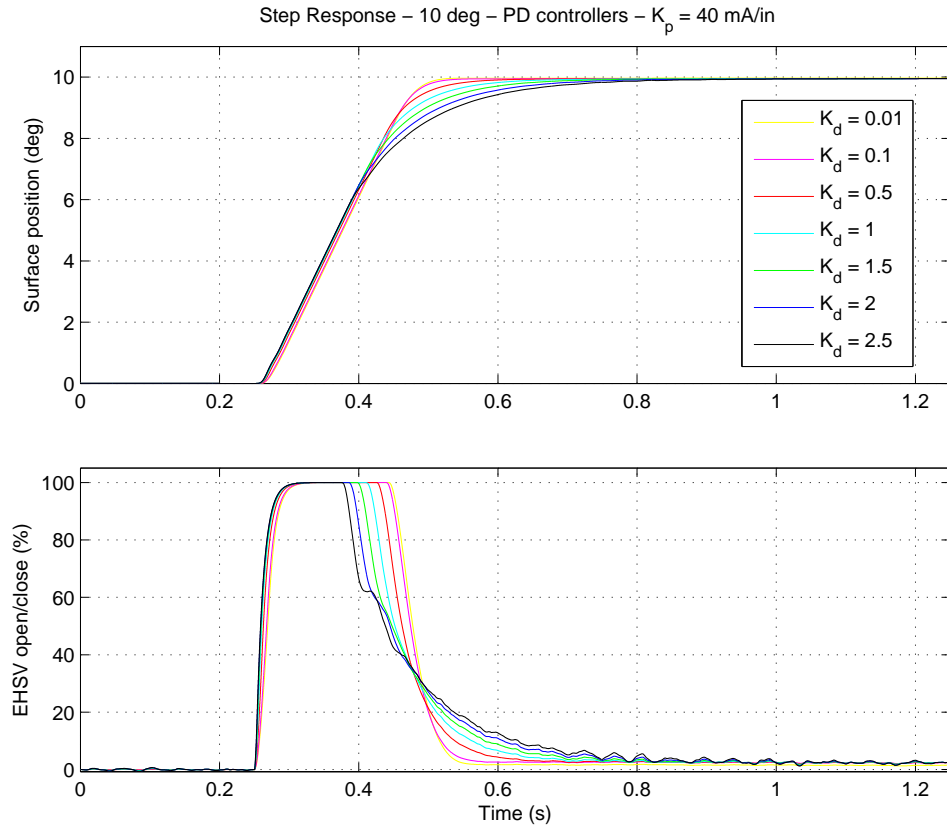


FIGURE 5.17 – Step Response for different derivative gains

The actuator frequency response in figure 5.18 shows the effect of different derivative gains in the frequency response. While increasing the derivative gain, for low frequencies, the phase and amplitude ratio of the frequency response decrease. For higher frequencies, the actuator gain response presents an increase, which reflects the less stable behavior observed for time response performance. In addition, for high derivative gains, the presence of resonance peaks above 10 Hz is observed.

The gain margin decays while increasing the derivative action. Above a certain derivative gain, the gain margin is not compliant with the requirement. The phase margin also degrades with the increase of K_d gain. The actuator bandwidth begins to increase with the derivative gain increase. The actuator becomes faster, but for a high gain actuator, the frequency response performance determines a very small bandwidth.

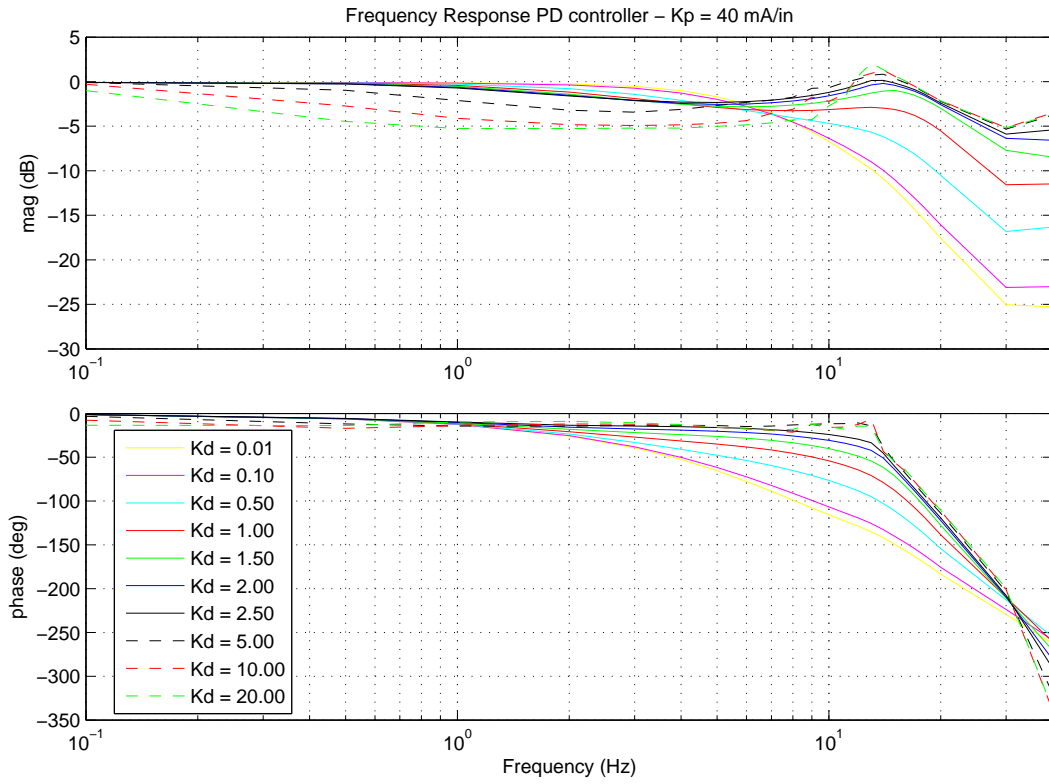


FIGURE 5.18 – Frequency Response for different derivative gains

TABLE 5.8 – Rudder Actuator Design - Frequency Response Requirements Compliance PD controller

PD controller - K_d variation - Frequency Response Performance						
Design parameter	Requirement	0.01	0.5	1.5	2.5	10
Gain margin (dB)	≥ 10	17.04	13.30	5.96	4.80	4.46
Phase margin (deg)	≥ 45	<i>inf</i>	<i>inf</i>	<i>inf</i>	127.17	113.12
Bandwidth (Hz)	<i>None</i>	6.57	5.72	20.21	21.94	0.71

The actuator dynamic stiffness response for different controller derivative gains is presented in figure 5.19. As it can be observed, increasing K_d helps to increase the actuator dynamic stiffness between 2 Hz and 12 Hz. However, when K_d reaches a certain value, the actuator dynamic stiffness response begins to reduce and violate the flutter suppression requirement.

For frequencies higher than 12 Hz, the increase of the derivative gain has always a harmful effect in the actuator's dynamic response. This occurs because the increase of the controller derivative gain will determine a system's bandwidth increase. The bandwidth increase leads the actuator to have a better response in some frequencies that were before

attenuated. Nonetheless, the phase delay increase leads to a degradation of the actuator's dynamic stiffness response, as it will be illustrated in figure 5.26.

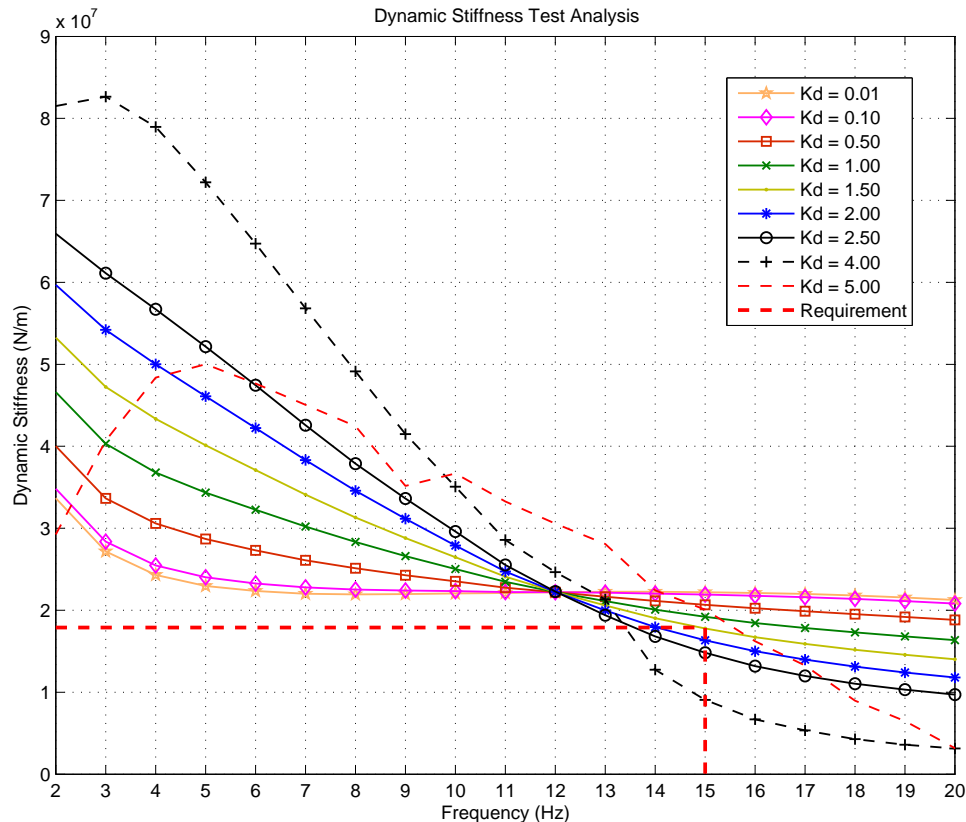


FIGURE 5.19 – Dynamic Stiffness test for different derivative gains

It can be concluded that increasing the controller derivative action determine an increase of the actuator dynamic stiffness, especially at frequencies between 2 Hz and 12 Hz. However, as the derivative gain increases, both the actuator's time response and frequency response start to present a degradation in performance and violate their design requirements.

5.2.1.3 Proportional Integral Derivative (PID) Controller

In this section, four different discrete PID controllers were implemented.

The proportional, integral and derivative gains were chosen based on the previous results obtained. The main criteria for choosing the PID gains was to identify those gains from P, PI, and PD control strategies that determined an actuator response that comply with time response, frequency response and dynamic stiffness.

Table 5.9 present the four PID controller that will be implemented and its gains.

TABLE 5.9 – Different PID designs proposed

PID controller design				
Parameter	PID 1	PID 2	PID 3	PID 4
K_p	40	60	40	40
K_i	$1E - 6$	$1E - 6$	$1E - 6$	$1E - 1$
K_d	0.5	0.5	0.8	0.5

From figure 5.20 and table 5.10, it is possible to observe that PID 1 and PID 4 controllers present very similar performance, this is due to the fact that the integral gain does not influence too much the actuator's time response. PID 2 and PID 3 controllers comply with all time response requirements.

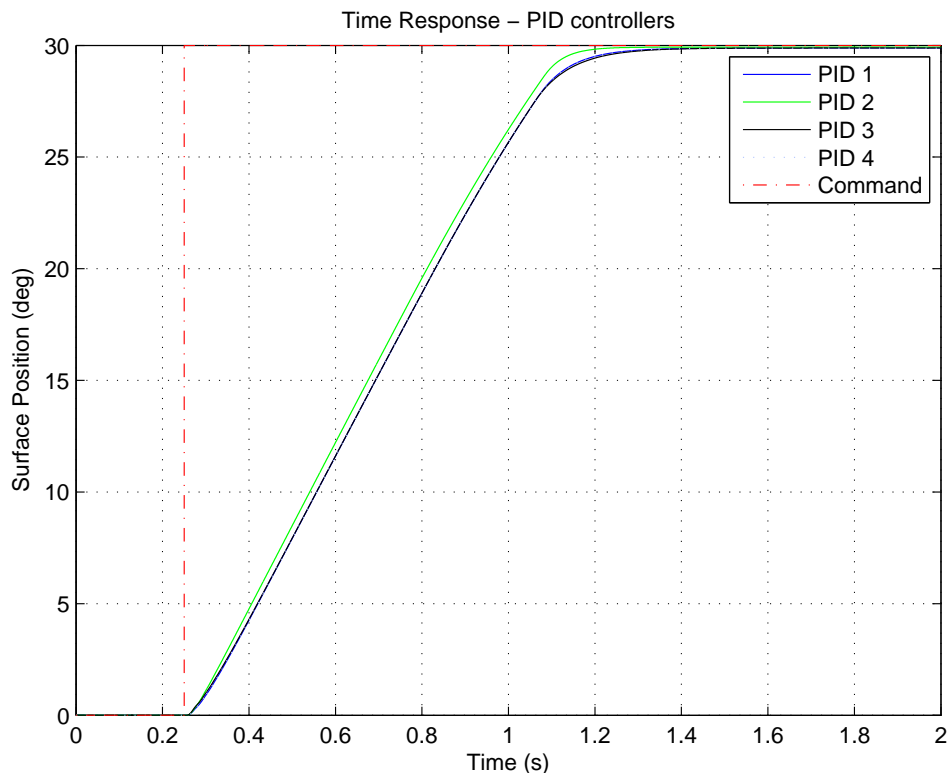


FIGURE 5.20 – Time Response for PID controllers

TABLE 5.10 – Rudder Actuator Design - Time Response Requirements Compliance PID controller

PID controller - Time Response Performance					
Design parameter	Requirement	PID 1	PID 2	PID 3	PID 4
Settling time (ms)	< 850	710	651	723	712
Steady State error (%)	< 1	0.17	0.12	0.17	0.20
Overshoot (%)	< 10	0.0	0.0	0.0	0.0
Minimum Average rate (deg/s)	> 32	34.85	35.09	34.79	34.85
Maximum Average rate (deg/s)	< 36	34.85	35.09	34.79	34.85

Figure 5.21 and table 5.11 summarize the PID controllers performance for frequency response. All PID configurations comply with the phase margin requirement. PID 3 is beyond the gain margin requirement, thus it is not an acceptable solution. In addition, PID 1 and PID 4 present very similar frequency response, what proves that the integral gain value does not have a great influence in the actuator's frequency response.

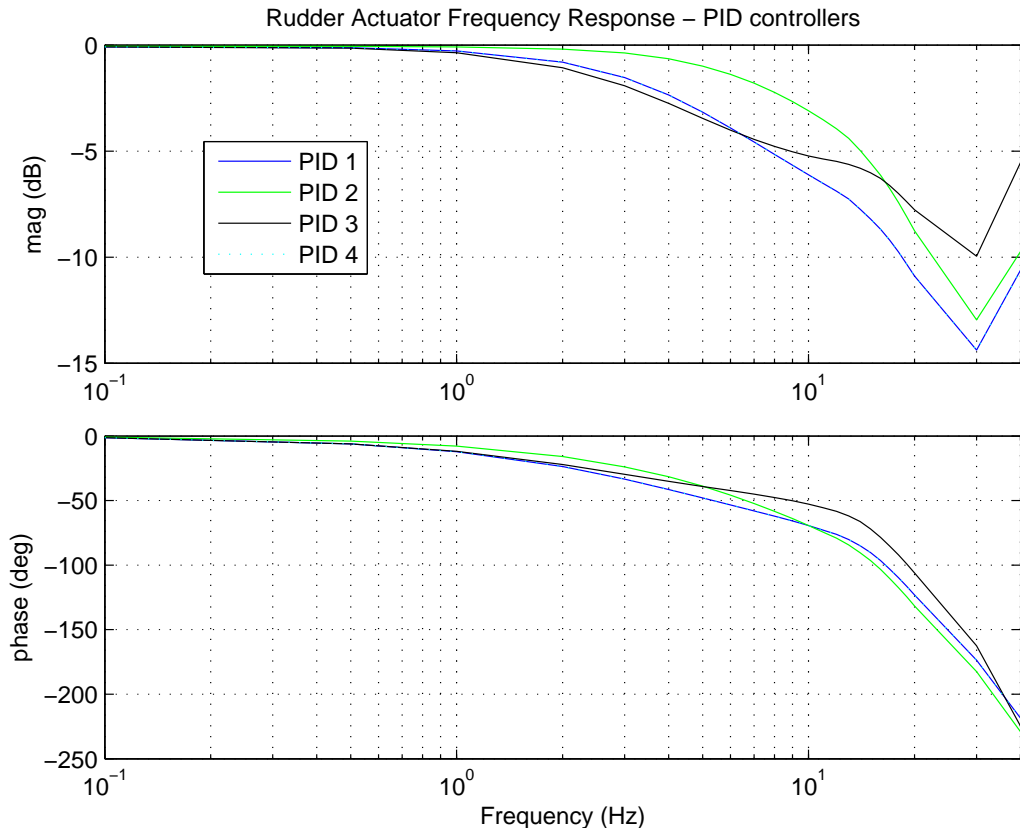


FIGURE 5.21 – Frequency Response for PID controllers

TABLE 5.11 – Rudder Actuator Design - Frequency Response Requirements Compliance PID controller

PID controller - Frequency Response Performance					
Design parameter	Requirement	PID 1	PID 2	PID 3	PID 4
Gain margin (dB)	≥ 10	13.85	12.75	8.71	13.85
Phase margin (deg)	≥ 45	<i>inf</i>	<i>inf</i>	<i>inf</i>	<i>inf</i>
Bandwidth (Hz)	<i>None</i>	4.90	9.90	4.48	4.90

Figure 5.22 shows the actuator's dynamic stiffness for all PID controllers. All PID configuration exceed the design requirement for dynamic stiffness. Among the four PID controller, PID 2 presents the worst performance, this is related to its high proportional gain. PID 1 and PID 4 have similar performance and present the best performance at high frequencies (above 15 Hz), while PID 3 has the best performance for low frequencies.

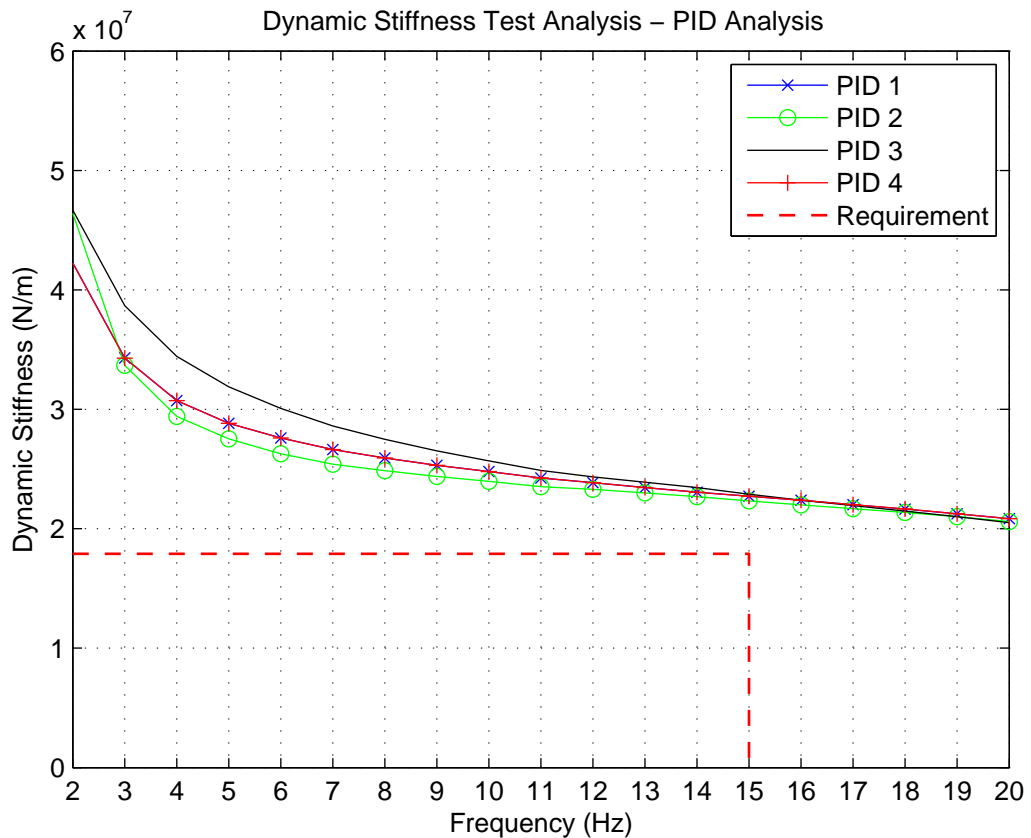


FIGURE 5.22 – Dynamic Stiffness test for PID controllers

It can be concluded that PID 1 presents the best performance among the four PID controller, since it has a better time response than PID 4, PID 3 fails the gain margin requirement, and PID 2 presents the worst dynamic stiffness response.

5.2.1.4 Classic Controllers comparison

In this section, it will be presented a comparison between the P, PI, PD and PID controllers. It will summarize the results for time response, frequency response and dynamic stiffness response for all four classic control strategies. The controller gains for all classic control strategies are shown on table 5.12.

TABLE 5.12 – Different classical controller design proposed

Classical controllers				
Parameter	P	PI	PD	PID
K_p	40	40	40	40
K_i	0.0	$1E - 6$	0.0	$1E - 6$
K_d	0.0	0.0	0.7	0.7

Figure 5.23 and table 5.13 illustrate that the P and PI controllers have the same performance for time response requirements. In addition, the PD and PID present the same performance for time response. It is important to notice that all control strategies are compliant with time response requirements.

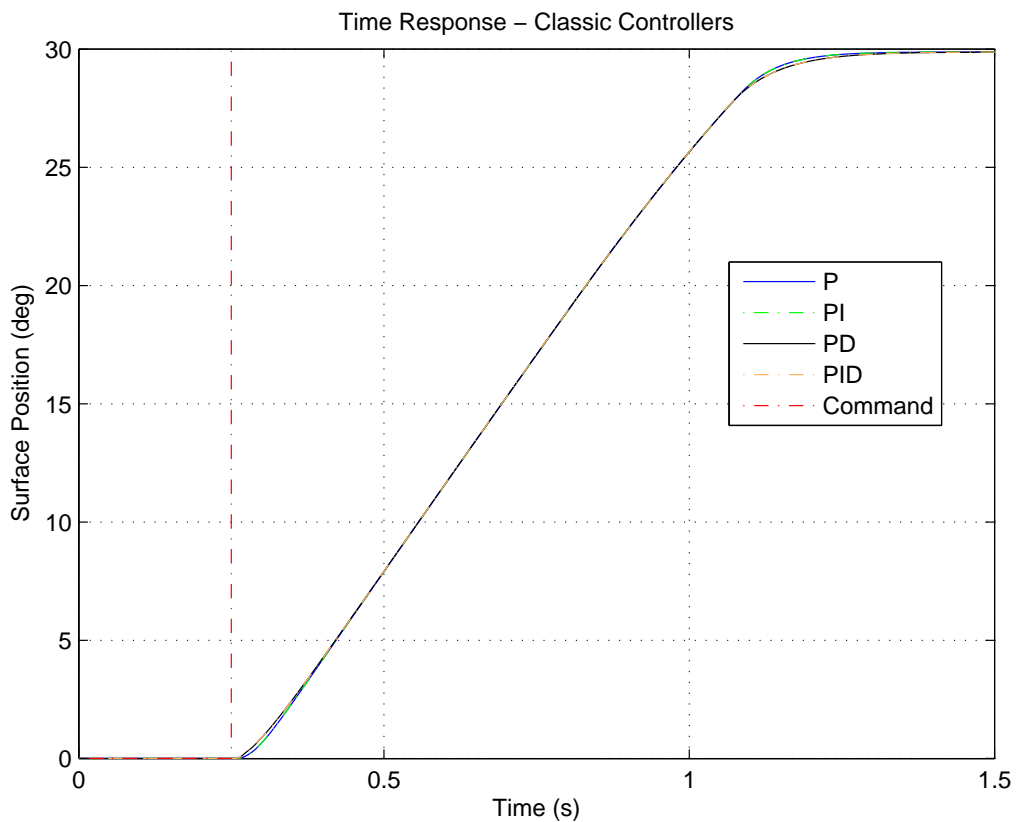


FIGURE 5.23 – Time response for different classic controllers

TABLE 5.13 – Rudder Actuator Design - Time Response Requirements Compliance Classic controllers

Classic controllers - Time Response Performance					
Design parameter	Requirement	P	PI	PD	PID
Settling time (ms)	< 850	690	690	710	710
Steady State error (%)	< 1	0.17	0.17	0.17	0.17
Overshoot (%)	< 10	0.0	0.0	0.0	0.0
Minimum Average rate (deg/s)	> 32	34.94	34.94	34.85	34.85
Maximum Average rate (deg/s)	< 36	34.94	34.94	34.85	34.85

Regarding the actuator frequency response shown in figure 5.24, it is possible to realize, from table 5.14, that the integral term does not affect the actuator's performance, since the gain margin, phase margin and bandwidth for P and PI are equal, and the same effect is observed in PD and PID controllers results. In addition, all control strategies are compliant with frequency response requirements.

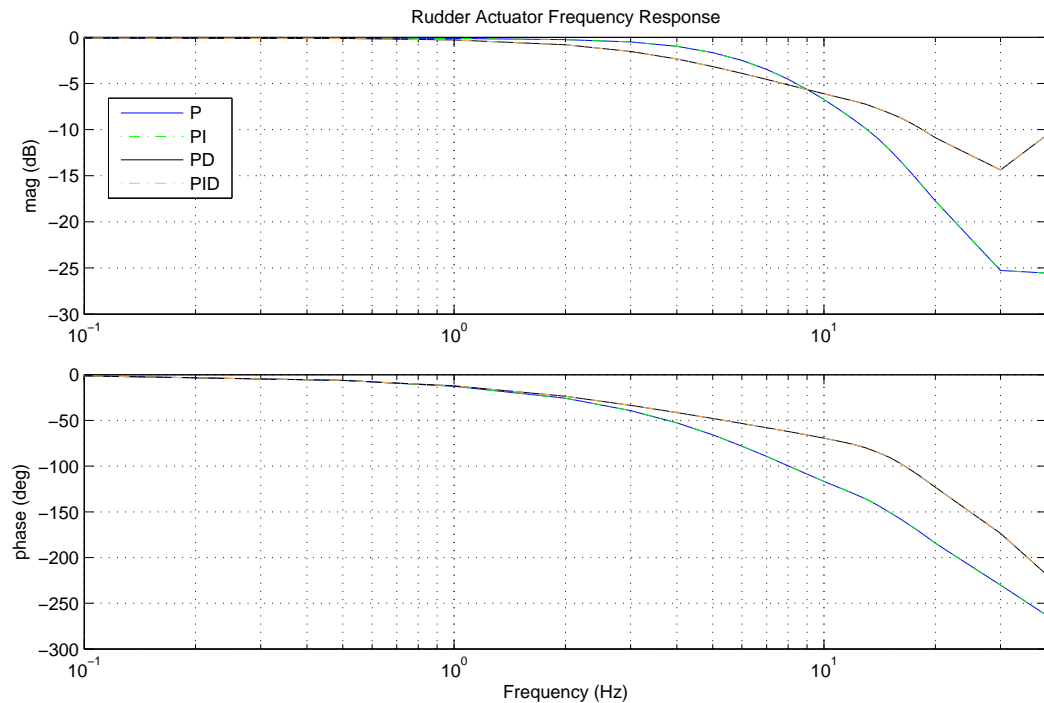


FIGURE 5.24 – Frequency response for different classic controllers

TABLE 5.14 – Rudder Actuator Design - Frequency Response Requirements Compliance
Classic controllers

Classic controllers - Frequency Response Performance					
Design parameter	Requirement	P	PI	PD	PID
Gain margin (dB)	≥ 10	17.04	17.04	13.85	13.85
Phase margin (deg)	≥ 45	<i>inf</i>	<i>inf</i>	<i>inf</i>	<i>inf</i>
Bandwidth (Hz)	<i>None</i>	6.60	6.60	4.90	4.90

Figure 5.25 shows the actuator dynamic stiffness for all four classic control strategies. Once more, it can be concluded that the integral term does not influence the actuator's dynamic stiffness response. The PD controller presents a better performance especially in the frequency band of 0.1 Hz and 12 Hz. However, for frequencies above 12 Hz, it has a worst performance compared with a pure proportional controller (P).

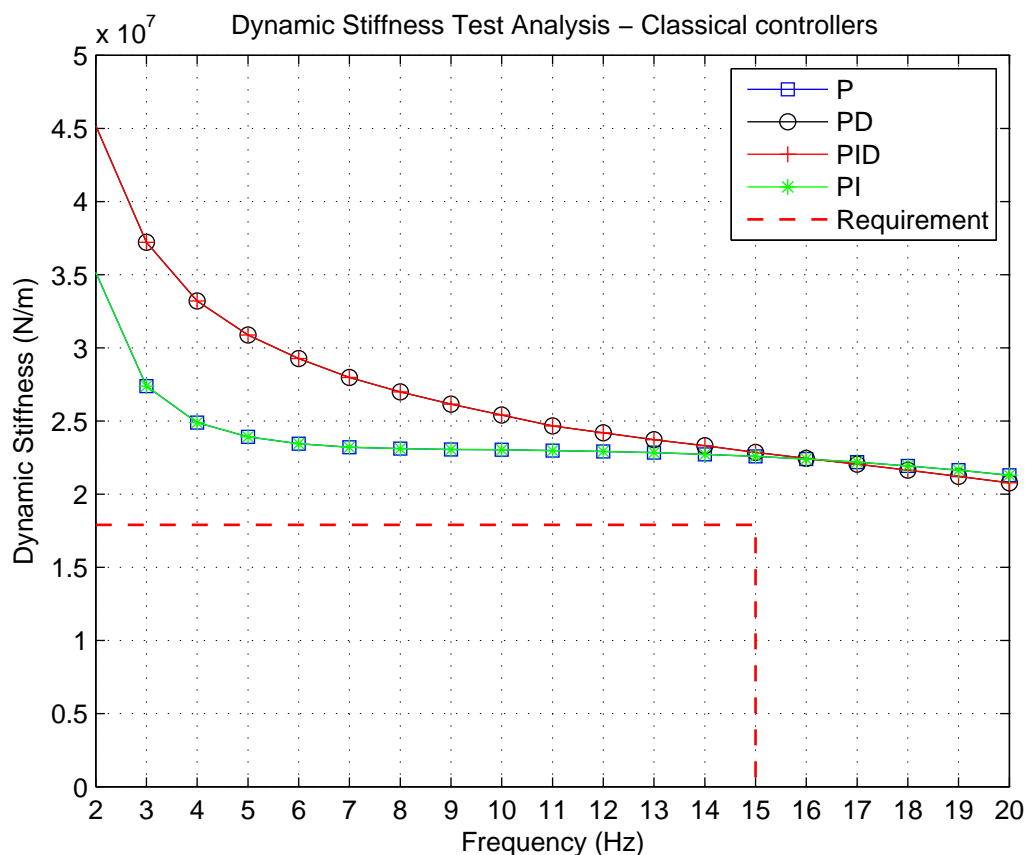


FIGURE 5.25 – Dynamic Stiffness for different classic controllers

In figure 5.26, the effect of the phase delay in the actuator dynamic stiffness response is observed: as it increases the dynamic stiffness response decreases. This is a rule for all the classic controllers analyzed.

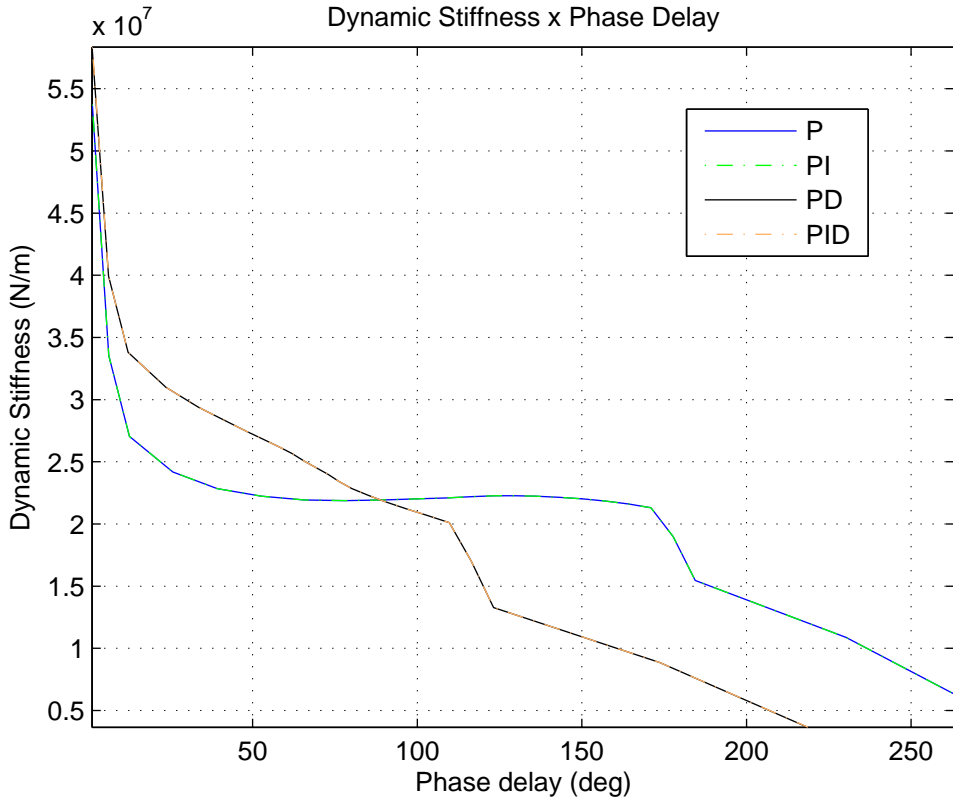


FIGURE 5.26 – Phase delay x Dynamic Stiffness

5.2.2 Modern Controller

This section presents the synthesis of modern control strategies in order to control the electrohydraulic actuator piston position. First, it is necessary to develop a linear model of the system, and then modern control strategies can be developed based on this linear model.

5.2.2.1 Electro-hydraulic Actuator Linear model

From the nonlinear model developed in chapter four (section 4.1), it is possible to obtain an electro-hydraulic actuator linear model, adopting the following assumptions:

- i No load applied to the actuator piston ($F_L = 0$ and $K_p = 0$);
- ii EHSV spool overlap neglected ($x_{ov} = 0$);
- iii EHSV spool position always positive ($x_v > 0$);
- iv Constant Bulk Modulus ($\beta(P_1, T) = \beta(P_2, T) = \beta_c$)

Those assumptions determine the following simplified nonlinear equations for the servo-controlled hydraulic actuator:

$$\ddot{x}_v = \frac{1}{A_s K_r} (K_i K_2 w_{n_e}^2 i - 2\xi_e w_{n_e} A_s K_r \ddot{x}_v - A_s K_r w_{n_e}^2 \dot{x}_v - K_2 K_w w_{n_e}^2 x_v) \quad (5.8)$$

$$\dot{P}_1 = \frac{\beta_c}{V_{01} + A_p x_p} (K_{CD} (\sqrt{P_S - P_1} (x_v x_w + A_{leak}) - \sqrt{P_1 - P_T} A_{leak} - A_{ext} \sqrt{P_1} - A_{int} \sqrt{P_1 - P_2}) - A_p \dot{x}_p) \quad (5.9)$$

$$\dot{P}_2 = \frac{\beta_c}{V_{02} - A_p x_p} (A_p \dot{x}_p + K_{CD} (\sqrt{P_S - P_2} A_{leak} - A_{ext} \sqrt{P_2} + A_{int} \sqrt{P_1 - P_2} - \sqrt{P_2 - P_T} (x_v x_w + A_{leak}))) \quad (5.10)$$

$$\ddot{x}_p = \frac{1}{m_p} (A_p (P_1 - P_2) - B_p \dot{x}_p) \quad (5.11)$$

Defining $\Delta P = P_1 - P_2$ and according to (CONTE; TROMBETII, 2000), the equations 5.8, 5.9, 5.10 and 5.11 can be linearized considering only the first order of Taylor expansion series. Hence, the electro-hydraulic actuator can be represented as:

$$\ddot{x}_v = k_{v1} x_v + k_{v2} \dot{x}_v + k_{v3} \ddot{x}_v + k_{vi} i \quad (5.12)$$

$$\dot{\Delta P} = \gamma_v x_v + \gamma_{\Delta P} \Delta P + \gamma_p x_p + \gamma_{pd} \dot{x}_p \quad (5.13)$$

$$\ddot{x}_p = \alpha_{\Delta P} \Delta P + \alpha_{pd} \dot{x}_p \quad (5.14)$$

where:

$$\begin{aligned} k_{v1} &= \frac{\partial \ddot{x}_v}{x_v} & k_{v2} &= \frac{\partial \ddot{x}_v}{\dot{x}_v} & k_{v3} &= \frac{\partial \ddot{x}_v}{\ddot{x}_v} & k_{vi} &= \frac{\partial \ddot{x}_v}{i} \\ \gamma_v &= \frac{\partial \dot{\Delta P}}{x_v} & \gamma_{\Delta P} &= \frac{\partial \dot{\Delta P}}{\Delta P} & \gamma_p &= \frac{\partial \dot{\Delta P}}{x_p} & \gamma_{pd} &= \frac{\partial \dot{\Delta P}}{\dot{x}_p} \\ \alpha_{\Delta P} &= \frac{\partial \ddot{x}_p}{\Delta P} & \alpha_{pd} &= \frac{\partial \ddot{x}_p}{\dot{x}_p} \end{aligned}$$

If we consider the following state-space vector X with input U and output Y :

$$X = \begin{bmatrix} x_v \\ \dot{x}_v \\ \ddot{x}_v \\ \Delta P \\ x_p \\ \dot{x}_p \end{bmatrix}$$

$$U = i$$

$$Y = \begin{bmatrix} x_v \\ \Delta P \\ x_p \end{bmatrix}$$

It is possible to obtain a state space model as follows:

$$\dot{X} = AX + BU \quad (5.15)$$

$$Y = CX + DU \quad (5.16)$$

where:

$$A = \begin{bmatrix} 0 & 1 & 0 & 0 & 0 & 0 \\ 0 & 0 & 1 & 0 & 0 & 0 \\ k_{v1} & k_{v2} & k_{v3} & 0 & 0 & 0 \\ \gamma_v & 0 & 0 & \gamma_{\Delta P} & \gamma_p & \gamma_{pd} \\ 0 & 0 & 0 & 0 & 0 & 1 \\ 0 & 0 & 0 & \alpha_{\Delta P} & 0 & \alpha_{pd} \end{bmatrix} \quad B = \begin{bmatrix} 0 \\ 0 \\ k_{vi} \\ 0 \\ 0 \\ 0 \end{bmatrix} \quad C = \begin{bmatrix} 1 & 0 & 0 & 0 & 0 & 0 \\ 0 & 0 & 0 & 1 & 0 & 0 \\ 0 & 0 & 0 & 0 & 1 & 0 \end{bmatrix} \quad D = 0$$

To obtain a specific linear model it is necessary to define an operation point, the equilibrium point of the system. The equilibrium point was numerically obtained using the Matlab *trim* function:

$$X_e = \begin{bmatrix} 0 \\ 0 \\ 0 \\ 0 \\ 0 \\ 0 \end{bmatrix}$$

$$U_e = 0$$

Using Matlab function *linmod*, the coefficient for the A and B matrices are obtained. The linearization process is described in details in Appendix A.

To validate the linear model, a current step input of 1 mA was performed in both linear and nonlinear model. The resulting time responses for the states x_v , \dot{x}_v , \ddot{x}_v , ΔP , x_p and \dot{x}_p are illustrated in figures 5.27, 5.28 and 5.29.

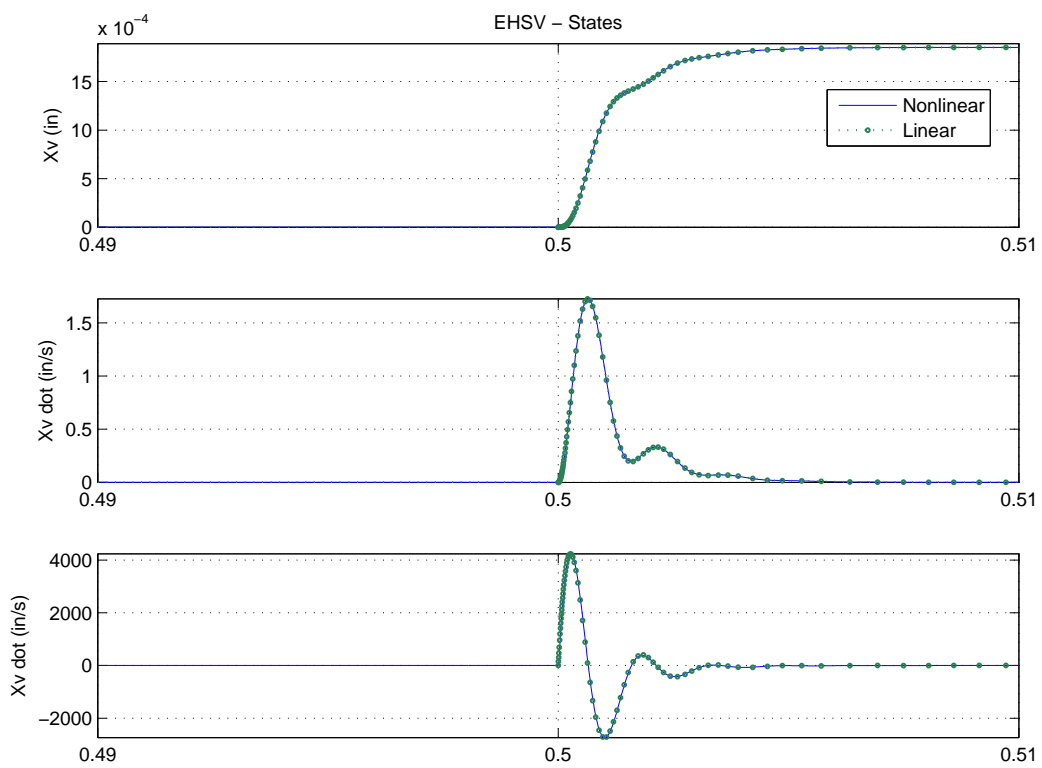


FIGURE 5.27 – Nonlinear and linear model comparison - EHSV 1st stage states - EHSV 1 mA step at 0.5 s

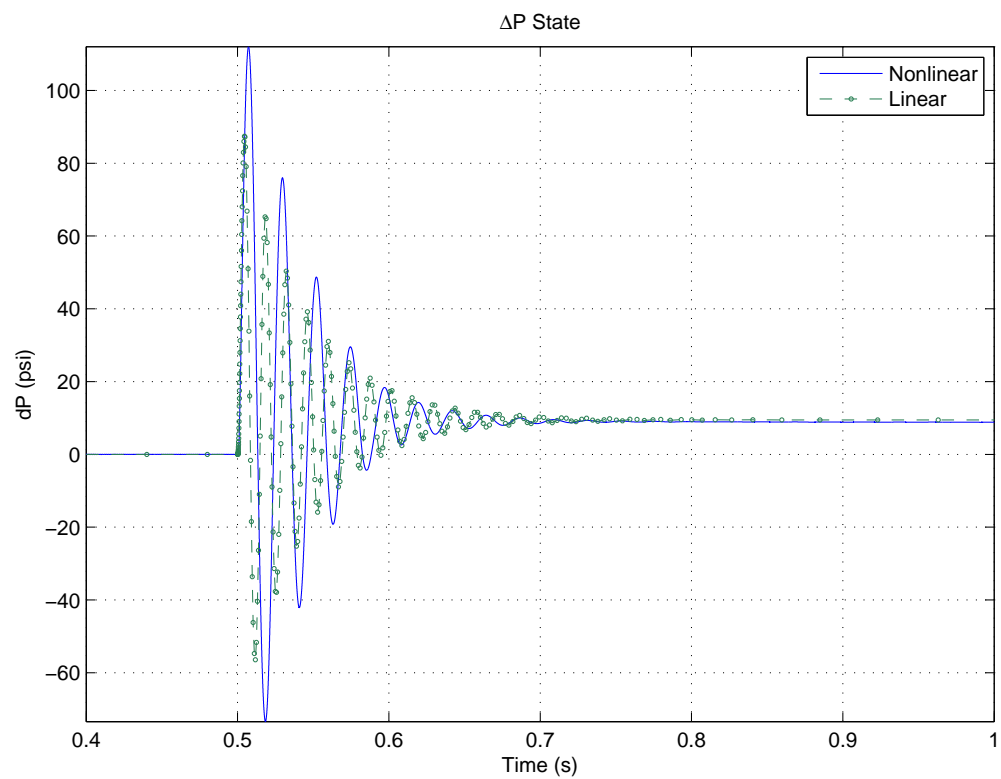


FIGURE 5.28 – Nonlinear and linear model comparison - ΔP state - EHSV 1 mA step at 0.5 s

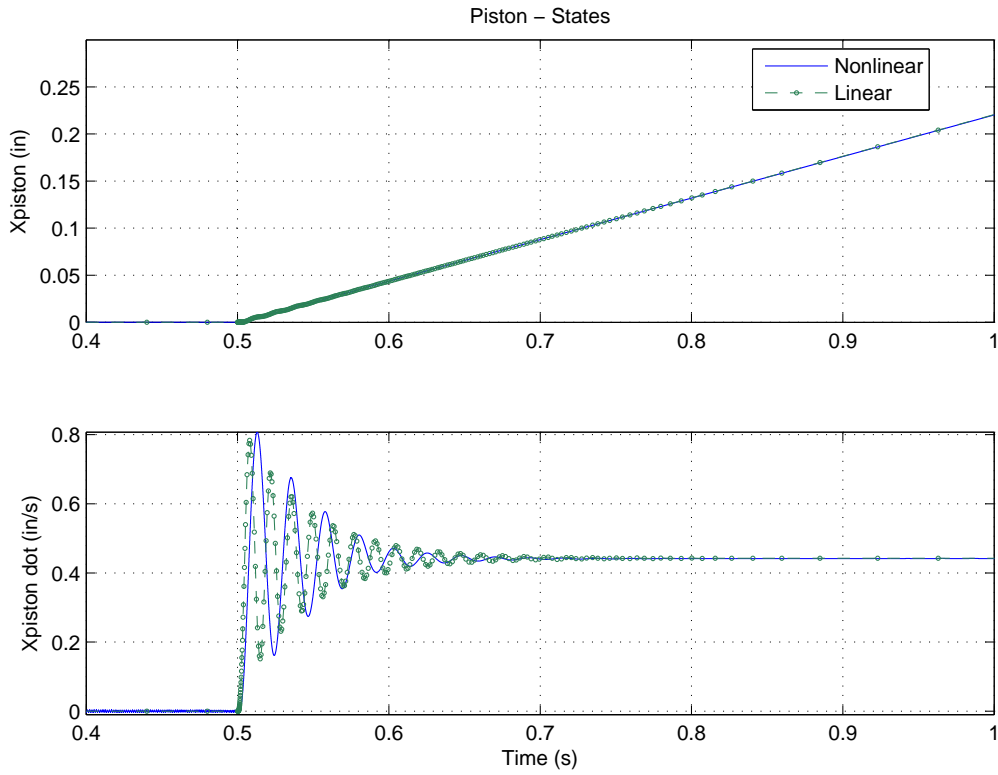


FIGURE 5.29 – Nonlinear and linear model comparison - Piston states - EHSV 1 mA step at 0.5 s

As it can be observed, the time response for both linear and nonlinear model have a satisfactory match for the state X and present an expected behavior for a current step in the EHSV: the spool position x_v stabilizes in a certain position, which generates a constant ΔP that determine a ramp in the hydraulic actuator piston position. It can be concluded that the linear model obtained is a good representation of the nonlinear model dynamics and can be considered validated.

The following eigenvalues for the linear model were obtained:

$$\text{Eigenvalues}_A = \begin{bmatrix} -1.342 \cdot 10^3 + i4.097 \cdot 10^3 \\ -1.342 \cdot 10^3 - i4.097 \cdot 10^3 \\ -9.524 \cdot 10^2 \\ -23.412 + i4.570 \cdot 10^2 \\ -23.412 - i4.570 \cdot 10^2 \\ 8.477 \cdot 10^{-4} \end{bmatrix}$$

There is one eigenvalue that has its real part positive, but as it is very close to zero, due to numerical approximations, it can be considered zero. This zero eigenvalue is expected and it represents the integral inherent action of the system due to the hydraulic

piston integral characteristics. The others eigenvalues have their real parts negative, which determine that those system modes are all stable. The three ones with the smallest real part correspond to the fast dynamics of the EHSV first stage, and the cylinder dynamics is represented by the two eigenvalues with a real part close to -23 .

5.2.2.2 State-Space Control

Once the electro-hydraulic actuator linear model was obtained and validated, a state-space feedback control strategy can be developed for the actuator's position control loop. Considering the following linear state space system:

$$\dot{X} = AX + BU \quad (5.17)$$

$$Y = CX \quad (5.18)$$

$$U = -KX \quad (5.19)$$

Hence, the linear system is transformed into:

$$\dot{X} = (A - BK)X \quad (5.20)$$

$$Y = CX \quad (5.21)$$

Choosing the eigenvalues of the matrix $A - BK$, by choosing the gain K , makes it possible to change the system dynamics with a full state feedback and control the actuator's piston position.

To provide a full state feedback, information about all the system complete state is necessary. However, the actuator model of this study measures, using sensors, only 3 system states: x_v , ΔP and x_p . Hence, an observer is necessary to reconstruct the system full state based on the system output (sensors) and input.

LINEAR REDUCED-ORDER OBSERVER

An observer is a dynamic system responsible to estimate the state of another dynamic system using the measured output and input of the later (FRIEDLAND, 1986). If the order of the observer is equal to the order of the observed system, the observer is defined as full-order state observer, if the observer order is less than the order of the observed system; the observer is defined as reduced-order state observer.

Having a partial observation of the state of the actuator system due to LVDT sensors, a reduced-order state observer is recommended to be implemented. The reduced-order

observer can be interpreted as a less expensive solution. However, it may have better properties especially with regard to robustness than a full-order solution, particularly when implemented in closed-loop control system (FRIEDLAND, 1986).

Dividing and rearranging the state of the system into directly measured (X_1) and non-directly measure (X_2) states:

$$X = \begin{bmatrix} X_1 \\ X_2 \end{bmatrix} = \begin{bmatrix} x_v \\ \Delta P \\ x_p \\ \dot{x}_v \\ \ddot{x}_v \\ \dot{x}_p \end{bmatrix}$$

Then, the linear system state-space model can be represented as:

$$\dot{X}_1 = A_{11}X_1 + A_{12}X_2 + B_1U \quad (5.22)$$

$$\dot{X}_2 = A_{21}X_1 + A_{22}X_2 + B_2U \quad (5.23)$$

$$Y = CX \quad (5.24)$$

where:

$$C = [I_{3x3} \mathbf{0}] \quad (5.25)$$

X_1 is the observation vector which comprises the directly measured state variables. Thus, the estimated states X_1^{obs} is equal to the system output, no observer is required.

$$X_1^{obs} = CX = X_1 = Y \quad (5.26)$$

The non-directly measured states (X_2) can be estimated by a reduced-order observer defined as:

$$X_2^{obs} = K_{obs}Y + z \quad (5.27)$$

and z is the state of a system of the same order as X_2 :

$$\dot{z} = A^{obs}z + LY + HU \quad (5.28)$$

The matrix A^{obs} , L and H are chosen to ensure that the states estimation error goes to zero independent of X , Y and U . The estimation error can be split into:

$$e_1 = X_1 - X_1^{obs} = 0 \quad (5.29)$$

$$e_2 = X_2 - X_2^{obs} \quad (5.30)$$

The estimation error from the directly measured states (e_1) is equal to zero and the estimation error from the observed states must have its convergence to zero guaranteed.

Defining:

$$\dot{e}_2 = \dot{X}_2 - \dot{X}_2^{obs} \quad (5.31)$$

and developing it based on 5.23, 5.24 and 5.26:

$$\dot{e}_2 = A_{21}X_1 + A_{22}X_2 + B_2U - K_{obs}(A_{11}X_1 - A_{12}X_2 - B_1U) - A^{obs}z - LY - HU \quad (5.32)$$

Substituting $Y = X_1$ and $z = X_2^{obs} - K_{obs}X_1$:

$$\dot{e}_2 = A_{21}X_1 + A_{22}X_2 + B_2U - K_{obs}(A_{11}X_1 - A_{12}X_2 - B_1U) - A^{obs}(X_2^{obs} - K_{obs}X_1) - LX_1 - HU \quad (5.33)$$

Then, the \dot{e}_2 can be written as:

$$\dot{e}_2 = (A_{21} - K_{obs}A_{11} + A^{obs}K_{obs} - L)X_1 + (A_{22} - K_{obs}A_{12} - A^{obs})X_2 + A^{obs}e_2 + (B_2 - K_{obs}B_1 - H)U \quad (5.34)$$

From (FRIEDLAND, 1986), to make the reduced-order observer independent from X_1 , X_2 and U , the matrix A^{obs} , L and H shall be:

$$A^{obs} = A_{22} - K_{obs}A_{12} \quad (5.35)$$

$$L = A_{21} - K_{obs}A_{11} + A^{obs}K_{obs} \quad (5.36)$$

$$H = B_2 - K_{obs}B_1 \quad (5.37)$$

And the error in estimation of X_2 is set to:

$$\dot{e}_2 = A^{obs}e_2 \quad (5.38)$$

Thus, the selection of K_{obs} must assure that the eigenvalues of matrix $A^{obs} = A_{22} - K_{obs}A_{12}$ lie in the left-half of the complex plane (stable poles) to guarantee that e_2 converges to zero. Once K_{obs} is chosen L and H can be found and the reduce-order state observer is completed.

Once the state of the system can be completely observed using sensors and reduce-order observer, full state feedback control laws can be implemented.

LINEAR QUADRATIC REGULATOR (LQR)

The linear quadratic regulator is one of the most common optimal control strategies. Given a single-input linear system:

$$\dot{X} = AX + BU \quad (5.39)$$

where $X \in \mathbb{R}^6$ and $U \in \mathbb{R}$, the following quadratic cost function is attempted to be minimized:

$$J = \int_0^\infty (X^T Q X + U^T R U) dt \quad (5.40)$$

where $Q \geq 0$ and $R > 0$ are semi-positive and positive definite matrices respectively. The cost function J represents a trade-off between the distance of the state from the origin and the cost of the control input.

From (ASTROM; MURRAY, 2009), the solution of the LQR problem is a linear control law:

$$u = -KX = -R^{-1}B^TPX \quad (5.41)$$

where P is a symmetric, positive definite matrix that solves the algebraic Riccati equation:

$$PA + A^T P - PBR^{-1}B^TP + Q = 0 \quad (5.42)$$

One advantage of the LQR synthesis is that the feedback control gain (K) can be set by weighting Q and R , few parameters. By setting Q and R weights, the control design can penalize the input versus the states and set the states that should remain small by putting higher weight coefficients. Generally, Q and R are chosen as diagonal matrices to facilitate the weight setting.

The first full state feedback gain synthesis attempt was using LQR, once the gain and

the matrix $A - BK$ eigenvalues placement was performed, a fine tuning of the control gain by changing the dominant resulting pole, the one which is closest to the origin, was done. The LQR gains used can be seen in Appendix A.

5.2.2.3 Modern Control Performance

From the LQR control strategy adopted, two implementations were evaluated. One with an analog controller that performs full-state feedback control with the help of a linear reduced order observer, and the other using a digital controller performing a partial-state feedback (output feedback) using only the sensors output (x_v , ΔP and x_p) to perform feedback control.

The modern controller full-state feedback gain matrix is the following:

$$K_{gain_{full}} = \begin{bmatrix} 2.430 \cdot 10^1 & 5.853 \cdot 10^{-4} & 1.692 \cdot 10^{-4} & 6.532 \cdot 10^{-4} & 5.728 \cdot 10^1 & -4.902 \cdot 10^{-3} \end{bmatrix}$$

The full-state feedback strategy place the system eigenvalues as follows:

$$Eigenvalues_{A-BK} = \begin{bmatrix} -1.322 \cdot 10^3 + i4.092 \cdot 10^3 \\ -1.322 \cdot 10^3 - i4.092 \cdot 10^3 \\ -9.69 \cdot 10^2 \\ -24.622 + i4.577 \cdot 10^2 \\ -24.622 - i4.577 \cdot 10^2 \\ -25.000 \end{bmatrix}$$

The modern controller partial-state feedback gain matrix is the following:

$$K_{gain_{partial}} = \begin{bmatrix} 2.430 \cdot 10^1 & 0 & 0 & 6.532 \cdot 10^{-4} & 5.728 \cdot 10^1 & 0 \end{bmatrix}$$

The partial feedback strategy using only the sensors output place the system eigenvalues as follows:

$$Eigenvalues_{A-BK} = \begin{bmatrix} -1.320 \cdot 10^3 + i4.092 \cdot 10^3 \\ -1.320 \cdot 10^3 - i4.092 \cdot 10^3 \\ -9.70 \cdot 10^2 \\ -24.418 + i4.581 \cdot 10^2 \\ -24.418 - i4.581 \cdot 10^2 \\ -24.944 \end{bmatrix}$$

As it can be seen, the full-state feedback and the partial-state feedback strategies determine a closed-loop system dynamics very similar. The eigenvalues from both strategies

are very close. Observing figure 5.30, the actuator step responses for a 30 degree surface command for both strategies have a very similar performance.

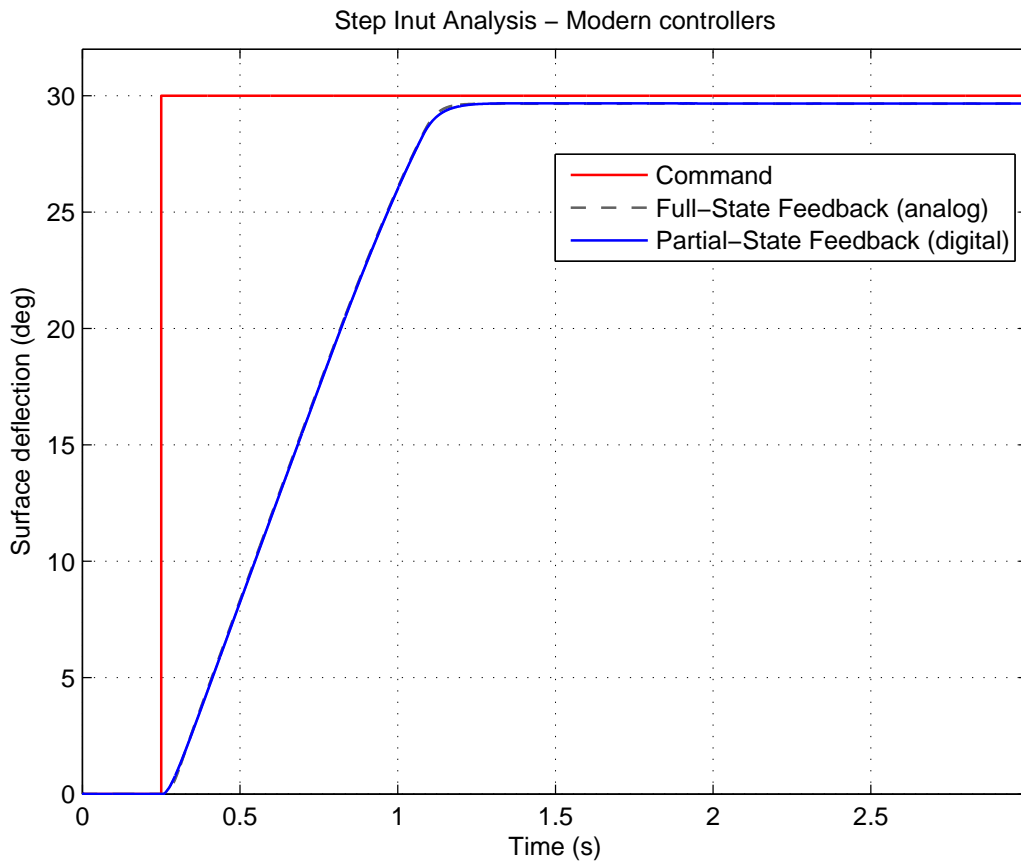


FIGURE 5.30 – Time Response for modern controllers

Table 5.15 summarizes the time response performance for the full-state feedback and partial-state feedback strategy. It can be concluded that both strategies are compliant with time performance requirements. The partial feedback presents the best settling time, however the full-state feedback determines the best surface average rate.

TABLE 5.15 – Rudder Actuator Design - Time Response Requirements Compliance Modern controllers

State feedback controller - Time Response Performance			
Design parameter	Requirement	FULL	PARTIAL
Settling time (ms)	< 850	660	641
Steady State error (%)	< 1	0.51	0.51
Overshoot (%)	< 10	0.0	0.0
Minimum Average rate (deg/s)	> 32	35.90	35.88
Maximum Average rate (deg/s)	< 36	35.90	35.88

The modern controllers step response performance lower step references is presented in figure 5.31. It can be observed that both modern control strategies do not present overshoot or steady-state error, and the control output (EHSV position) works in the saturation region for a great part of the rising time.

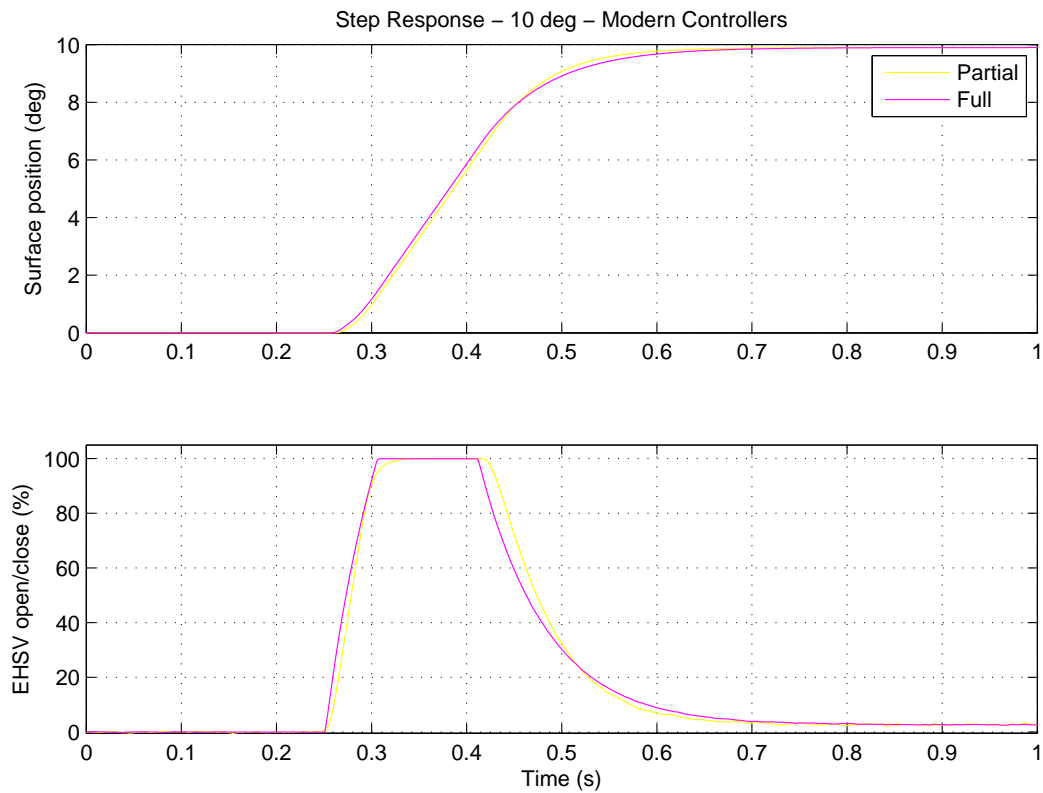


FIGURE 5.31 – Time Response for modern controllers

The frequency response for the state control feedback strategies are presented in figure 5.32 and results are summarized in table 5.16. As it can be observed, the partial-state feedback presents a higher bandwidth than the full state feedback; also, it has a smaller gain margin than the full state feedback.

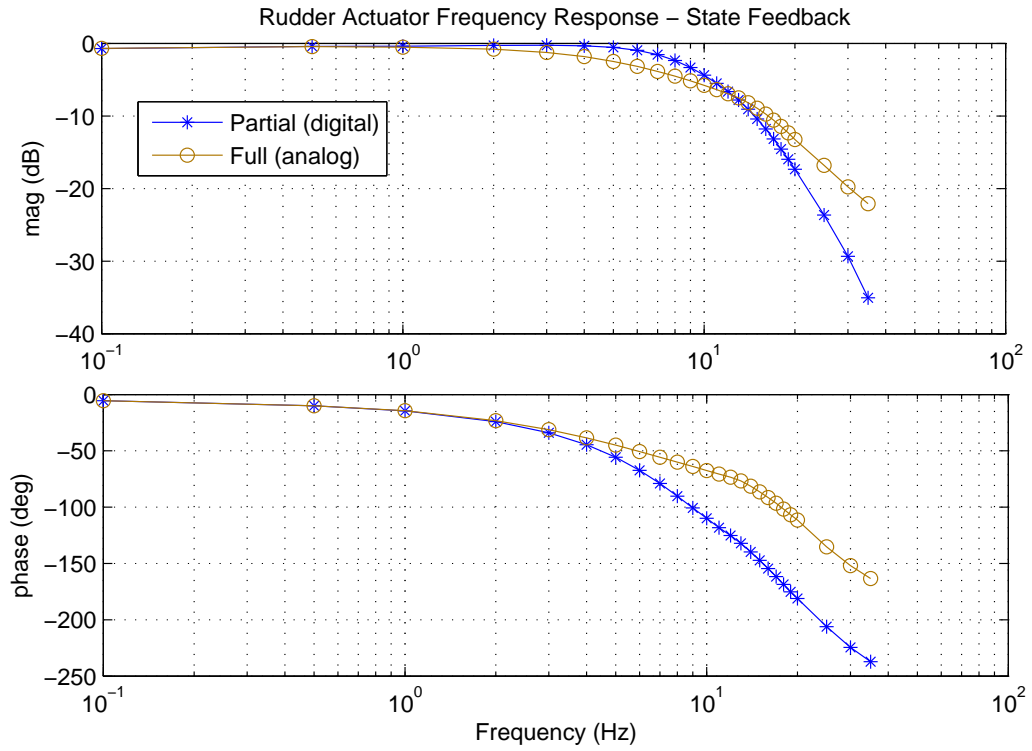


FIGURE 5.32 – Frequency Response for modern controllers

TABLE 5.16 – Rudder Actuator Design - Frequency Response Requirements Compliance Modern controllers

State Feedback - Frequency Response Performance			
Design parameter	Requirement	FULL	PARTIAL
Gain margin (dB)	≥ 10	25.44	17.11
Phase margin (deg)	≥ 45	<i>inf</i>	<i>inf</i>
Bandwidth (Hz)	<i>None</i>	6.76	9.36

A comparison between the dynamic stiffness performance of the actuator with a modern state-space controller with partial/full state feedback and classical proportional and proportional-derivative is presented in figure 5.33.

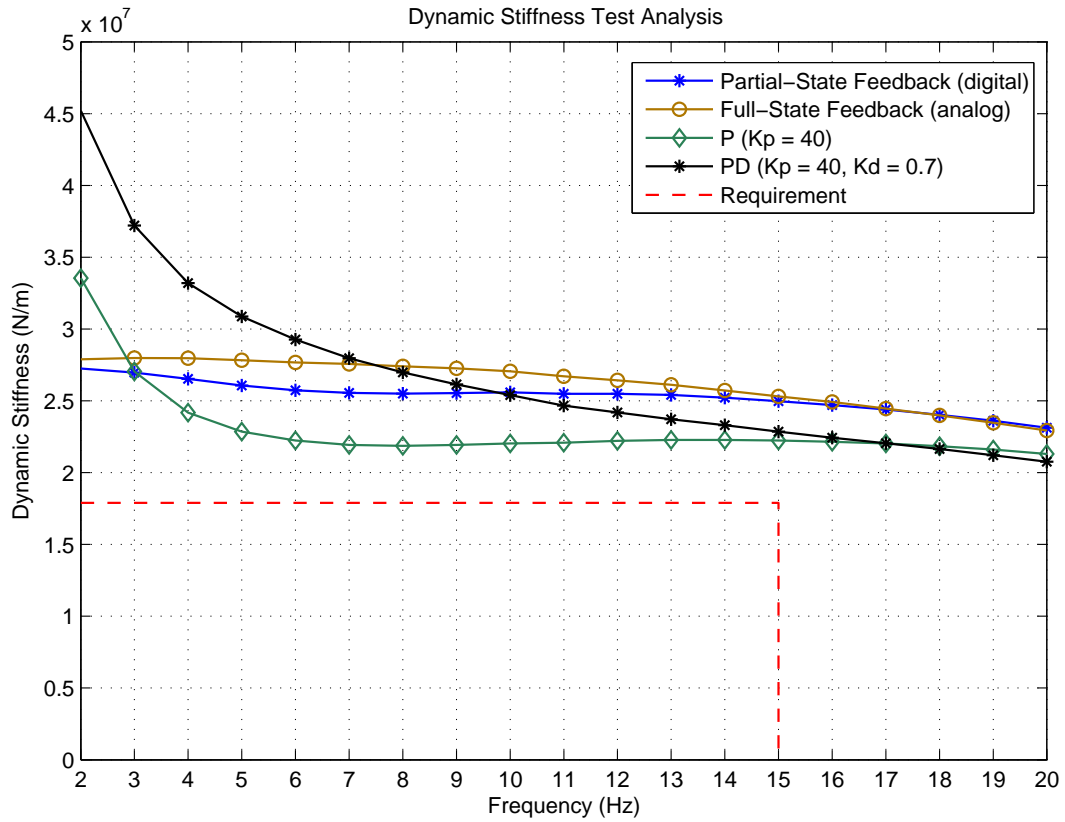


FIGURE 5.33 – Dynamic Stiffness for modern controllers

The full state-feedback determines a dynamic stiffness enhancement over the frequencies above 3 Hz, and the partial state feedback has a quite similar performance. When compared to the classical P and PD, both modern control strategies have better performance for frequencies above 10 Hz and do not present a degradation in performance, as the PD has for high frequencies.

Therefore, compared to the classical control approaches (P and PD), the modern controllers present a very good time and frequency response, which are compliant with the control loop requirements and both state-space feedback strategies bring benefit to the actuator's dynamic stiffness response. They are compliant to the dynamic stiffness design requirement and present an important enhancement effect for high frequencies.

6 Flight Control Actuator New Design

Having a significant enhancement of the actuator's dynamic stiffness with the help of position control techniques, as seen in the previous chapter, it is possible to evaluate if a redesigned actuator with a reduced piston area would comply with its design requirements without violating the minimum dynamic stiffness necessary for flutter suppression.

It is important to highlight that the redesigned actuator would have smaller hydraulic consumption and would be lighter than the previous design, bringing important benefits to the overall aircraft performance.

This chapter aims to provide the results obtained with a redesigned hydraulic actuator with its position controlled by different control techniques developed in the previous chapter.

6.1 Rudder actuator new design

The actuator new design was based on the original design developed in chapter 3. The new actuator design consists of:

- i reducing piston seal by one size number (from -328 to -327);
- ii maintaining rod size per original design;
- iii maintaining EHSV per original design;
- iv no change in kinematics: stroke, RLC triangle per original design.

Tables 6.1 and 6.2 illustrate the new actuator design. As expected, the design has a negative margin for dynamic stiffness requirement and a smaller stall load due to the reduced actuator area. The new piston and rod seal size are displayed on table 6.1, they determine a reduction of 18.10% of the actuator original area.

TABLE 6.1 – Rudder Actuator New design

Final Actuator New Design	
Piston Seal number	327
Rod Seal number	221
Actuator area (A_{act})	$1.901in^2$

TABLE 6.2 – New Rudder Actuator against Requirements

New Actuator Design Margin			
Design parameter	Requirement	New Design	Margin (%)
Stall load (lbf)	4545.57	5417.85	19.20
$K_{act}(N/m^2)$	$1.79E + 7$	$1.47E + 7$	-17.88

6.2 Actuator Redesign Performance

Once the previous actuator new design is concluded, the new design validation against requirements is performed by simulation. The actuator performance for time and frequency response and the actuator's dynamic stiffness are presented in this section for different control loop configurations:

- i Proportional controller
- ii Proportional-Derivative controller
- iii Partial-State Feedback controller
- iv Full-State Feedback controller

All control loops are digital implementation, except for the full-state feedback controller, which is an analog implementation.

The control gains for the modern controllers were set based on the previous development described in chapter 4 and based on an updated linear model. The digital controller gains were not modified, because the gains set in chapter 4 presented a good performance for this actuator.

TABLE 6.3 – Classical controller gains

P and PD controller design		
Parameter	P	PD
K_p	40	40
K_d	0.0	0.7

The modern controller gain matrix are:

$$K_{gain_{full}} = \begin{bmatrix} 2.708 \cdot 10^1 & 4.855 \cdot 10^{-3} & 1.475 \cdot 10^{-6} & 2.035 \cdot 10^{-4} & 7.332 \cdot 10^1 & -4.809 \cdot 10^{-3} \end{bmatrix}$$

$$K_{gain_{partial}} = \begin{bmatrix} 2.708 \cdot 10^1 & 0 & 0 & 2.035 \cdot 10^{-4} & 7.332 \cdot 10^1 & 0 \end{bmatrix}$$

6.2.1 Time Response

The step response of the new actuator for different control strategies can be observed in figure 6.1.

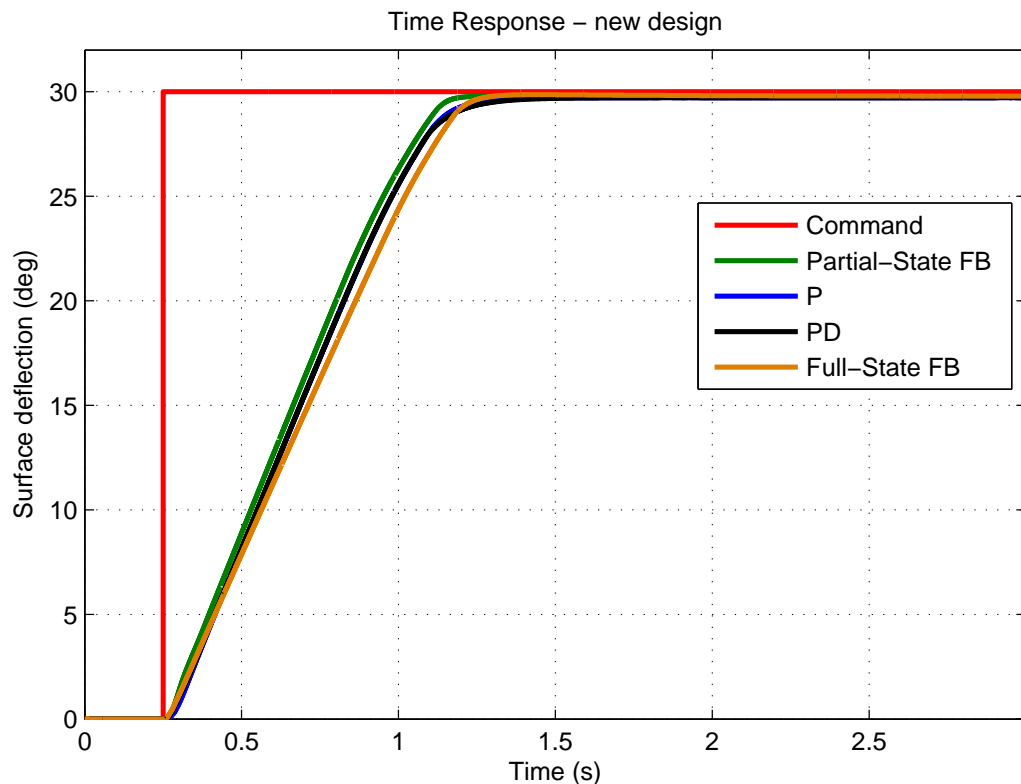


FIGURE 6.1 – Time Response - Different controllers - new design

Table 6.4 summarize the time response performance for different controllers. All time responses are compliant with requirements. The pure proportional and the proportional-derivative controllers present the higher settling time and a similar nominal surface rate and steady state error. The modern controllers have a better settling time performance and a smaller steady state error than the classical strategies. However, the full-state feedback has the smallest average rate among all controllers. None of the control strategies determines a surface position overshoot in the step response.

TABLE 6.4 – Rudder Actuator New Design Time Response Requirements Compliance

Time Response Performance					
Design parameter	Requirement	P	PD	Partial	Full
Settling time (ms)	< 850	724	761	640	715
Steady State error (%)	< 1	0.43	0.43	0.32	0.31
Overshoot (%)	< 10	0.0	0.0	0.0	0.0
Minimum Average rate (deg/s)	> 32	35.23	35.22	35.81	32.89
Maximum Average rate (deg/s)	< 36	35.23	35.22	35.81	32.89

The modern controllers present a step response performance quite similar to the classical strategies, highlighting a very good settling time and a small steady state error.

6.2.2 Frequency Response

The new actuator frequency response is illustrated in figure 6.2.

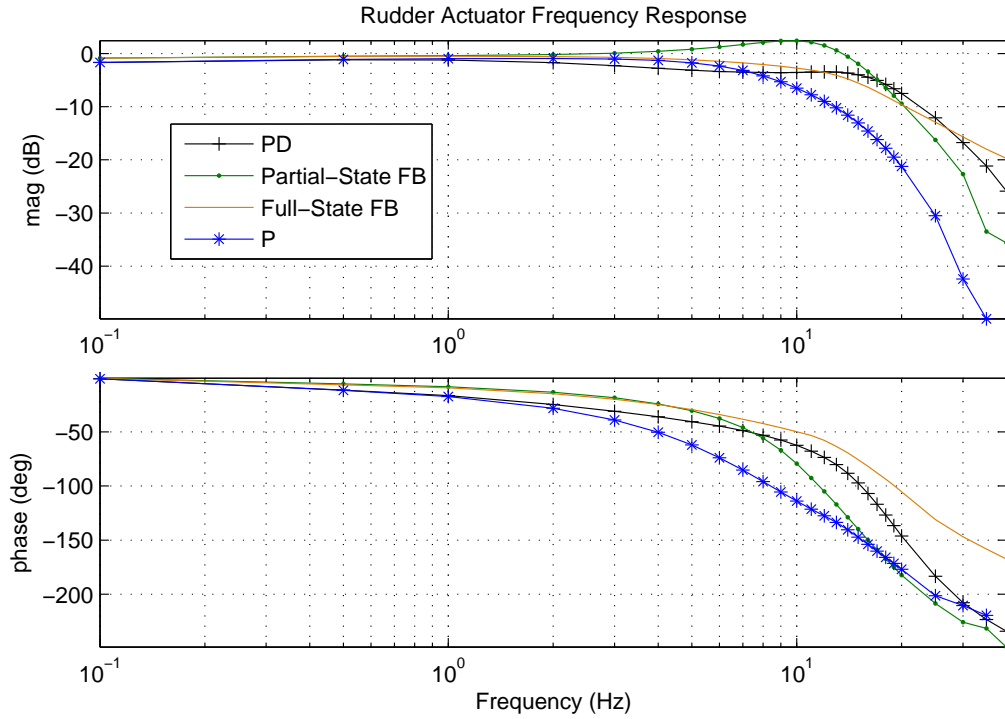


FIGURE 6.2 – Frequency Response - Different controllers - new design

From table 6.5, it is possible to conclude the proportional gain has the best gain margin among all the implemented control strategies, but with the worst bandwidth among the control strategies evaluated. All the controllers determine a frequency response with an infinite phase margin except for the partial-state feedback strategy. In addition, the partial-state feedback and the PD controllers have a large bandwidth (around 16 Hz) at the expense of gain margins. The full-state feedback presents a very good bandwidth (around 12 Hz) with a gain margin very close to the proportional controller.

TABLE 6.5 – Rudder Actuator New Design - Frequency Response Requirements Compliance

Frequency Response Performance					
Design parameter	Requirement	P	PD	Partial	Full
Gain margin (dB)	≥ 10	22.36	11.70	8.96	22.07
Phase margin (deg)	≥ 45	<i>inf</i>	<i>inf</i>	56.80	<i>inf</i>
Bandwidth (Hz)	<i>None</i>	8.43	16.36	16.30	12.61

6.2.3 Dynamic Stiffness

The new actuator's dynamic stiffness response is presented in figure 6.3.

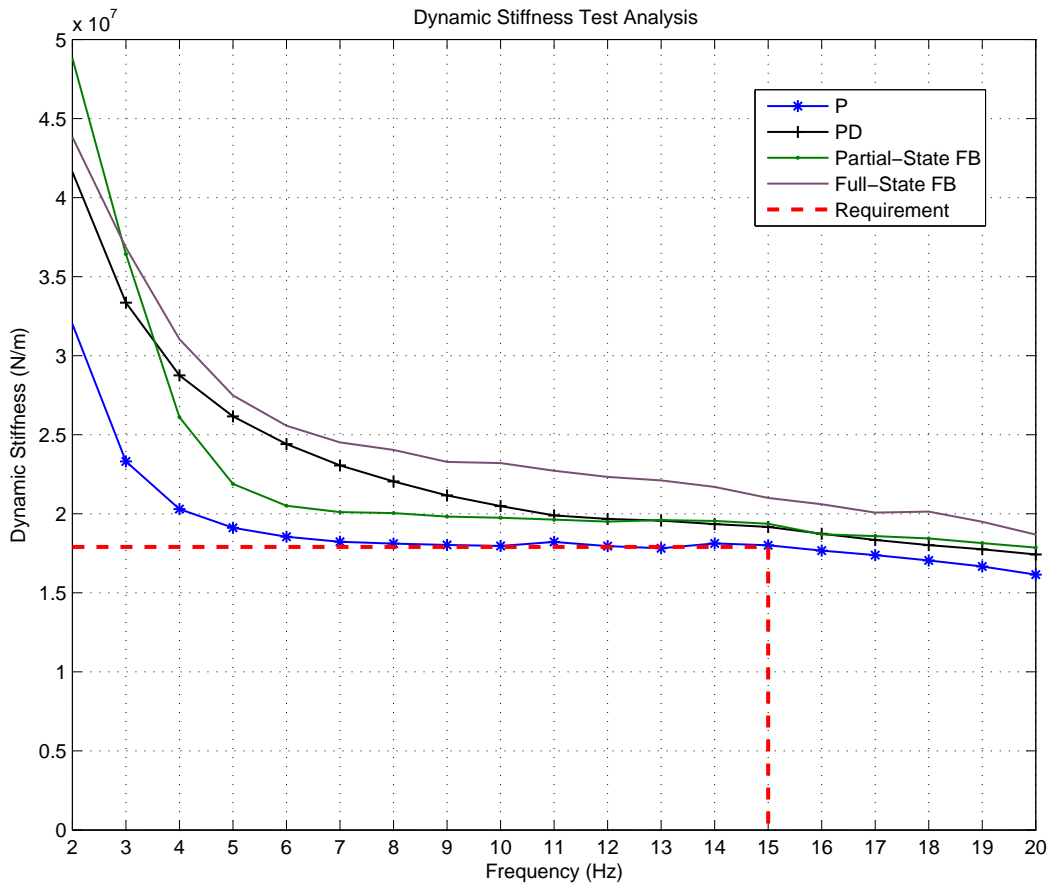


FIGURE 6.3 – Dynamic Stiffness - Different controllers - new design

As expected the simple proportional gain violates the requirement at infinite frequency (15 Hz). The PD and partial-state feedback present a better performance with a dynamic stiffness enhancement over the entire frequency range, as can be seen in figure 6.3. The full-state feedback presents the highest dynamic stiffness enhancement in the frequency range above 10 Hz and exceed the requirement in all the frequency range.

It can be concluded that the reduced size actuator with modern control strategies (full-state and partial-state feedback) is compliant with all time and frequency response requirements and has a dynamic stiffness response that exceeds the flutter suppression requirement.

6.3 Actuator Design Comparison

In this section, it is performed a performance comparison between the old rudder actuator, a preliminary design, with a proportional control loop (the aerospace industry standard solution) and the new actuator, an optimal design, with a reduced area and

full-state feedback controller.

Table 6.6 presents the comparison the main requirements and characteristics of the both actuator solutions.

TABLE 6.6 – Rudder Actuator New Design Frequency Response Requirements Compliance

Performance Comparison				
Design parameter	Requirement	Preliminary design	Optimal design	Δ (%)
Settling Time (ms)	< 850	690	715	+3.62
Nominal Rate (deg/s)	[32, 36]	34.94	32.89	-5.87
Steady State Error (%)	< 1	0.18	0.31	NA
Overshoot (%)	< 10	0.0	0.0	0.0
Gain margin (dB)	≥ 10	18.38	22.07	+20.07
Phase margin (deg)	≥ 45	inf	inf	NA
Bandwidth (Hz)	<i>None</i>	6.60	12.61	+91.06
Dynamic Stiffness margin @15Hz (%)	NA	24.2	17.3	NA
Piston Area (in^2)	NA	2.32	1.90	-18.10
Seal size number	NA	328 – 221	327 – 221	NA
Average Flow (gpm)	NA	3.64	2.79	-23.35

The new design presents a very similar step response performance compared with the old actuator. The new nominal rate is a little lower but is still compliant with no overshoot. The new actuator's frequency response performance is better than the old one, having a bigger gain margin and bandwidth, while maintaining an infinite phase margin. The piston area is around 18% smaller than the original actuator, and the hydraulic flow consumption 23% smaller than the first design. In addition, the new design has a very good dynamic stiffness margin at the critical infinite flutter frequency (15 Hz) around 17%, which is just a little bit smaller than the original margin from the first actuator design.

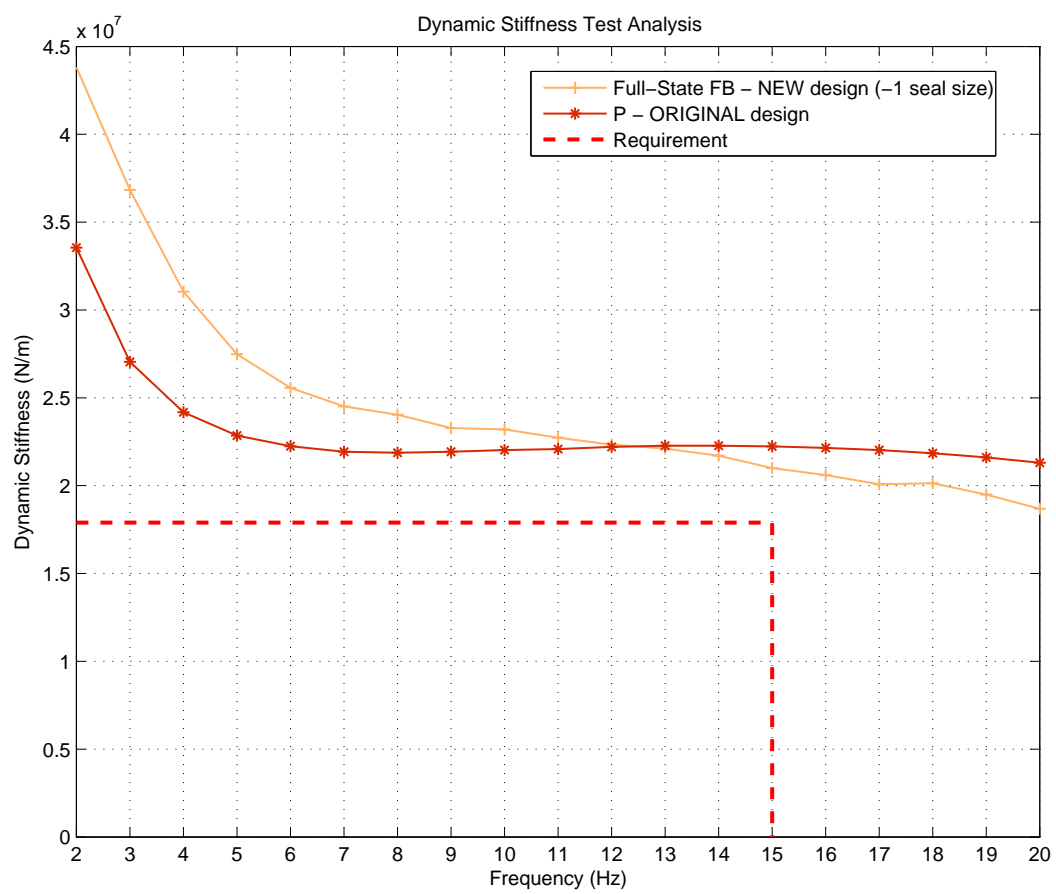


FIGURE 6.4 – Dynamic Stiffness - Preliminary vs. Optimal design comparison

7 Conclusion

A traditional flight control actuator's design was developed taking into account the actuator's kinematics, time and frequency response requirements, and hinge moment capability. As well, flutter suppression requirement, represented by the actuator's dynamic stiffness, and the use of standard seals were considered. The dynamic stiffness requirement was the dominant requirement to determine the piston area of the actuator final design.

A simulation model of the electro-hydraulic actuator was constructed based on (CONSTANTINO, 2010). The model of this work accommodate the variation of the hydraulic fluid bulk modulus due to hydraulic fluid pressure, temperature and percentage of entrained air. In addition, it included the LVDT sensors error and dynamic response. The electro-hydraulic servo valve was modified to allow the use of industry catalog parameters; the same motivation led the change of the inlet check valve. The rudder actuator design was validated and the actuator had its performance evaluated with the help of the simulation model.

In order to determine the influence of some electro-hydraulic actuator parameters in the actuator's performance, a parametric study was performed. From this parametric study, it could be concluded that the increase of EHSV flow gain and the control loop proportional gain will bring benefit to the actuator's time and frequency response, but not for the actuator's dynamic stiffness. As the EHSV flow gain and the control loop proportional gain increase the dynamic stiffness decrease and may lead to a violation of the dynamic stiffness requirement.

In addition, from this parametric study, an actuator's internal leakage increase showed a dynamic stiffness response degradation. Thus, if it were possible to design an actuator with minor internal leakage, this would enhance the overall dynamic stiffness response. The control loop's update rate also showed a major influence in the actuator's dynamic stiffness, since as it was increased the actuator's dynamic stiffness presented an enhancement.

Different actuator's position control classic strategies, commonly adopted in the aerospace industry, were evaluated. The PI strategy did not bring major benefits to the actuator

performance. Thus, the integral action did not have major influence in the dynamic stiffness. The PD controller was the classical controller that was able to comply with time and frequency response requirements and determined an enhancement of the dynamic stiffness response for frequencies up to 15 Hz, approximately. For frequencies above this value, the PD controller has a worse performance than the pure proportional controller (P).

The synthesis of a modern control strategy was performed. The actuator linear model was obtained and a LQR initial state-control gain was calculated. Based on the dynamic stiffness response performance, a fine-tuning in the eigenvalues of the initial LQR strategy was performed. A linear reduced-order observed was implemented to allow the estimation of the system complete state variables, and a full-state feedback in an analog controller was implemented. Also, considering only the output feedback of the measured states (x_v , ΔP and x_p), a partial-state feedback was implemented in a digital controller. The modern control strategies presented a very good performance, which was compliant with time and frequency response requirements. In addition, those strategies presented a dynamic stiffness enhancement especially for frequencies above 10 Hz.

Based on the performance of the modern controllers, it was to redesign the actuator: reducing the piston seal size by one dash number (-328 to -327) while maintaining the same manifold and valves of the previous design. Both classical and modern control strategies were implemented and the performance were very satisfactory for time and frequency response requirements. However, the classical controllers violate the dynamic stiffness requirement, while the partial-state and full-state feedback control bring the actuator to be compliant with dynamic stiffness requirement.

In conclusion, by taking credit of the performance of a modern control strategy, the traditional flight control actuator's design can be optimized. It is possible to reduce the actuator size, reducing its hydraulic consumption and weight, while maintaining the compliance with time and frequency response and dynamic stiffness requirement. Thus, by introducing a new control strategy approach to the actuator's piston position control, it is possible to optimize the actuator size and comply with extremely demanding design requirements.

7.1 Future Works

In this section, a few future work suggestions are presented. They would improve the flexibility of the constructed actuator model and would allow deeper analysis.

To improve reusability of the actuator model constructed, it would be interesting to configure the actuator mass estimation and metal stiffness as a function of the piston area size. In a more complex approach, a finite element analysis would be valuable to have a

more detailed actuator stiffness data.

In this thesis, the hydraulic fluid considered is the AS1241, Type IV, Class 1. To allow the design of hydraulic actuators for different applications, it would be necessary to include different types of hydraulic fluids (MIL-H-5606, AS1241 Type V, etc.); they would have different physical properties and bulk modulus characteristics and consequently would have major influence in the actuator performance.

The digital/analog conversions and sensors models may be expanded to incorporate with more details delays, gains variations and voltage conversions that are present in real industry applications. This would certainly influence the actuator's frequency response and dynamic stiffness.

To improve the discrete PID implemented in this work, it would be interesting to implement the derivative action with its input based on the sensor output and not the error, this would prevent an excessive control action for step commands.

The dynamic stiffness and flutter analysis would be refined by including backlash effects in the model, because it would be possible to reproduce the rig test environment into the simulation model.

A robustness analysis would be interesting to determine the controller performance sensitivity to important parameters such as the control surface inertia and stiffness, actuator's piston area tolerances, and supply and return pressure variations, for example.

In order to allow different installation configurations of the hydraulic actuator in the aircraft, it would be interesting to include the toggle link kinematics in the model.

To help safety analysis studies of flight control actuators and system monitors development, it would be an interesting approach to consider automatic failure scenarios, such as EHSV spool hardover, seal leakage and other electronic failures.

It would be interesting the development of an actuator's design optimization algorithm to perform the system's eigenvalues placement with controller gains as optimization variables. This algorithm can define the dynamic stiffness and hydraulic consumption as cost functions with restrictions such as minimal rate and overshoot (time response) and gain margin, phase margin and minimal bandwidth (frequency response). This optimization would determine a more efficient actuator control loop's design.

In addition, a good path forward is to complete the study of the ON/OFF controller presented in Appendix A. This study should include the use of PWM (Pulse-width modulation) drivers in the EHSV current and compare them with the controllers implemented in this work. The PWM could also overcome the influence of the EHSV deadband non-linearity in the step response.

Bibliography

AIR1362B. Aerospace hydraulic fluids physical properties. **Society of Automotive Engineers International**, Rev B, 2008.

ARP490F. Electrohydraulic servovalves. **Society of Automotive Engineers International**, Rev F, 2008.

AS4716B. Gland design, o-ring and other elastomeric seals. **Society of Automotive Engineers International**, Rev B, 2011.

ASTROM, K. J. **Control System Design - Lecture Notes for ME 115A.** [S.l.]: University of California Santa Barbara, 2002.

ASTROM, K. J.; MURRAY, R. M. **Feedback Systems - An introduction for Scientists and Engineers.** [S.l.]: Princeton University Press, 2009.

ASTROM, K. J.; WITTENMARK, B. **Computer-Controlled Systems - Theory and Design.** [S.l.]: Prentice Hall, 1997.

BLAIGNAN, V. B.; SKORMIN, V. A. Stiffness enhancement of flight control actuator. **IEEE Transactions on Aerospace and Electronic Systems**, v. 29, n. 2, p. 380–390, 1993.

CONSTANTINO, C. A. **Hydraulic Actuation System Modeling: An Analysis of High Frequency Modelling.** 2010. 121 p. Dissertação (Master in Engineering) — ITA, São José dos Campos, 2010.

CONTE, J. P.; TROMBETII, T. L. Linear dynamic modelling of a uni-axial servo-hydraulic shaking table system. **Earth Quake Engineering and Structural Dynamics**, 2000.

CORTELLINE, C. H.; GOES, L. S. On the air in servo valve hydraulic control systems. **Brazilian Conference on Dynamics, Control and their Applications**, n. 9, 2010.

DAEROSPACE. <http://www.daerospace.com/>. [S.l.]: visited in May/2015, 2015.

FRIEDLAND, B. **Control System Design: An Introduction to State-Space Methods.** 1st. ed. United States: McGraw-Hill, 1986.

HODGES, P. **Hydraulic Fluids.** 1st. ed. United Kingdom: Butterworth-Heinemann, 1996.

- KASHI, K.; SOFFKER, D. Model-based estimation of force and displacement of a hydraulic cylinder. **7th International Symposium on Advanced Vehicle Control**, 2004.
- KURODE S., D. P.; SHIRALKAR, A. Modelling of electro-hydraulic servovalve and robust position control using sliding mode technique. **1st International Conference on Machine and Mechanisms**, p. 607–614, 2013.
- LEECO. **Technical Hydraulic Handbook**. 11. ed. [S.l.], 2009.
- MACROSENSORS. [S.l.], 2015. Disponível em: <<http://www.macrosensors.com/>> - visited in Mar/2015>.
- MERRITT, H. E. **Hydraulic Control Systems**. [S.l.]: John Wiley & Sons, 1967.
- MIL-A-8870C. Airplane strength and rigidity vibration, flutter and divergence. **Society of Automotive Engineers International**, 1993.
- PARKER. **Parker O-ring Handbook**. [S.l.], 2007.
- PRATT, R. W. **Flight Control Systems: practical issues in design and implementation**. 1st. ed. United Kingdom: John Wiley & Sons, 2000.
- RABIE, M. G. **Fluid Power Engineering**. 1st. ed. [S.l.]: McGraw-Hill, 2009.
- SCHMIDT, L. V. **Introduction to Aircraft Flight Dynamics**. [S.l.]: AIAA, 1998.
- THAYER, W. J. **Transfer Functions for Moog Servovalves**. East Aurora, 1965. (RR 95-02).
- THOMPSON, D. F.; PRUYN, J. S.; SHUKLA, A. Feedback design for robust tracking and robust stiffness in flight control actuator using a modified qft technique. **Proceedings of the American Control Conference**, 1999.
- WOODWARD. <http://www.woodward.com/>. [S.l.]: visited in May/2015, 2015.
- WRIGHT, J.; COOPER, J. E. **Introduction to Aircraft Aeroelasticity and Loads**. [S.l.]: John Wiley & Sons, 2007.
- YANADA, H.; KHAING, W.; TRAN, X. Effect of friction on simulation of a hydraulic actuator. **3rd International Conference on Design Engineering and Science**, p. 175–180, 2014.

Appendix A - General Topics

A.1 ON-OFF Controller

The ON-OFF controller strategy is one of the simplest feedback control strategies and can be described as follows, according to (ASTROM, 2002):

$$u = \begin{cases} u_{max} & e > h_{max} \\ u_{min} & e < h_{min} \end{cases}$$

Where u is the control signal and e is the error signal, which is the difference between the reference signal and the system output. The ON-OFF controller hysteresis is represented by h_{max} and h_{min} .

In the actuator control loop, the error is defined as the difference between the actuator command signal and the actuator position output signal measured by the piston LVDT, the control signals $u_{max} = 10\text{ mA}$ and $u_{min} = -10\text{ mA}$ correspond to the maximum and minimum current command to the EHSV.

The ON-OFF controller error hysteresis is influenced by the error of the piston position LVDT sensor. The hysteresis sensibility characterization was performed to evaluate the impact on the actuator performance; the hysteresis bandwidth is expressed as a percentage of the LVDT error signal.

From figure A.1, it is possible to observe the actuator's response for a step command of 30 degrees of amplitude for different hysteresis errors.

The actuator performance pass the surface average rate requirement, as seen on table A.1, but the oscillatory behavior when it reaches the desired position may induce structural problems to the aircraft as presented in (CONSTANTINO, 2010). For higher hysteresis error values, the ON-OFF controller generates higher oscillatory time responses.

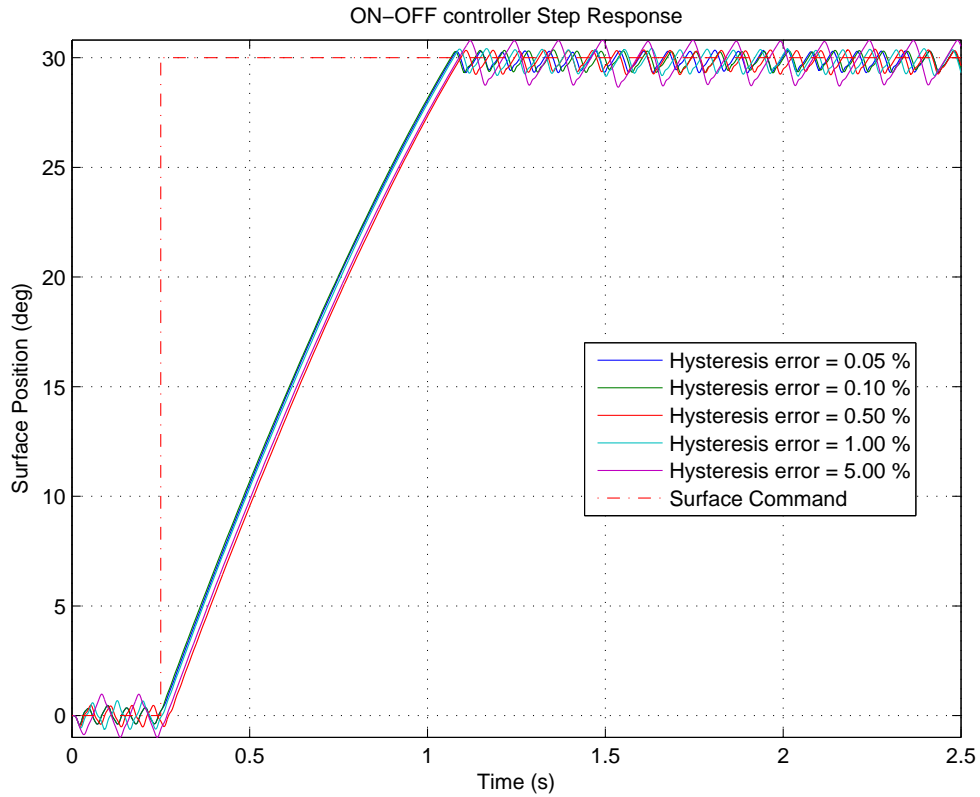


FIGURE A.1 – Time Response - ON-OFF controller

TABLE A.1 – Rudder Actuator Design - Time Response Requirements Compliance ON-OFF controller

ON-OFF controller - Hysteresis Error - Time Response Performance						
Design parameter	Requirement	0.05%	0.10%	0.50%	1.00%	5.00%
Settling time (ms)	< 850	2449	2457	2462	<i>inf</i>	<i>inf</i>
Steady State error (%)	< 1	0.13	0.45	0.35	1.13	1.05
Overshoot (%)	< 10	1.0	1.0	1.2	1.3	2.6
Minimum Average rate (deg/s)	> 32	36.18	36.17	35.37	35.06	39.10
Maximum Average rate (deg/s)	< 36	36.18	36.17	35.37	35.06	39.10

Observing the figure A.2, the ON-OFF controller with different hysteresis error generates an actuator frequency response that has resonance peaks between 5 Hz and 10 Hz. For the phase response, the ON-OFF controller shifts to right as the hysteresis error value becomes higher. From table A.2, it is observed that a higher hysteresis error value determines worst actuator's frequency response performance.

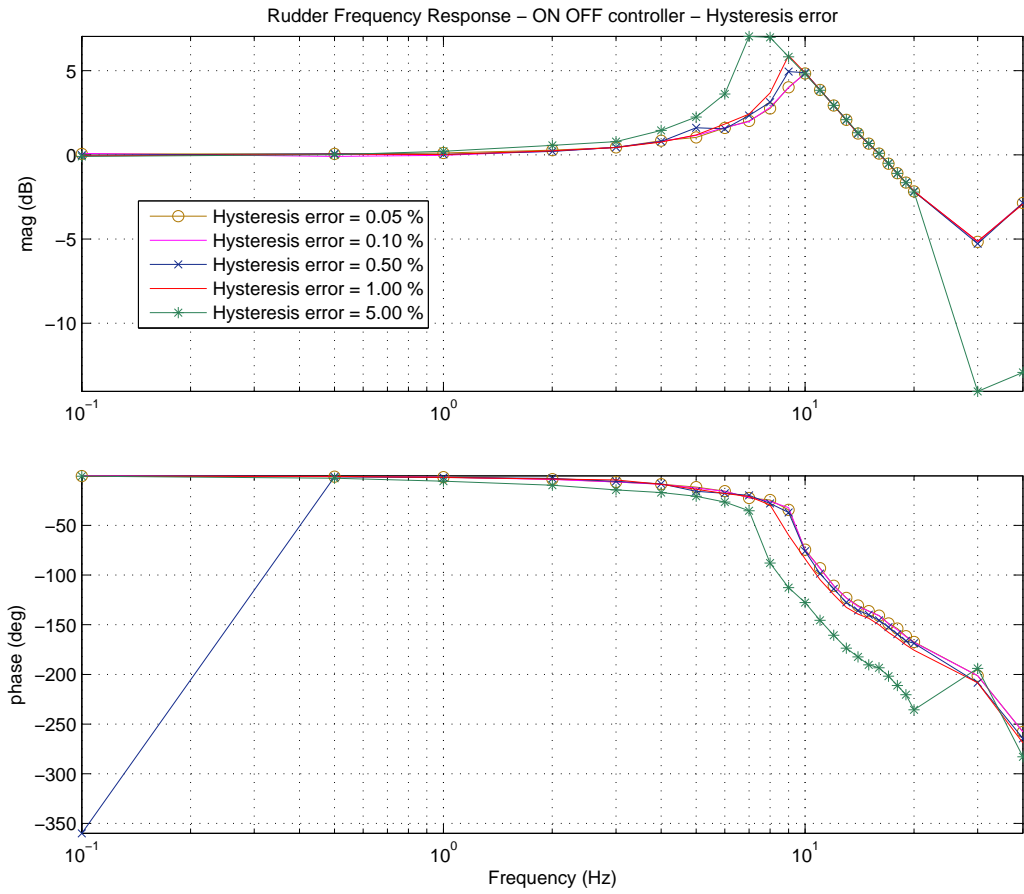


FIGURE A.2 – Frequency Response - ON-OFF controller

TABLE A.2 – Rudder Actuator Design - Frequency Response Requirements Compliance
ON-OFF controller

ON-OFF controller - Hysteresis Error - Frequency Response Performance						
Design parameter	Requirement	0.05%	0.10%	0.50%	1.00%	5.00%
Gain margin (dB)	≥ 10	3.28	3.25	3.05	2.55	-1.53
Phase margin (deg)	≥ 45	38.09	38.11	33.75	29.18	-14.66
Bandwidth (Hz)	<i>None</i>	23.00	22.50	22.72	23.03	20.74

The actuator's dynamic stiffness with an ON-OFF controller violates the flutter suppression design requirement, as shown in figure A.3 for all hysteresis error values.

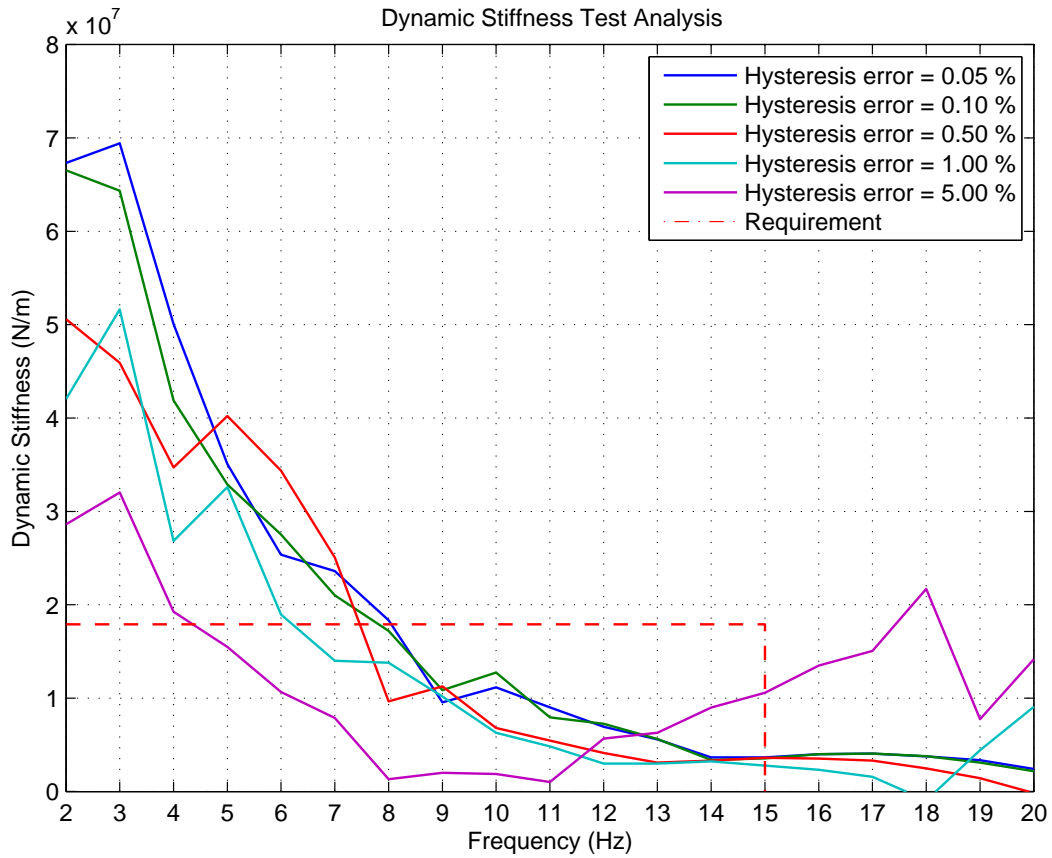


FIGURE A.3 – Dynamic Stiffness - ON-OFF controller

It can be concluded that the ON-OFF controller topology is not acceptable to be implemented in a real flight control actuator. Although it partially complies with time and frequency response's design performance, the ON-OFF controller fails in the dynamic stiffness requirement.

A.2 Electro-hydraulic Actuator State-space model

In this section, it will be presented the numerical state-space model for the electro-hydraulic actuator developed in this work.

The linear system obtained using Matlab *trim* and *linmod* functions is presented below:

$$\begin{bmatrix} \dot{x}_v \\ \ddot{x}_v \\ \dddot{x}_v \\ \dot{\Delta P} \\ \dot{x}_p \\ \ddot{x}_p \end{bmatrix} = \begin{bmatrix} 0 & 1 & 0 & 0 & 0 & 0 \\ 0 & 0 & 1 & 0 & 0 & 0 \\ -1.77 \cdot 10^{10} & -2.11 \cdot 10^7 & -3.64 \cdot 10^3 & 0 & 0 & 0 \\ 2.30 \cdot 10^7 & 0 & 0 & -9.36 \cdot 10^{-2} & 8.16 \cdot 10^1 & -9.63 \cdot 10^4 \\ 0 & 0 & 0 & 0 & 0 & 1 \\ 0 & 0 & 0 & 2.18 & 0 & -4.67 \cdot 10^1 \end{bmatrix} \begin{bmatrix} x_v \\ \dot{x}_v \\ \ddot{x}_v \\ \Delta P \\ x_p \\ \dot{x}_p \end{bmatrix} + \begin{bmatrix} 0 \\ 0 \\ 3.28 \cdot 10^7 \\ 0 \\ 0 \\ 0 \end{bmatrix} i$$

$$\begin{bmatrix} x_v \\ \Delta P \\ x_p \end{bmatrix} = \begin{bmatrix} 1 & 0 & 0 & 0 & 0 & 0 \\ 0 & 0 & 0 & 1 & 0 & 0 \\ 0 & 0 & 0 & 0 & 1 & 0 \end{bmatrix} \begin{bmatrix} x_v \\ \dot{x}_v \\ \ddot{x}_v \\ \Delta P \\ x_p \\ \dot{x}_p \end{bmatrix}$$

The linear model was obtained by breaking the nonlinear actuator model into three models:

- i- EHSV 1st stage dynamics;
- ii- EHSV 2nd stage and ΔP dynamics;
- iii- Piston dynamics.

The nonlinear model breakdown was necessary due to numerical limitations encountered while applying *trim* and *linmod* functions to the complete nonlinear actuator model.

The *trim* function is responsible to obtain the steady state parameters of a Simulink model, and it was used to obtain the system operating points.

The *linmod* function obtains the linear model of a system for a specific operating point and it is necessary to specify the inputs and outputs in the Simulink model to be linearized.

As described in chapter 5, the linearization point is obtained with the *trim* function help:

$$X_e = \begin{bmatrix} x_{ve} \\ \dot{x}_{ve} \\ \ddot{x}_{ve} \\ \Delta P_e \\ x_{pe} \\ \dot{x}_{pe} \end{bmatrix} = \begin{bmatrix} 0 \\ 0 \\ 0 \\ 0 \\ 0 \\ 0 \end{bmatrix} \quad U_e = i_e = 0$$

Figure A.4 shows the EHSV first stage dynamics model. This model was extracted from the nonlinear actuator model and it was performed the linearization to obtain the linear dynamics for the EHSV states x_v , \dot{x}_v and \ddot{x}_v . The integrators initial condition values, representing $(x_v, \dot{x}_v$ and $\ddot{x}_v)$, were set to zero, according to the desired linearization point.

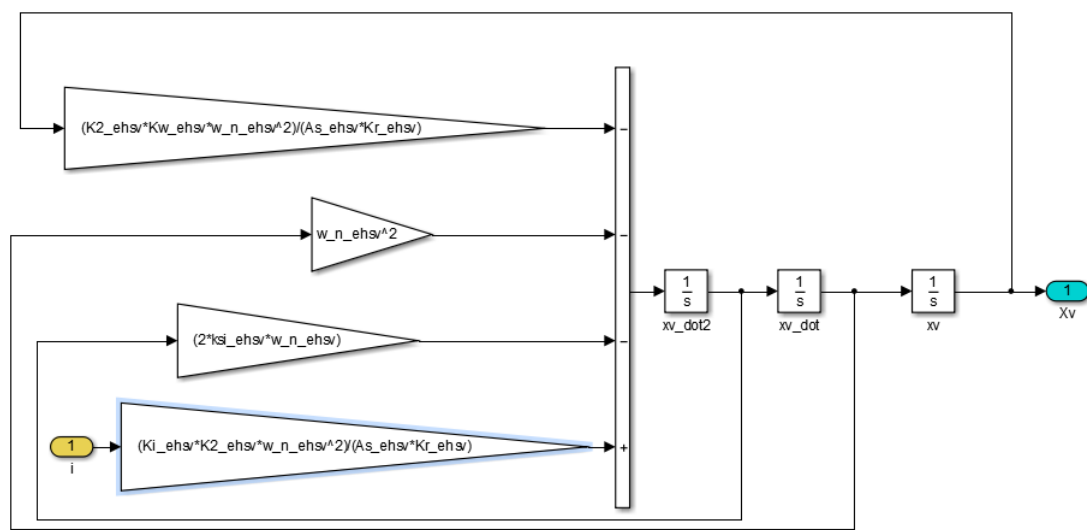
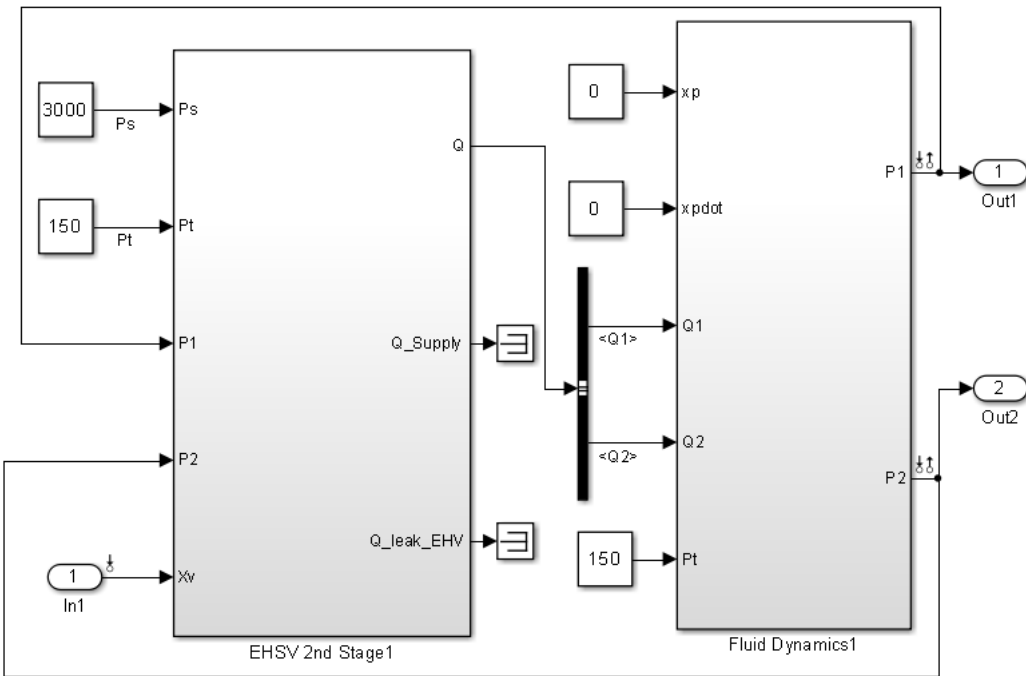
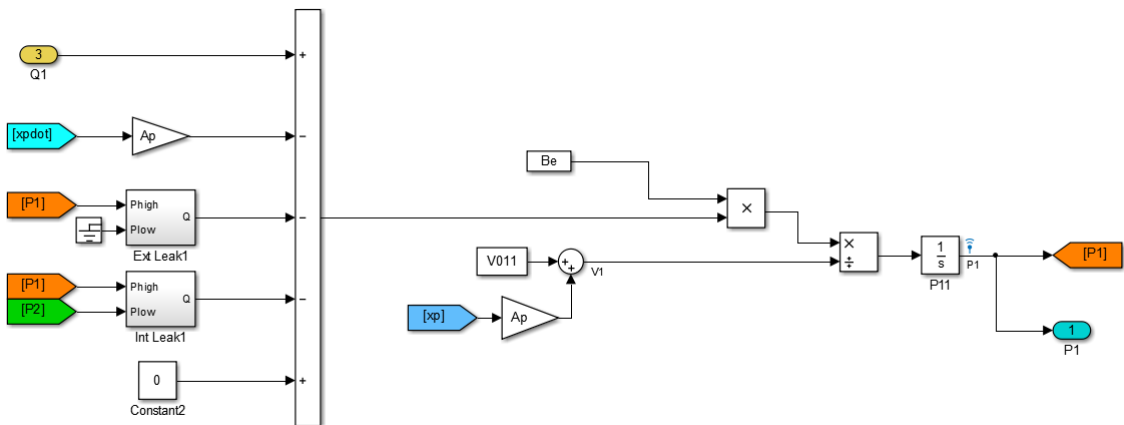


FIGURE A.4 – EHSV first stage dynamics model

Figure A.5 illustrates the Simulink model of the EHSV 2nd stage and the pressures dynamics of the actuator's chambers. This model was extracted from the nonlinear actuator model in order to obtain the numerical linearization of the ΔP state variable. From chapter 5, ΔP was defined as $\Delta P = P_1 - P_2$. Thus, the operating point is defined as $\Delta P_e = P_{1e} - P_{2e} = 1500 - 1500 = 0$, and, consequently, the pressures dynamics integrators initial condition values were fixed to 1500 psi. The supply and return pressure were fixed to 3000 psi and 150 psi, respectively. The states x_p , \dot{x}_p initial conditions were fixed to zero, their linearization point value. The anti-cavitation valves were removed from the fluid dynamics block, and the Bulk Modulus was considered constant, those modifications can be seen in the detailed pressure dynamics of chamber 1 model in figure A.6.

FIGURE A.5 – EHSV 2nd stage and ΔP dynamicsFIGURE A.6 – Simplified P_1 dynamics

The piston dynamics model is observed in figure A.7. The integrator initial values for x_p and \dot{x}_p are set to their linearization point. The piston load is set to zero due to the no-load assumption from the linear model construction. Also, the friction is eliminated together with the actuator stroke mechanical stops.

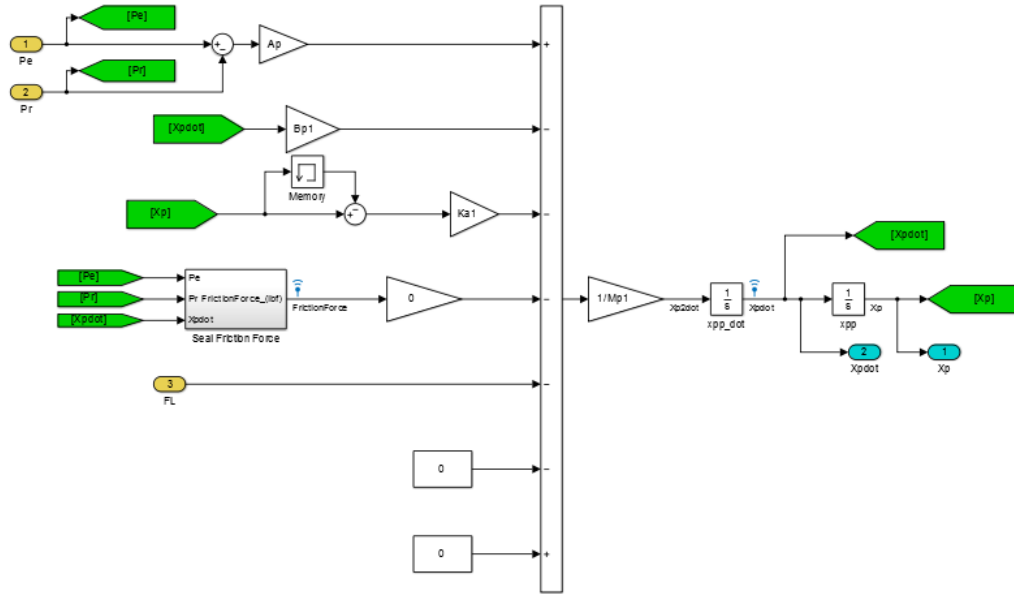


FIGURE A.7 – Simplified Piston dynamics model

Running trim and linmod functions into the described previous models, the linear system matrix A and B coefficients can be obtained.

A.3 Modern controller with Pressure sensor noise

This section is complementary to the chapter 5 results and it presents the effect of a failure in the actuator's Δ pressure sensor in the actuator performance. This failure induces a noise into the sensor's measurement output. In the figure A.8, it is possible to observe the sensor output with and without measurement noise. To simulate the measurement noise, Matlab/Simulink White Noise block was used.

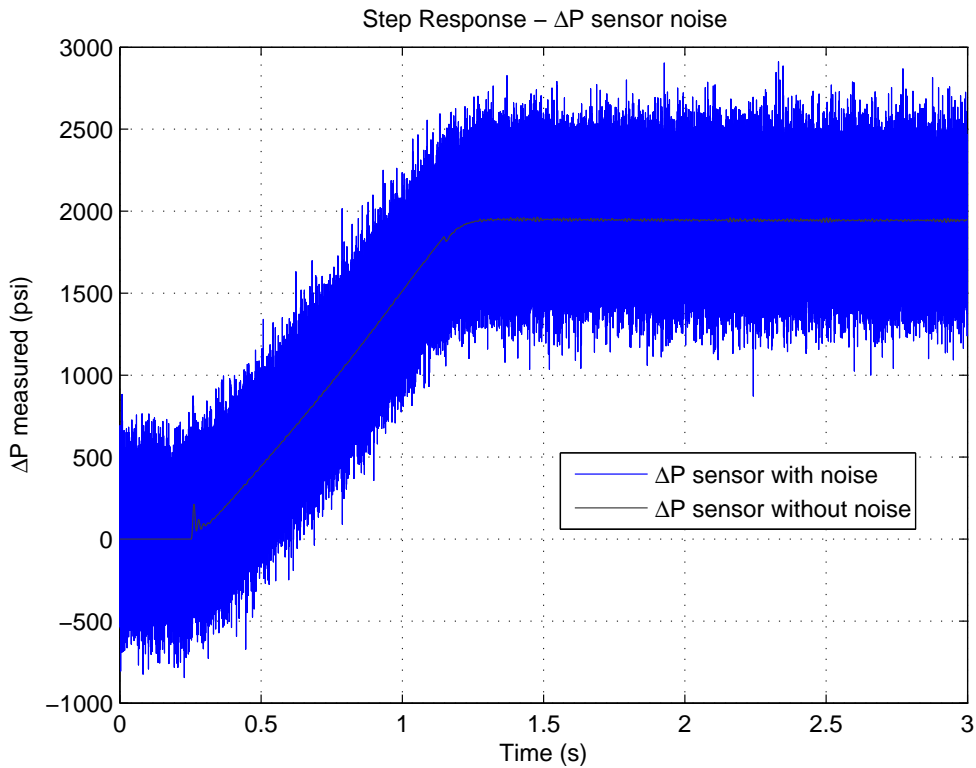


FIGURE A.8 – Δ pressure sensor output with noise

Figure A.9 shows the actuator's step response for partial and full state feedback control, both cases present the measurement noise from the ΔP sensor. From table A.3, it is possible to observe that the actuator with full-state feedback control comply with all time response requirements. The partial-state feedback actuator do not comply with the average rate. It is possible to conclude that even with the noise from the differential pressure sensor, the modern controllers present a very good time response performance.

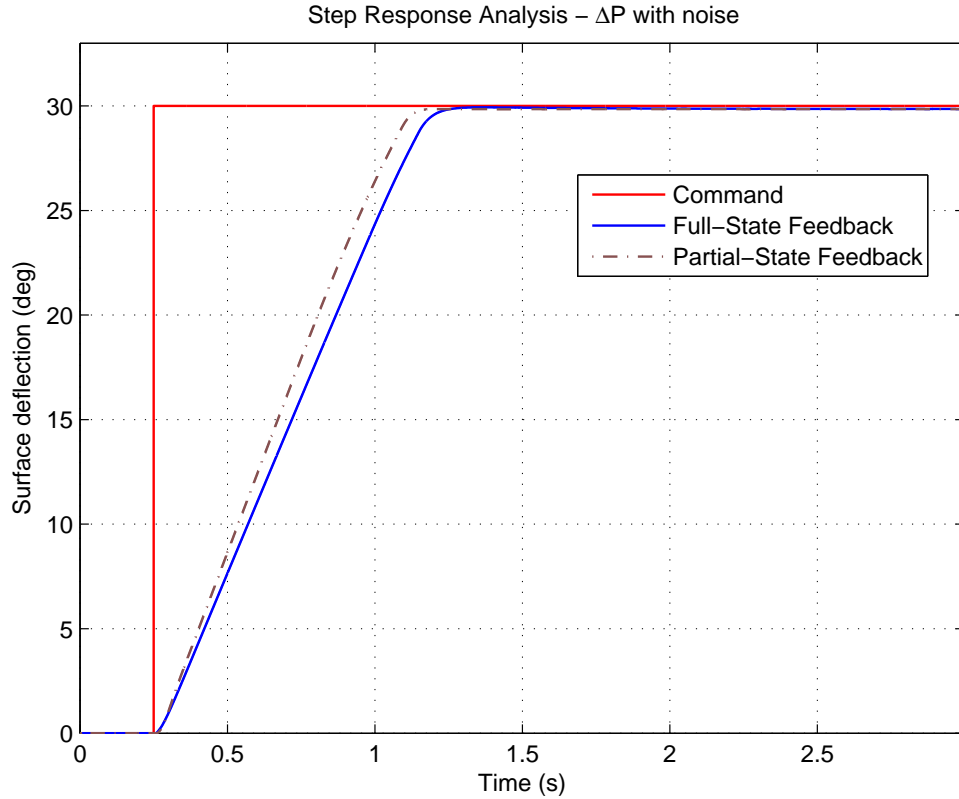


FIGURE A.9 – Actuator’s time response for modern controller and with ΔP sensor noise

TABLE A.3 – Actuator’s time response for modern controller and with ΔP sensor noise

Time Response Performance			
Design parameter	Requirement	Partial	Full
Settling time (ms)	< 850	612	684
Steady State error (%)	< 1	0.24	0.22
Overshoot (%)	< 10	0.0	0.0
Minimum Average rate (deg/s)	> 32	36.10	33.35
Maximum Average rate (deg/s)	< 36	36.10	33.35

Figure A.10 shows the actuator’s frequency response for partial and full state feedback control, both cases present the measurement noise from the ΔP sensor. From table A.4, it is possible to observe that the actuator with full-state and partial-state feedback control are still compliant with all frequency response requirements. The partial-state feedback actuator has a smaller bandwidth than the full-state feedback, and a smaller phase margin. Thus, the partial-state feedback performance is more sensitive to the ΔP sensor measurement noise than the full-state feedback.

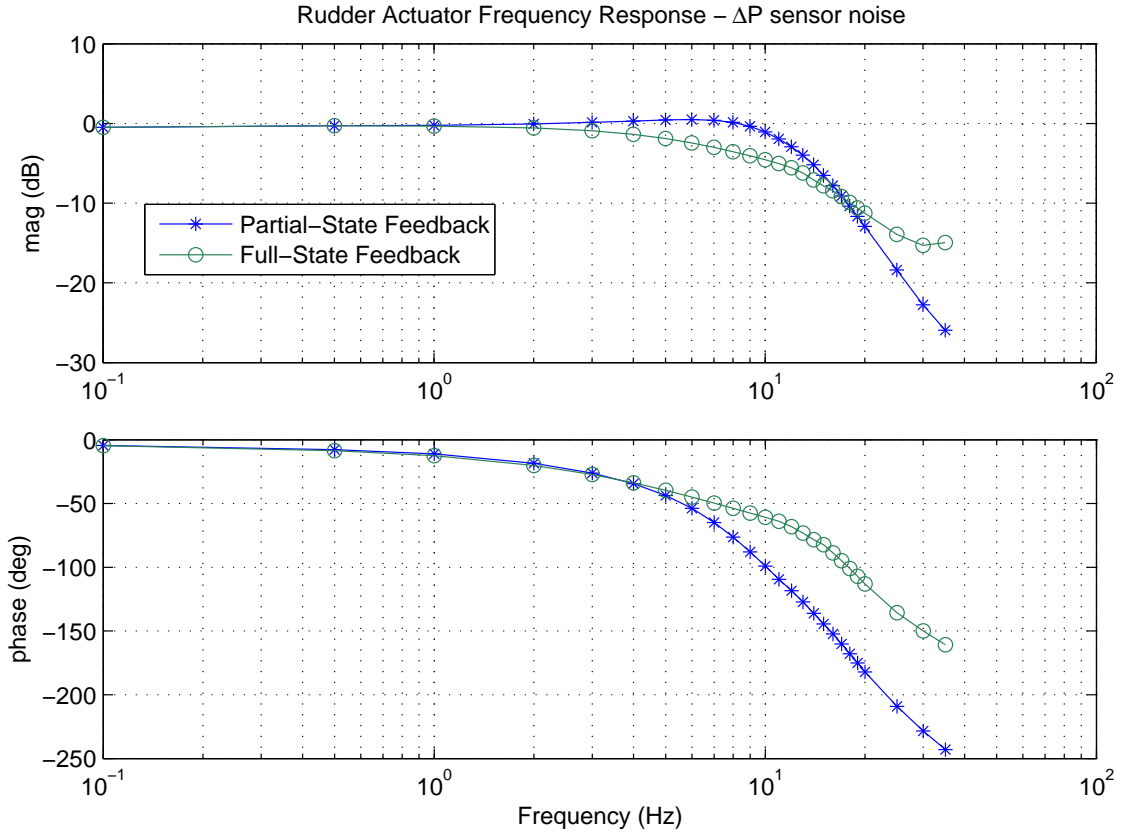


FIGURE A.10 – Actuator’s frequency response for modern controller and with ΔP sensor noise

TABLE A.4 – Actuator’s frequency response for modern controller and with ΔP sensor noise

Frequency Response Performance			
Design parameter	Requirement	Partial	Full
Gain margin (dB)	≥ 10	12.53	14.36
Phase margin (deg)	≥ 45	100.41	inf
Bandwidth (Hz)	<i>None</i>	12.53	7.90

Regarding the actuator’s dynamics, figure A.11 shows a comparison between the modern controller performance with and without the presence of measurement noise of the ΔP sensor output. It can be concluded that for both modern controllers the measurement noise affects the dynamic stiffness performance for frequencies above 10 Hz. The partial-state feedback presents the worst performance with the presence of noise, and the full-state feedback in the presence of measurement noise presents degradation in performance especially for high frequencies.

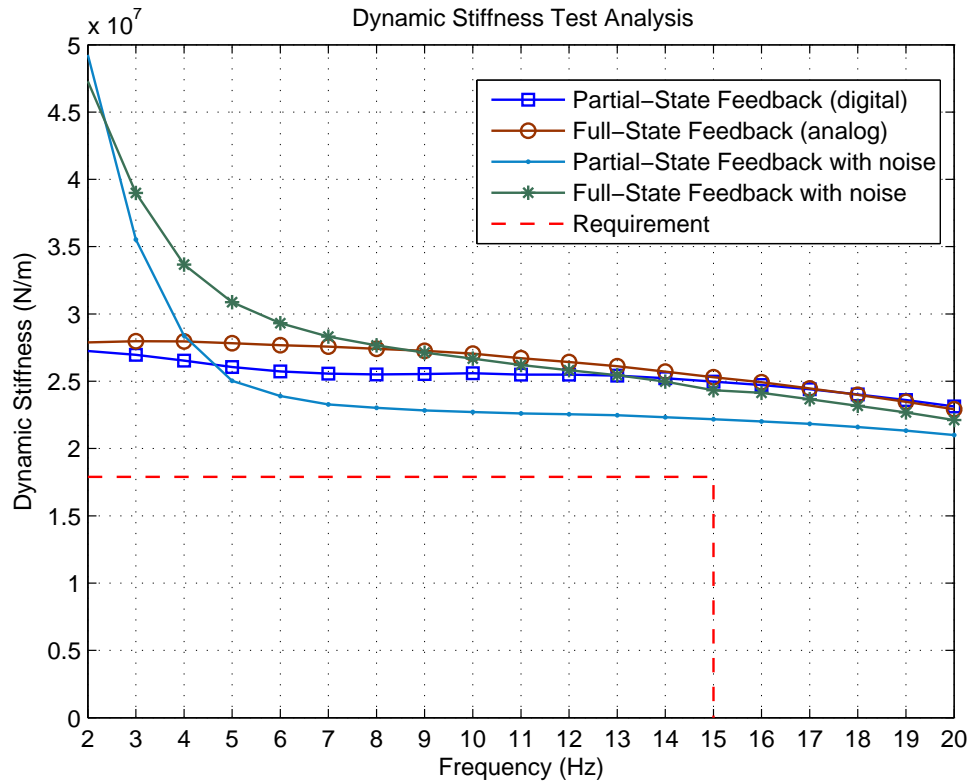


FIGURE A.11 – Dynamic Stiffness performance comparison for modern controller with and without ΔP sensor noise

It is possible to conclude that even in the presence of measurement noise in the ΔP sensor, the modern controllers determine an actuator performance that is still compliant with its design requirements. However, there is a degradation in performance, especially for the actuator's dynamic stiffness, when compared to the chapter 4 results obtained without ΔP sensor measurement noise.

Annex A - Aeroelastic and Safety Requirements

A.1 Control surface flutter suppression requirements

25.629 Aeroelastic stability requirements.

(a) General. The aeroelastic stability evaluations required under this section include flutter, divergence, control reversal and any undue loss of stability and control as a result of structural deformation. The aeroelastic evaluation must include whirl modes associated with any propeller or rotating device that contributes significant dynamic forces. Compliance with this section must be shown by analyses, wind tunnel tests, ground vibration tests, flight tests, or other means found necessary by the Administrator.

(b) Aeroelastic stability envelopes. The airplane must be designed to be free from aeroelastic instability for all configurations and design conditions within the aeroelastic stability envelopes as follows:

(1) For normal conditions without failures, malfunctions, or adverse conditions, all combinations of altitudes and speeds encompassed by the V_D/M_D versus altitude envelope enlarged at all points by an increase of 15 percent in equivalent airspeed at both constant Mach number and constant altitude. In addition, a proper margin of stability must exist at all speeds up to V_D/M_D and, there must be no large and rapid reduction in stability as V_D/M_D is approached. The enlarged envelope may be limited to Mach 1.0 when M_D is less than 1.0 at all design altitudes, and

(2) For the conditions described in §25.629(d) below, for all approved altitudes, any airspeed up to the greater airspeed defined by;

(i) The V_D/M_D envelope determined by §25.335(b); or,

(ii) An altitude-airspeed envelope defined by a 15 percent increase in equivalent airspeed above V_C at constant altitude, from sea level to the altitude of the intersection of 1.15 V_C with the extension of the constant cruise Mach number line, M_C , then a linear variation in equivalent airspeed to $M_C + .05$ at the altitude of the lowest V_C/M_C intersection; then, at higher altitudes, up to the maximum flight altitude, the boundary defined by a .05 Mach increase in M_C at constant altitude.

(c) Balance weights. If concentrated balance weights are used, their effectiveness and strength, including supporting structure, must be substantiated.

(d) Failures, malfunctions, and adverse conditions. The failures, malfunctions, and adverse conditions which must be considered in showing compliance with this section are:

(1) Any critical fuel loading conditions, not shown to be extremely improbable, which may result from mismanagement of fuel.

(2) Any single failure in any flutter damper system.

(3) For airplanes not approved for operation in icing conditions, the maximum likely ice accumulation expected as a result of an inadvertent encounter.

(4) Failure of any single element of the structure supporting any engine, independently mounted propeller shaft, large auxiliary power unit, or large externally mounted aerodynamic body (such as an external fuel tank).

(5) For airplanes with engines that have propellers or large rotating devices capable of significant dynamic forces, any single failure of the engine structure that would reduce the rigidity of the rotational axis.

(6) The absence of aerodynamic or gyroscopic forces resulting from the most adverse combination of feathered propellers or other rotating devices capable of significant dynamic forces. In addition, the effect

of a single feathered propeller or rotating device must be coupled with the failures of paragraphs (d)(4) and (d)(5) of this section.

(7) Any single propeller or rotating device capable of significant dynamic forces rotating at the highest likely overspeed.

(8) Any damage or failure condition, required or selected for investigation by §25.571. The single structural failures described in paragraphs (d)(4) and (d)(5) of this section need not be considered in showing compliance with this section if;

(i) The structural element could not fail due to discrete source damage resulting from the conditions described in §25.571(e), and

(ii) A damage tolerance investigation in accordance with §25.571(b) shows that the maximum extent of damage assumed for the purpose of residual strength evaluation does not involve complete failure of the structural element.

(9) Any damage, failure, or malfunction considered under §§25.631, 25.671, 25.672, and 25.1309.

(10) Any other combination of failures, malfunctions, or adverse conditions not shown to be extremely improbable.

(e) Flight flutter testing. Full scale flight flutter tests at speeds up to V_{DF}/M_{DF} must be conducted for new type designs and for modifications to a type design unless the modifications have been shown to have an insignificant effect on the aeroelastic stability. These tests must demonstrate that the airplane has a proper margin of damping at all speeds up to V_{DF}/M_{DF} , and that there is no large and rapid reduction in damping as V_{DF}/M_{DF} is approached. If a failure, malfunction, or adverse condition is simulated during flight test in showing compliance with paragraph (d) of this section, the maximum speed investigated need not exceed V_{FC}/M_{FC} if it is shown, by correlation of the flight test data with other test data or analyses, that the airplane is free from any aeroelastic instability at all speeds within the altitude-airspeed envelope described in paragraph (b)(2) of this section.

A.2 Safety requirements - Flight Control System

25.671 General.

(a) Each control and control system must operate with the ease, smoothness, and positiveness appropriate to its function.

(b) Each element of each flight control system must be designed, or distinctively and permanently marked, to minimize the probability of incorrect assembly that could result in the malfunctioning of the system.

(c) The airplane must be shown by analysis, tests, or both, to be capable of continued safe flight and landing after any of the following failures or jamming in the flight control system and surfaces (including trim, lift, drag, and feel systems), within the normal flight envelope, without requiring exceptional piloting skill or strength. Probable malfunctions must have only minor effects on control system operation and must be capable of being readily counteracted by the pilot.

(1) Any single failure, excluding jamming (for example, disconnection or failure of mechanical elements, or structural failure of hydraulic components, such as actuators, control spool housing, and valves).

(2) Any combination of failures not shown to be extremely improbable, excluding jamming (for example, dual electrical or hydraulic system failures, or any single failure in combination with any probable hydraulic or electrical failure).

(3) Any jam in a control position normally encountered during takeoff, climb, cruise, normal turns, descent, and landing unless the jam is shown to be extremely improbable, or can be alleviated. A runaway of a flight control to an adverse position and jam must be accounted for if such runaway and subsequent jamming is not extremely improbable.

(d) The airplane must be designed so that it is controllable if all engines fail. Compliance with this requirement may be shown by analysis where that method has been shown to be reliable.

FOLHA DE REGISTRO DO DOCUMENTO

1. CLASSIFICAÇÃO/TIPO DM	2. DATA 25 de março de 2015	3. DOCUMENTO Nº DCTA/ITA/TC-018/2015	4. Nº DE PÁGINAS 175
5. TÍTULO E SUBTÍTULO: Dynamic Stiffness Enhancement of a Flight Control Actuator using control techniques			
6. AUTOR(ES): Heric Martinez Santos Ballesteros			
7. INSTITUIÇÃO(ÓES)/ÓRGÃO(S) INTERNO(S)/DIVISÃO(ÓES): Instituto Tecnológico de Aeronáutica – Divisão de Engenharia Mecânica – ITA/IEM			
8. PALAVRAS-CHAVE SUGERIDAS PELO AUTOR: Atuador; Rigidez Dinâmica; Flutter			
9. PALAVRAS-CHAVE RESULTANTES DE INDEXAÇÃO: Atuador; Rigidez Dinâmica; Flutter			
10. APRESENTAÇÃO: <input type="checkbox"/> Nacional <input checked="" type="checkbox"/> Internacional ITA, São José dos Campos. Curso de Mestrado Profissional. Programa de Pós-Graduação em Engenharia Aeronáutica e Mecânica. Área de Sistemas Aeroespaciais e Mecatrônica. Orientador: Prof. Dr. Alberto Adade Filho. Coorientador: MSc. Raphael das Neves Calvo. Defesa em 23/10/2015. Publicada em 25/10/2015.			
11. RESUMO: <p>Em sistemas de comandos de voo, atuadores eletrohidráulicos são responsáveis por mover as superfícies de controle primário das aeronaves atendendo requisitos de desempenho, como resposta temporal e em frequência. Outra responsabilidade dos mesmos é a supressão de flutter da superfície de controle, atendendo requisitos de rigidez dinâmica e de amortecimento. Em um projeto clássico de atuador, o cumprimento de tais requisitos gera atuadores não-ótimos, penalizando o desempenho da aeronave. O objetivo deste trabalho é investigar diferentes estratégias de controle de posição do atuador que atendam os requisitos de desempenho e aumentem a rigidez dinâmica do atuador.</p> <p>Uma metodologia clássica de dimensionamento de atuadores primários é desenvolvida e validada utilizando um modelo baseado em (CONSTANTINO, 2010) com modificações para a análise de rigidez dinâmica. O desempenho do atuador para diferentes controladores clássicos (P, PI, PD, PID) é analisado, e uma abordagem de controle moderno usando a estratégia de controle LQR com um observador linear de ordem reduzida, além de uma realimentação de estado parcial, usando apenas variáveis medidas, são desenvolvidas. Ambas estratégias apresentaram bom desempenho, superando o do controle PD, e aumentando a rigidez dinâmica do atuador especialmente para frequências acima de 10 Hz.</p> <p>O desempenho dos controladores modernos permitiu a redução da área do pistão em um selo. O atuador com área reduzida operando com realimentação de estados ou de saída apresentou um excelente desempenho e uma melhoria notável da rigidez dinâmica. Assim, é possível projetar um atuador de comandos de voo otimizado, utilizando uma abordagem de controle moderno, que reduziria o consumo hidráulico, o peso e tamanho do atuador, trazendo benefícios para o desempenho da aeronave.</p>			
12. GRAU DE SIGILO: <input type="checkbox"/> OSTENSIVO <input checked="" type="checkbox"/> RESERVADO <input type="checkbox"/> CONFIDENCIAL <input type="checkbox"/> SECRETO			